Enthalpies of CH_4 and CO_2 Hydrate Formation and Dissociation Using Residual Thermodynamics

Master of Science Thesis in Process Technology

Specialisation in Separation Technology

By

Petter Berge Gjerstad

Department of Physics and Technology

University of Bergen, Norway

October 2019

Abstract

The problem in the processing industries regarding the formation of gas hydrate in pipelines or equipment have inspired much of the research for better understanding of hydrates. The world's increasing demands for more energy opens for hydrate as a potential energy source. For the duration of the last few years, there have been ideas involving using hydrate, since it is a solid phase, as a better transport of gases such as methane (CH_4). Carbon capture involving storage of carbon dioxide (CO_2) as hydrate in empty reservoirs would help lower the greenhouse gas emission. This requires better knowledge and technology within the hydrate field, but the theory of hydrates among scientists is not necessarily in agreement.

Even though hydrate was discovered in the 1800s, any precise method of determining the heat of hydrate formation or dissociation is widely spread. The equilibrium pressure and temperature for hydrates are well known and in good agreement among scientists. The approaches of measuring or calculating the enthalpy changes of hydrate phase transition are implemented by using experiments, the Clapeyron equation or the Clausius-Clapeyron equation. The deficiency of information or the estimation of hydration numbers makes the experimental results challenging to trust or rely on. Clausius-Clapeyron equation, which is a simplified version of the Clapeyron equation, is very popular for calculating the heat of hydrate dissociation but is inaccurate at higher pressures compared to the Clapeyron equation.

The Clapeyron approach relies on equilibrium conditions, and since hydrates cannot reach equilibrium in real life, approaches that can calculate for non-equilibrium systems would be a better choice. Since the enthalpy change is directly coupled to the change in free-energy, by calculating the change in free-energy of the phase change, we can directly calculate the heat of hydrate formation and dissociation using residual thermodynamics. The method of using residual thermodynamics for hydrate calculation is proposed in this work and is not limited to heterogeneous hydrate formation from liquid water and hydrate phase, but can be used to calculate for homogeneous hydrate formation from dissolved hydrate formers in liquid water also. In this work, the enthalpy of hydrate formation for both CH_4 and CO_2 hydrates along with hydration numbers have been calculated using residual thermodynamics at equilibrium conditions from temperatures of 273.16 K to 290.0 K. These values have also been compared with other works recorded in literature based on experimental works, Clapeyron equation and Clausius-Clapeyron equation.

Acknowledgement

I would like to express my gratitude and appreciation to my former supervisor, Professor Bjørn Kvamme, who introduced me to hydrates and the theory behind it and also allowed me to participate on articles to be published in scientific journals. Even though he could not be my supervisor anymore, he was still contacting me through e-mails and even met me in person to discuss my master thesis. Professor Kvamme has a hectic schedule, but he always responds to e-mails whenever there are any questions about hydrates.

I want to give big gratitude to Mr Solomon Aforkoghene Aromada and Professor Tatiana Kuznetsova, who could step in as my supervisors at such short notice. Even though Solomon is a self-funded PhD-candidate busy working on his thesis and has a family to take care of, he did not hesitate to become my new supervisor. We have been working together on several hydrate projects since 2017, and with his expertise, I knew Mr Aromada was the right person for this supervisor job.

Both Mr Aromada and Prof. Kuznetsova have been accommodating since the beginning. Prof. Kuznetsova is always supportive if I have any question or problem, and she does not give up until the issue is resolved or answered.

Finally and not least, I want to thank my family and friends for all the support I received over the years.

List of publications and conference papers

Kvamme, B., Aromada, S.A., Kuznetsova, T., Gjerstad, P.B., Canonge, P.C., Zarifi, M., "Maximum tolerance for water content at various stages of a natuna production", *Heat and Mass Transfer*, **2018**

Kvamme, B., Aromada, S.A., Saeidi, N., Hustache, T., Gjerstad, P., "Hydrate Nucleation, growth and induction", *ACS Omega*, **2019**, (submitted and waiting for acceptation)

Kvamme, B., Aromada, S.A., Gjerstad, P.B., "Consistent enthalpies of hydrate formation and dissociation using residual thermodynamics", *Chem.Eng.Data*, **2019**

Kvamme, B., Wei, N., Sun, W., Aromada, S.A., Gjerstad, P.B., Zarifi, M., "A Residual thermodynamic scheme for calculation of enthalpy for hydrate formation and dissociation", *ICGH10*, **2019**, (submitted and waiting for acceptation)

Publications included in this thesis

Appendix A:

Kvamme, B., Aromada, S.A., Kuznetsova, T., Gjerstad, P.B., Canonge, P.C., Zarifi, M., "Maximum tolerance for water content at various stages of a natuna production", *Heat and Mass Transfer*, **2018**

Table of Contents

List of Figures

List of Tables

Nomenclature

$\AA$	Angstrom
δ	Partial charge
P	Pressure
P	Number of phases (Gibbs phase rule)
T	Temperature
T_R	Actual temperature divided by critical temperature
$T_{0,R}$	273 Kelvin divided by the actual temperature
R	Universal gas constant
R	Radius of hydrate core
R^*	Critical radius for the hydrate core
ρ_N^H	Molar density of hydrate
γ	Interface free energy
γ_i	Activity coefficient of a component
γ_i^∞	Activity of a component at infinite dilution
μ	Chemical potential
μ_i^H	Chemical potential of component i in hydrate cavity
μ_i^{gas}	Chemical potential of component i in hydrate former phase
μ_i^{water}	Chemical potential of component i in liquid/gas or solid water

$\mu_{H_2O}^{Water}$	Chemical potential of water in liquid/gas or solid water
$\mu_{H_2O}^{0,H}$	Chemical potential of water in empty hydrate cavity
μ_i^{∞}	Chemical potential of a component at infinite dilution
G_i^{Ψ}	Gibbs free energy of a component at a phase ψ
ΔG	Change in Gibbs free energy
ΔG^{Total}	Total change in Gibbs free energy
Δg_{ik}^{inc}	Impact on hydrate water from the inclusion of guest i in cavity k
H	Hydrate
H	Enthalpy
H_{ik}^{R}	Residual enthalpy of a component inside the cavity
ΔH	Change in Enthalpy
ΔS	Change in Entropy
x_i^H	Mole fraction of component i in hydrate
x_{ik}^H	Mole fraction of component i in cavity k
$x_{H_2O}^H$	Mole fraction of water in the hydrate
y_i^{gas}	Mole fraction of component i in hydrate former phase
J	Mass transport rate
J_0	Mass transport flux

β	The inverse of Boltzmann's constant multiplied with temperature
m	Mass
$c \text{ and } c^{eq}$	Supersaturated and equilibrium concentration
C	Number of components (Gibbs phase rule)
F	Degree of freedom
A	Surface area of a crystal
K	Overall transfer coefficient
K_d	Diffusion coefficient
K_r	Reaction coefficient
K_B	Boltzmann's constant
U	Internal energy
$U_{ik}^{residual}$	Residual contribution of energy for guest in the cavity
S	Entropy
N_j^i	Number of particles of component j in phase i
n	Hydration/Occupation number
$\Delta U \text{ or } dU$	Change in internal energy
V	Vapour
V	Volume
V_{ik}	Volume of the component in the cavity
v_m	Molar volume

v_k	Fraction of cavity-type k per water molecule
h_{ik}	Canonical cavity partition function of component i in cavity k
θ_{ik}	Filling fraction of component in cavity k
b	The volume occupied by one mole of the molecules
a	The average attraction between particles
ϕ	Fugacity coefficient
f	Fugacity
f_i^0	Fugacity for an ideal solution at a reference state
A	Helmholtz
z	Compressibility coefficient
z_{ik}	Compressibility factor for guest inside the cavity
W	Work energy
Q	Heat energy
$L \text{ or } L_w$	Liquid/Liquid water

1 Introduction

Gas hydrates are known to appear in seafloor sediments at several regions around the world, seemingly not confined to certain latitudes. Hydrates are very efficient gas collectors, and it is estimated that 1 m^3 of methane hydrate can release about 164 m^3 of methane (CH_4) gas under standard temperature and pressure conditions (STP) [1]. It has been anticipated that over 15 x 10^{12} toe (ton of oil equivalent) of gas hydrate exists around the globe. Only 17-20% of this resource can supply the energy demand of the world for 200 years [2].

Release of the methane gas into the atmosphere is considering to be a threat to the global climate system due to its properties as a potent greenhouse gas. This can cause even more hydrate dissociation in sediments or in the permafrost due to the change in temperature, releasing even more greenhouse gas [3]. Natural gas hydrates as an energy source are limited by the technology of production. Several methods have been proposed, such as pressure reduction, dissociation by hot steam (thermal stimulation), but they are too expensive.

Pilot tests have been faced with trouble due to freezing, and other problems include sand and water production. A new, and perhaps better approach is by injection of CO_2 into hydrate reservoir, replacing the methane inside the hydrate [4]. This technology for natural gas production is also of great interest due to storing CO_2 in reservoirs, as a replacement for releasing it into the atmosphere. Hydrate research is essential for future work. The history of hydrate research is widespread, the first report is nearly 200 years old, and hydrate research has played a leading role in the development of modern science. Hydrate scientists these days encounter an impressive number of practical challenges.

The control of hydrate formation, decomposition or hydrate structure, in connection with the transportation of gas in pipelines, the sequestration of CO_2 (carbon capture and storage), or the recovery of natural gas from hydrates. Locating and estimating the quantity of gas in natural formations in linking with energy reserves and the potential for global climate change [5] is also a challenge. In this thesis, we will investigate how widespread the different values of enthalpy of hydrate formation and dissociation in different works of literature have become with different approaches, such as Clapeyron, Clausius-Clapeyron and experimental. In addition to this, a suggestion of how and why we should use residual thermodynamics as the most suitable approach for calculating hydrate phase transitions.

1.1 Motivation

Any production of natural gas from hydrates requires a supply of heat. If the pressure of a hydrate deposit is reduced to below hydrate stability pressure, the heat of dissociation must still be supplied. Adding heat to dissociate natural gas hydrate obviously needs information on the heat of hydrate dissociation. During the injection of carbon dioxide into a methane hydrate reservoir, a new carbon dioxide hydrate will be formed, and the released heat of formation will be used for dissociation of the methane hydrate. Reliable data for heats of formation and dissociation for hydrates of carbon dioxide and methane hydrate is therefore essential.

As a first step in the direction of this goal, it is crucial to evaluate what is available of experimental data and theoretical methods for calculating these hydrate phase transition enthalpies. The second step is to either extend or modify existing models or develop new models for enthalpies of hydrate formation and hydrate to fit the needs discussed above. In addition to the needs for enthalpy of hydrate phase transitions as part of concept studies for hydrate production, there is a need for consistent enthalpies in kinetic theories for a hydrate phase transition. Some existing theories are based on gradients of independent thermodynamic variables (temperature and pressure).

Thermodynamic consistency, however, implies that the resulting thermodynamic variable is consistently related. Enthalpy is uniquely related the free energy by trivial thermodynamic relationships. Models for describing free energy changes related to hydrate phase transitions will, therefore, have a corresponding unique enthalpy change based on the same models.

This type of consistent approach will apply to Phase Field Theory, Classical Nucleation Theory, Multicomponent Diffuse Interface Theory and any other kinetic theory for phase transition, which is complete. By complete means that there is implicit coupling between mass transport, heat transport and the thermodynamics of the phase transition.

1.2 Objective and scope

One of the main goals of this thesis is to show how wide the variation, confusion and uncertainty within the hydrate literature are, more specifically, the enthalpies of formation and dissociation for methane and carbon dioxide hydrates. The other one is to justify the use of residual thermodynamics in calculations involving hydrate phase transitions.

To achieve these objectives:

- Research for information available in works of literature involving enthalpies of hydrate formation and dissociation for methane (CH_4) and carbon dioxide (CO_2). Experimental data is preferred.
- Evaluate the different available experimental data
- Evaluate the other approaches such as Clapeyron equation and Clausius-Clapeyron equation
- Introduce the basic theory of hydrates and how residual thermodynamics can be used to calculate the heat of formation and dissociation of hydrates.
- Calculate the enthalpy of CH_4 and CO_2 hydrate formation using residual thermodynamics at equilibrium conditions within the same range of temperatures as the other literature.
- Make the results easily accessible for other readers and researchers for further work. This can be done by inserting the values into a table.
- Compare results from residual thermodynamics with available literature.

1.3 Scientific methods

Evaluation of the phase transition of hydrate formation or dissociation discussed in this work requires scientific methods such as molecular dynamics (MD) simulation. MD is a computer simulation technique useful for analysing the physical movements of molecules and atoms (nanoscale) that is allowed to interact with each other for a fixed period of time and provides a view of the dynamic development of a hydrate system [6]. However, MD is limited to small volume and time scales (nanoseconds), considering that hydrate formation and dissociation is a relatively slow process. Other techniques, such as density functional theory (DFT) and phase-field theory (PFT) [7] can also be used to study the formation or dissociation of hydrates. The concept of density functional theory is that the kinetics of a phase transition is proportional to the changes of molecular structures but are limited to geometric scales.

These structures are directly related to the free energy, and this is where phase-field theory (PFT) comes in. PFT makes it possible to scale up and are only limited to the thermodynamic description, yet, it requires a considerable amount of computer power to do the simulations and using much time to run the simulations. The CPU time would rise more than proportional to the number of components, where the integration over concentration includes a differential equation of the fourth-order in compare to phase-field, which only goes to second-order differential equations [8].

The choice of the scientific method for this work is a technique called free energy minimisation and is based on classical thermodynamics. Residual thermodynamics will be applied for all the components and phases via the application of the Soave-Redlich-Kwong (SRK) equation of state. The parameters required by the SRK, such as the chemical potential of liquid water and chemical potential for empty hydrate structure have been obtained by molecular dynamics simulations (MD).

The Monte Carlo approach [9] was used to evaluate the differences in enthalpies of hydrate formation. The result and outcomes in this thesis are based on the theory and programming codes by Professor Bjørn Kvamme. These codes, written in a FORTRAN language and run from a Microsoft Developer studio, provide the desired variables. By using software such as MATLAB, these values can be plotted, and figures are the preferred method to presents the results individually, and also for comparing with other literature research.

2 Hydrate

Gas hydrates are solid non-stoichiometric crystalline structures that look like ice but are different in various ways. Unlike ice, gas hydrates can form at temperatures above zero degrees Celsius, as long pressure is high enough. Such circumstances often occur in oil and gas wells, but also in pipeline equipment. Gas hydrate is hydrogen-bonded water molecules that form a cage-structure which traps small-sized molecules as guest molecules [10]. An empty hydrate without a gust molecule is not thermodynamically stable. Guest molecules prevent the hydrate lattice from collapsing and help to stabilise the hydrate. Hydrocarbon components such as methane (CH_4), ethane (C_2H_6) and propane (C_3H_8) are some of the typical guests that are not too large or too small to fit into water cavities.

Non-hydrocarbon also, such as carbon dioxide (CO_2), nitrogen (N_2) and hydrogen sulphide (H_2S) are prevalent as guest molecules. Natural gas hydrates, usually methane, occur in the pore spaces under ocean sediments or continental sedimentary rock formation [11], and it has been estimated that about 97% of all-natural gas hydrates have been located offshore and only 3% on land [2]. Over the past century, fossil fuels have supplied the majority of china's energy. Their extensive consumption of energy has led to a shortage and environmental pollution. China's research on gas hydrates is progressing rapidly but is still in an early developing stage [12]. Gas hydrates may be an alternative energy source for the future, but it also causes problems in the industries. Processing plants transporting hydrocarbons are always accompanied by reservoir water. Under the right conditions with high pressure and low enough temperature, water combined with hydrocarbons can form hydrates that cause plugging in pipelines or damage on expensive equipment.

To avoid hydrate formation during transportation and pressure reduction or heating is not an option, there are other alternatives. Adding chemical inhibitors such as methanol or ethanol changes the thermodynamic properties of the system by lowering the chemical potential of liquid water, making it more stable. Another option is by lowering the fraction of water in the gas phase by dehydration. In fact, rusty pipelines are found to increase the risk of liquid water drop out (that is causing hydrate formation) by a factor of 18 due to adsorption on hematite (rust) [13]. Hydrate formation during transportation of natural gas will not be a topic for this thesis, much of this is already covered in a previously published work by our research group and can be found in appendix A.

2.1 History of hydrates

One of the first known discovery of hydrates was either done by Joseph Priestly in 1778 or by Sir Humphrey Davy in 1810. This is because there is some uncertainty if the experiments completed by Priestley with vitriolic air (SO_2) at temperatures under the freezing point were an observation of ice or hydrate. Sir Humphrey Davy did his experiments with chlorine (Cl_2) at temperatures above the freezing point, making this the first discovery of "warm ice". At that time, neither of the experiments got any attention among scientists or industrialists. It only became an academic interest later as a laboratory curiosity to establish which compounds were able to form hydrates and to describe the composition between the water molecules and the guest molecules. During this time, fossil fuel such as oil and gas became a central source of energy. For transportation, large gas pipelines were constructed in the USA in the 1920s, and the formation of plugs during cold periods became a significant problem. These were misjudged as solid ice, not gas hydrate. It was not until the American chemist E.G Hammerschmidt identified the problem as hydrate plugging in 1934 that created the beginning of modern research for hydrate.

The challenges to predict and prevent hydrate formation in pipelines and equipment during transport or processing has required vast amounts of effort and research. Most of these are connected with the work of D. Katz and R. Kobayashi who devoted all their scientific lives to hydrates. These pioneers gave rise to new technology and techniques. The determination of the two hydrate crystals s(I) and s(II) were reported by a group of the German scientist Von Stackelberg in 1949 after two decades of X-ray hydrate crystal diffraction experiments. A statistical theory for hydrates based on its structure was first proposed by Van Der Waals and Platteeuw in 1959. In 1967, a group of Russian researchers led by Makogon discovered the massive field of natural gas hydrates in the permafrost region. It has been estimated that the total energy in resources of methane worldwide, is twice the amount of all the combined fossil fuel energy reserve [14]. With the world's increasing demand for energy, gas hydrates might be used as an alternative energy source as our technology and knowledge improve. Methane (CH_4) is a potent greenhouse gas, around 25 times more aggressive than CO_2. The dissociation of methane hydrate in the permafrost leaking into the atmosphere is an environmental threat. Thermodynamically, methane hydrates are more unstable than Carbon dioxide hydrates. This opens up the opportunity to replace the CH_4 molecules in the hydrate with CO_2, a win-win situation where CO_2 gets injected and provided long-term storage for CO_2 in the form of a hydrate, but at the same time releasing natural gas for energy [15].

2.2 Hydrate structures, filling and stabilisation of cavities

The structure of the gas hydrate depends on the guest molecules. There are three common structures; structure (I), (II) and (H). Only structure (I) and structure (II) are usually found in petroleum production and processing. Structure (H), the third hydrate structure is not as ordinary as the other two structures and will not be relevant for this thesis, but information on its geometry can be found in Table 2.1. A typical hydrate structure, shown in Figure 2.1, is composed of cages, also known as cavities. In particular, the 5^{12}, forms a building block for all the three hydrate structures, as shown in Figure 2.2. It is composed of 12 pentagonal faces, formed by H_2O-molecules linked together by hydrogen-bond, with oxygen at each vertex [16]. The free diameter of the 5^{12} cages is 5.1 Å (angstrom) and allows small molecules like methane (4.36 Å) to stay inside. There are no chemical bonds between the cage and the guest molecules. When a 5^{12} cavity is connected to others, a body-centred cubic crystal of 5^{12} cavities forms, and it is called hydrate structure (I).

Because the 5^{12} cavities cannot fill space without strains on the hydrogen-bond, a secondary cavity is required, $5^{12}6^2$. This is with both 12 original pentagonal faces and two new hexagonal, strain-reliving faces. The 5^{12} is often referred to as the small cavity and the $5^{12}6^2$ as the large cavity of structure (I). Formation of a structure (I) hydrate crystal, requires 2 small and 6 large cavities, as shown in Figure 2.2. Structure (I) hydrate have a total sum of 46 water molecules in all the cavities. The diameter of the large cavity, $5^{12}6^2$, is around 5.86 Å.

This allows a molecule of ethane (5.5Å), which is the second most common component of natural gas, to fit inside the large cavity. The methane molecule is too small to prop open the large $5^{12}6^2$ cavities, although it can fit inside. In a mixture of both CH_4 and C_2H_6, methane occupies mostly in the small cavity and only a slight number of the large cavity.

Structure (I) hydrate is suitable for small components such as CH_4, C_2H_6, CO_2 and H_2S, but larger molecules such as propane (6.3 Å) and i-butane (6.5 Å) are too big to fit inside $5^{12}6^2$ cavities. A larger cavity, $5^{12}6^4$ with a diameter of 6.66 Å forms around the molecule. This cavity has 12 pentagonal and 4 hexagonal faces. Again, the 5^{12} cavities cannot fill all the space alone, but the large $5^{12}6^4$ cavities help. By combining 16 small 5^{12} cavities and 8 large $5^{12}6^4$ cavities, the hydrate structure (II) is formed and contains 136 water molecules in total. A summary of the different hydrate structures is shown in Table 2.1.

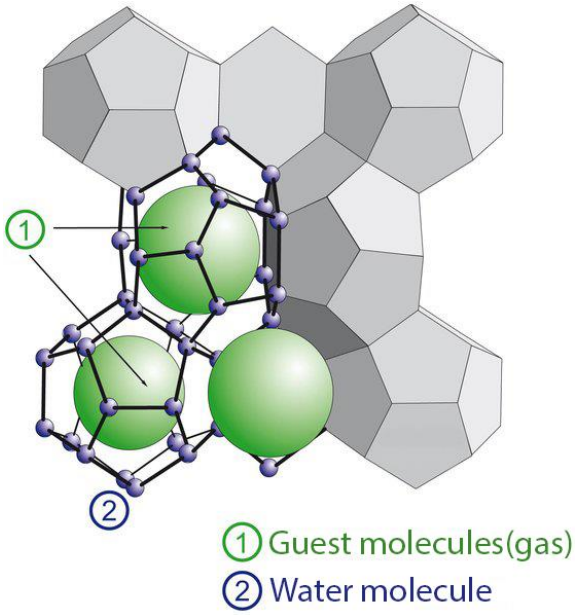

Figure 2.1: Illustration of a typical gas hydrate structure, where the water molecules bonds and forms cages that trap the gas molecules (such as methane, ethane, etc.) inside. Adapted from [17].

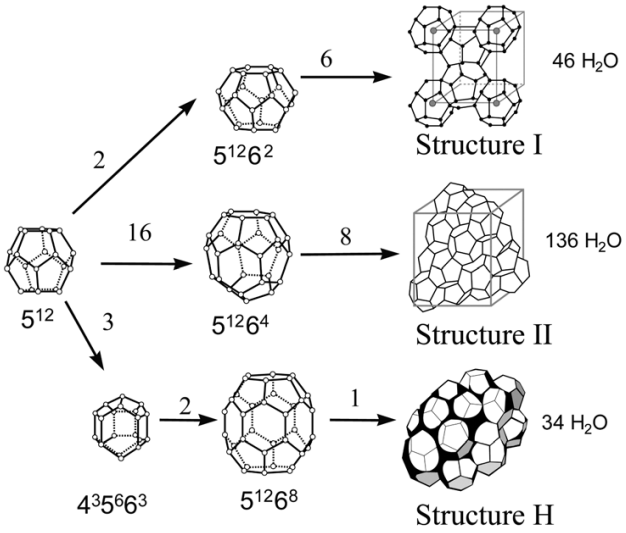

Figure 2.2: Illustration of how the different hydrate structures are formed [18]. From left, the small 5^{12} cavity acts as a building block to be merged with larger cavities and form hydrate structures.

Table 2.1: Geometry of hydrate crystal structures, adapted from Sloan [19].

Hydrate crystal structure	**I**		**II**		**H**		
Cavity type	**Small**	**Large**	**Small**	**Large**	**Small**	**Medium**	**Large**
Description	5^{12}	$5^{12}6^2$	5^{12}	$5^{12}6^4$	5^{12}	$4^3 5^6 6^3$	$5^{12}6^8$
Number of cavities/unit cell	2	6	16	8	3	2	1
Average cavity radius[a] (Å)	3.95	4.33	3.91	4.73	3.94	4.04	5.79
Variation in radius (%)	3.4	14.4	5.5	1.73	4.0	8.5	15.1
Number of water molecules per cavity[b]	20	24	20	28	20	20	36
Number of water molecules per unit cell	46		136		34		
Examples of guest molecules	Methane, ethane, carbon dioxide		Propane, iso-butane		Methane + neohexene, Methane + cycloheptane		

[a] *The average cavity radius will vary with temperature, pressure and guest composition. One angstrom is equal to* 1.0×10^{-10} *meters*

[b] *Number of oxygen atoms at the periphery of each cavity*

Several factors keep cavities stable; The volume of the guest molecule makes it difficult for the H_2O in the cavity wall to collapse. In hydrates, the actual stabilisation depends on the van der Waals-attraction, which are the short-range interactions between the guest and the water molecules [20]. Hydrogen sulphide, H_2S, is a very aggressive hydrate former and it stabilizes both small and large cavities of the structure I hydrate. The H_2S molecule is slightly polar compared to the nonpolar component like methane. Due to its effect of dipole moment, H_2S has a unique effect on hydrate stability. When it rotates inside the water cavity, it exposes an average positive charge outward because of the positively charged hydrogen atoms pointing outward towards the cavity walls, as shown in Figure 2.3.

The cavity walls have an average negative charge and face inward in the cavity. Strongly polar molecules would destroy hydrate lattice by destroying hydrogen bonds, but the dipole moment of H_2S is strong enough to have strong coulombic attraction towards the cavity wall, but weak enough not to make it collapse. For H_2S the average coulombic effect gives extra stabilisation, while for CO_2 the average coulombic effect gives some destabilisation effect.

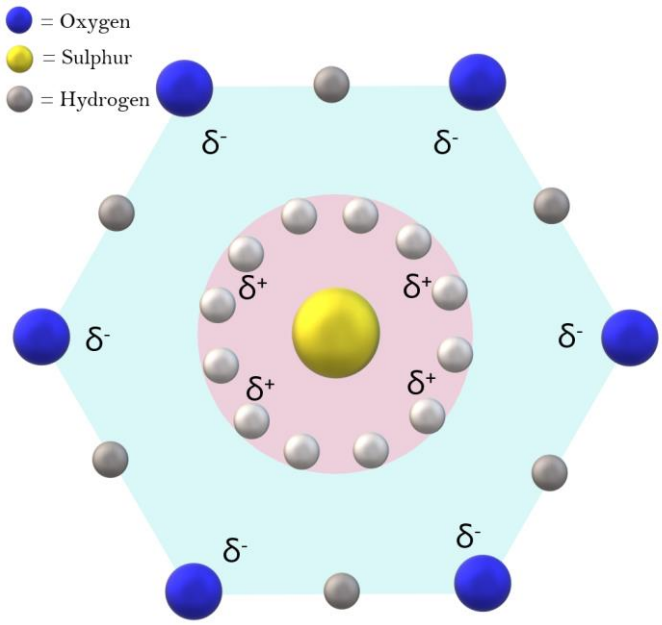

Figure 2.3: A two-dimensional illustration of how the H_2S molecule help stabilising the hydrate from inside the cavity. The oxygen and hydrogen atoms of water molecules form the surrounding cavity wall. The hydrogen in the water wants to line along with the water connection, but the other hydrogen atoms go in and out of the cavity, resulting in an average negative charge facing inwards. Although H_2S has a positive partial charged at its centre, an average positive charge is facing outwards due to rotation inside the hydrate cavity. Adapted from [20]

3 Kinetics of hydrate formation

Hydrate formation is a three-step process which involves hydrate nucleation, growth, and induction. Each step is described in their own subsection and is based on a previously published paper [21], but simplified. Hydrate formation and dissociation are processes that involve many competing phases and represents non-equilibrium scenarios. A lot of research groups treat the phase transitions as equilibrium reactions because the reactions can occur pretty quick. In reality, hydrate systems can barely achieve equilibrium. The Gibbs phase rule, which relates to the degree of freedom that a mixture of components and phases have in a closed system, states that hydrate systems are in a non-equilibrium state [22]. In the hydrate reservoir, where both temperature and pressure are given locally by process control or hydrodynamic flow, the hydrate system can never reach equilibrium. Even for a simple system of pure CH_4 in contact with water ends up with a maximum one thermodynamic variable that can be specified for achieving equilibrium. This is why equilibrium curves are always measured by keeping either the pressure or temperature fixed and monitoring the phase transition of hydrate through a slow variation of the other variable.

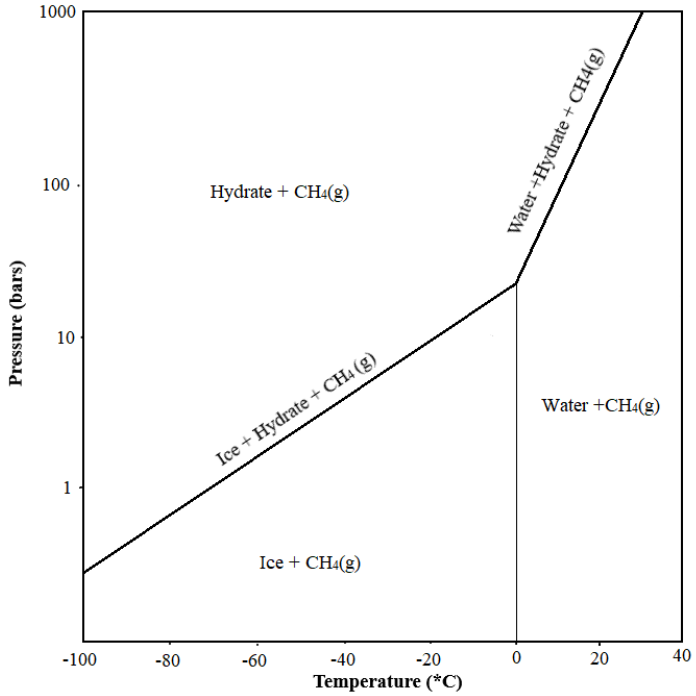

Figure 3.1: A typical three-phase equilibrium pressure diagram for methane hydrate as a function of temperature. Adapted from [23]. The diagram is just for illustrating the effects of pressure and temperature in a hydrate system, and the data point should not be used for any calculation. A proper equilibrium curve for CH_4 and CO_2 can be found on page 58.

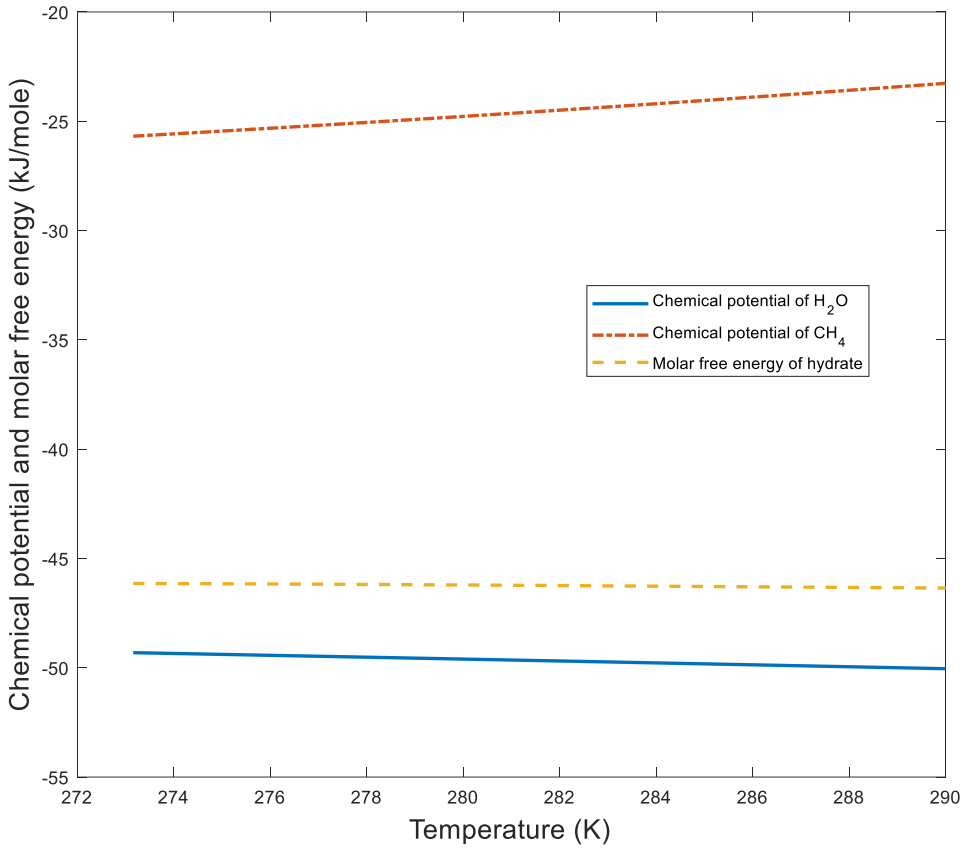

Figure 3.2: The chemical potential for CH_4 and water in the hydrate along the equilibrium curve, respectfully. The dashed line in the centre is the molar free energy of the hydrate.

Figure 3.1 shows a typical equilibrium curve for methane hydrate. Every pressure and temperature conditions to the left of the equilibrium curve are stable for hydrate formation. Conditions to the right of the equilibrium curve are not stable for hydrate formation. Hydrates under such conditions would dissociate into liquid water and hydrate former gas. There is nothing new about this figure, and there are several equilibrium codes published that can calculate that curve. Figure 3.2 shows the chemical potential of water and methane in the hydrate as well as the molar free energy of the hydrate along the hydrate equilibrium curve. Gibbs free energy is a measurement of the energy available in a system to drive a reaction. It's not possible to determine the absolute value, but the change in energy can be calculated, as shown:

$$\Delta G = \Delta H - T\Delta S \tag{3.1}$$

Where ΔG is the change in free energy, ΔH is the change in enthalpy, and ΔS is the change in entropy.

A system at equilibrium is the point which no net change occurs over time, so no change in enthalpy and entropy makes ΔG = 0. All systems seek naturally towards states with the lowest possible free energy. This is because a lower free energy state is less likely to drive a reaction. In a non-equilibrium system, there is no rule that controls the chemical potential of each component to be equal across the phase boundaries. So, for a methane hydrate formation to occur, the free energy for the hydrate phase must be lower than the free energy for methane in its pure gas phase and the free energy for the water phase. Since the chemical potentials of hydrate formers (guest components) can be different at various phases, it is also possible for various formation-routes to create different types of hydrates.

For a simple system of water and methane under hydrate conditions, where the effects of the solid surface are neglected, the free energy change of the hydrate formation on the interface is formulated in equation 3.2 and illustrated in Figure 3.3.

$$\Delta G^{H_1} = \left[x_{H_2O}^{H_1} \left(\mu_{H_2O}^{H_1}(T,P,\vec{x}^{H_1}) - \mu_{H_2O}^{water}(T,P,\vec{x}) \right) + \sum_j x_j^{H_1} \left(\mu_j^{H_1}(T,P,\vec{x}^{H_1}) - \mu_j^{gas}(T,P,\vec{y}^{gas}) \right) \right] \quad (3.2)$$

The delta symbol, Δ, is the change in free energy and the superscript H_1 indicates the specific hydrate formation route. x is the mole fraction in liquid water or hydrate (superscript) and y is the mole fraction in hydrate former phase. The vector sign denote the mole fraction of all the components in the actual phase. Superscripts H_2O and *j* denote water and hydrate formers (guest), μ is the chemical potential. Other factors as heat and mass transport play an essential role in hydrate formation. As the hydrate film on the water surface emerge and closes in, the mass transport of hydrate builders becomes very slow.

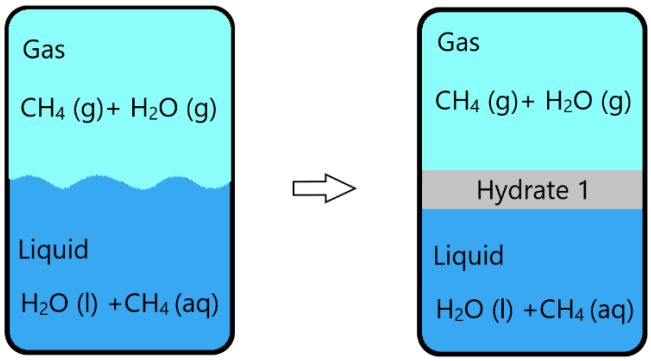

Figure 3.3: Formation of hydrate film at the interface between the liquid water and methane gas.

Since the initial hydrate film limits mass transport across the interface and thus hydrate formation at the interface, this opens up a second route towards hydrate formation where it uses the hydrate former that is already dissolved in the liquid water. Since this is a non-equilibrium situation, the chemical potential of methane dissolved in water does not necessarily be the same for methane in the gas phase. For this reason, the composition will be different from the first hydrate, and so will the equation to calculate the free energy, shown in equation 3.3 denoted H_2.

$$\Delta G^{H_2} = \left[x_{H_2O}^{H_2} \left(\mu_{H_2O}^{H_2}(T,P,\vec{x}^{H_2}) - \mu_{H_2O}^{water}(T,P,\vec{x}) \right) + \sum_j x_j^{H_2} \left(\mu_j^{H_2}(T,P,\vec{x}^{H_2}) - \mu_j^{water}(T,P,\vec{x}) \right) \right] \quad (3.3)$$

Formation of hydrate via the H_2 route will be limited to the concentration of hydrate formers in the liquid water. It is more likely that heterogeneous methane hydrate formation occurs at the hydrate/water interface region due to higher methane concentrations, as shown in Figure 3.4, but homogeneous hydrate formation inside the water solution is also achievable.

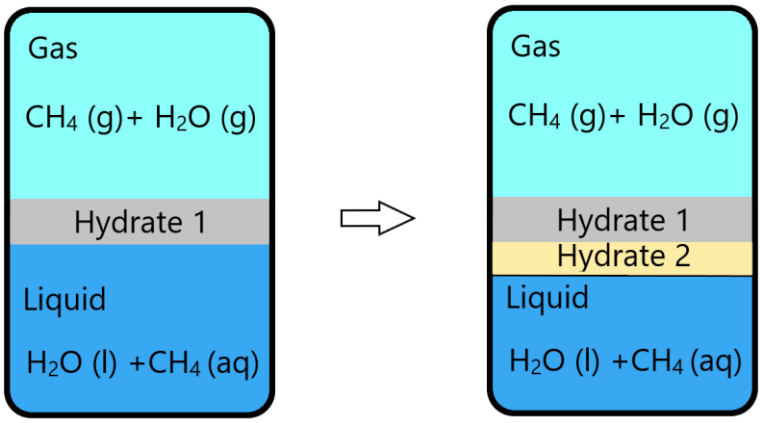

Figure 3.4: Formation of methane hydrate between the hydrate film and water interface.

There is a third, but a possible theoretical route to hydrate formation, H_3, shown in Figure 3.5. The free energy is given by equation (3.4).

$$\Delta G^{H_3} = x_{H_2O}^{H_3}\left(\mu_{H_2O}^{H_3}(T,P,\vec{x}^{H_3}) - \mu_{H_2O}^{gas}(T,P,\vec{y}^{gas})\right) + \sum_j x_j^{H_3}\left(\mu_j^{H_3}(T,P,\vec{x}^{H_3}) - \mu_j^{gas}(T,P,\vec{y}^{gas})\right) \quad (3.4)$$

The gas region contains hydrate former and a small amount of dissolved water, but due to limited mass and heat transport, it's unlikely for this hydrate formation to occur. However, if water condenses out on the hydrate film, a limited amount of hydrate can be formed.

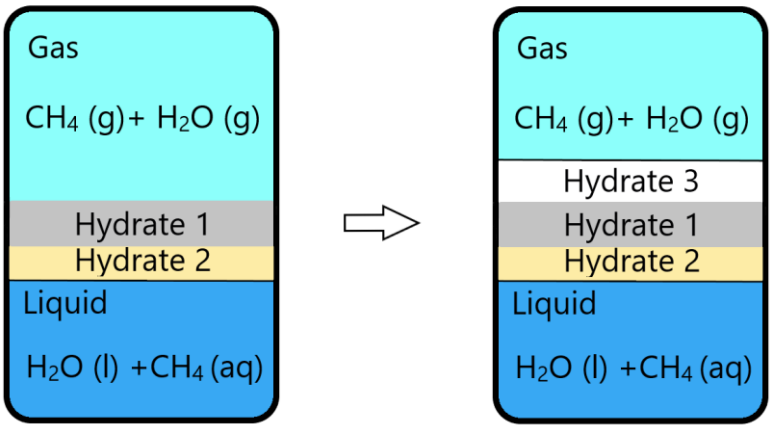

Figure 3.5: An illustration of the third hydrate formation route. Since gases conduct heat very poorly and can only have a limited concentration dissolved, it's not a thermodynamically favourable route.

Using the Gibbs phase rule for a simple system of methane and water, using 3 different hydrates, gives the number of freedom to -1. This means both temperature and pressure are highly overdetermined in terms of the possibility for equilibrium. The concept of the Gibbs phase rule is explained in section 3.4 on page 32.

The classical nucleation theory can be used to described hydrate formations, and the mass transport rate expressed as:

$$J = J_0 e^{-\beta \Delta G^{Total}} \quad (3.5)$$

Where the J_0 in equation 3.5 is the mass transport flux that's supplying building blocks for the hydrate growth. To give it in better perspective, J_0 would be the supply of methane to the

interface growth in equation 3.2 and diffusion rate for dissolved methane to crystal growth from aqueous solution in equation 3.3. The supply of H_2O by diffusion through a gas is the limiting mass transport rate in equation 3.4. For homogeneous hydrate formation in equation 3.3 and 3.4, the units for J_0 will be moles/m^{3}s, and for heterogeneous hydrate growth in equation 3.2, will be moles/m^{2}s. J has the same units as J_0. β is the inverse of the gas constant multiplied with the temperature and ΔG^{Total} is the molar free energy change of the phase transition.

The total change in Gibbs free energy consists of two competing processes:

$$\underline{\Delta G}^{Total} = \underline{\Delta G}^{Phase\ transition} + \underline{\Delta G}^{Push\ work} \tag{3.6}$$

The lines below the symbols indicate extensive properties and have the unit of Joule. The phase transition contributes to a negative free energy change and is described in equation 3.2 to 3.4 as examples. The push work, also known as the penalty, gives a positive contribution to the free energy. As the hydrate core is growing, work is required to push the surrounding molecules away to give space for the new phase.

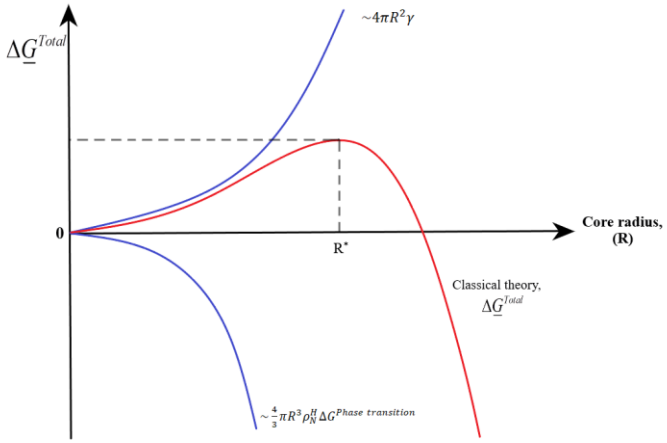

Figure 3.6: Schematic representation of the classical theory, where the total change in free energy is a function of the nucleus radius. The critical radius, R*, represents the radius at maximum ΔG. Crystal radius beyond this point is where the "benefit" is dominating, and stable growth is achieved. Adapted from *[24]*

Since the molar densities of hydrate and liquid water are relatively close, it should be a fair approximation to multiply $\Delta G^{\text{Phase Transition}}$ with the molar density of hydrate, ρ_N^H, times the volume of the hydrate core, as shown:

$$\Delta G^{Total} = \frac{4}{3}\pi R^3 \rho_N^H \Delta G^{Phase\ transition} + 4\pi R^2 \gamma \tag{3.7}$$

The γ is the interface free energy between the hydrate and the surrounding phase. Since the easiest shape of a hydrate crystal is a sphere, the volume and surface area with its radius R, are used in the calculation, as shown in equation 3.7. At a certain radius, the benefit of phase transition is dominating over the "penalty work", and this allows for stable nucleus growth. This point is the were the free energy is at its maximum peak, and the nucleus radius is called the critical radius, illustrated in Figure 3.6. By differentiation of equation 3.7 with respect to R, results in the equation 3.8, where the critical radius indicated by the superscript (*) on R. In temperature ranges between 274 - 278K and pressures above 150 bars, the typical critical hydrate core radius lies between 18 and 22 Angstroms.

$$R^* = -\frac{2\gamma}{\rho_N^H \Delta G^{Phase\ transition}} \tag{3.8}$$

3.1 Hydrate nucleation

The transition from an unstable growth over to a stable growth is called nucleation and is part of the hydrate formation. The nucleation process happens very fast, in just a few nanoseconds, and there are basically two different approaches for modelling the nucleation part [25]. The main difference of the hypotheses is about where the initial nucleation process takes place, at the liquid water interface or towards the hydrate former part of the interface. Christiansen and Sloan's [26] hypothesis from 1994, proposed that water molecules form clusters around dissolved guest molecules and then combines to form unit cells. When the size of agglomerated clusters reaches critical, growth begins. The other hypothesis was published by Kvamme [27] in 1996. He proposed that the initial nucleation takes part towards the gas/water interface where the water molecule first forms partial, and then complete cages around the adsorbed species. At the gas/vapour side of the surface, clusters get together and grow until the critical size are achieved for stable growth.

3.2 Hydrate Growth

The second step in hydrate formation is stable growth. This process also occurs fast, but is often limited by mass and heat transfer. Once the hydrate film at the interface between hydrate former and water grows thick enough, mass transport becomes limited and may control the growth rate. In the classical theory of hydrate formation, a variety of different routes is possible;

- Heterogeneous formation: where the different components enter the hydrate from different phases.
- Homogeneous formation: where all the components are extracted from the same phase.

Hydrate formation on the interface between the gas (or liquid) and water are heterogeneous and is the most common studies [21]. Homogeneous nucleation can occur in the bulk of water with dissolved hydrate formers and nucleate towards mineral surfaces in such as natural sediments or a pipeline. There are two primary models for hydrate growth, the work by Englezos et al. [28] in 1987 and the later modified version by Skovborg and Rasmussen [29] in 1994. The crystal growth rate change is frequently expressed in terms of:

$$\frac{dm}{dx} = KA(c - c^{eq}) \tag{3.9}$$

Where A represents the surface area of crystal, c and c^{eq} the supersaturated and equilibrium concentration. K represents an overall transfer coefficient expressed in terms of diffusion and reaction coefficients k_d and k_r as [15]:

$$\frac{1}{K} = \frac{1}{K_d} + \frac{1}{K_r} \tag{3.10}$$

By assuming ideal liquid solutions, conservation of mass and constant temperature and pressure, then the concentrations in equation (3.9) can be replaced by fugacity as in the Englezos model. Rasmussen and Skovborg simplified this approach by using a single rate constant related to the hydrate/liquid water interface area and differences in mole fraction of the hydrate former at the interface and bulk [25].

3.3 Induction times

Induction is the third stage of hydrate formation, and it is frequently misinterpreted as the nucleation time. It can be defined as the time needed to reach visible hydrate. This is the stage in which the growth rate for the hydrate becomes massive [19]. The massive growth is often delayed by several factors, most often mass transport limitations. An experiment was constructed by a research group to measure the induction time [30]. A cell made of a plastic cylinder cut in half, with a diameter of 4 cm and length of 10 cm. These two half-cylinders are then squeezed together against a 4 mm thick plastic spacer which then gives an empty space for fluids surrounded by a medium that will not be affected by magnetic radiation. This enables the Magnetic Resonance Imaging (MRI) to trace the dynamics of the hydrate phase transition. The experiment was conducted at $4\,^{\circ}C$ (277 K) and 83.75 bar(1200psig) with methane as hydrate former. Since the resolution of the MRI experiments was limited to the order of 300 microns, it was not able to detect the nucleation stage and the first stages of growth. The MRI-results in Figure 3.7, shows the induction time, the time for onset of massive hydrate growth, to be just about 100 hours. This is far beyond any reasonable value for nucleation times. Monitoring techniques or visual observation will often lead to incorrect interpretations of induction times as nucleation times [31]. Phase Field Theory (PFT) modelling, which can reproduce the experimental observation, supports this.

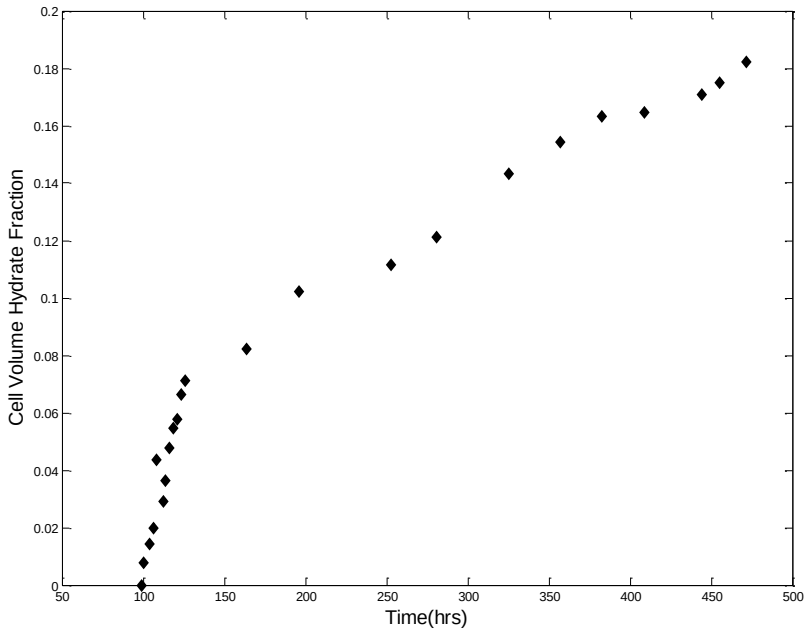

Figure 3.7: Experimental data for methane hydrate formation at 84 bars and 277 K [27].

3.4 Gibbs phase rule

A phase is a section of space, a thermodynamic system, in which all physical properties of a material are substantially equal. In other words, a phase is a region of material that is chemically identical, physically distinct, and (often) mechanically separable [32]. J. Willard Gibbs expressed his results in 1875, also known as Gibbs phase rule, and is built on the fundamental principles of thermodynamics and makes it possible to predict if a system of phases can reach equilibrium. It basically describes how many independent thermodynamic variables needed to be defined for the system to reach equilibrium [33].

$$F = C - P + 2 \tag{3.11}$$

The F in equation 3.11 is the number of independent variables (degree of freedom), C is the number of components, and P is the number of phases. In nature and industries, phase changes are controlled by pressure and temperature, hence the additional two in the equation. A simple system of liquid water and methane gas, where C=2 and P = 2(gas, liquid), results in F = 2 independent variables which are already given as pressure and temperature. This means the system can reach equilibrium. However, this is very unlikely in dynamic situations such as gas transport in pipelines due to the continuous flow.

If hydrate is introduced to the system, the number of independent variables reduces to F=1, due to the third phase P =3 (gas, liquid, hydrate). In this case, the system is overdetermined as the number of independent variables is lower than the number of variables already defined. Hydrates can therefore never reach equilibrium but will strive towards the lowest possible free energy. Nevertheless, in a non-equilibrium system, the chemical potential for a hydrate former in different phases are different because of the 1st and 2nd laws of thermodynamics which determine the distribution of masses over the various possible phases [21].

4 Thermodynamics

Thermodynamics is a compilation of beneficial mathematical relations between quantities, all of which is independently measurable. Even though thermodynamics tells us nothing of any kind of the microscopic description of macroscopic changes, it is useful because it can be used to quantify many unknowns. Thermodynamics is beneficial because specific quantities are easier to measure than others. The laws of thermodynamics offer a sophisticated mathematical expression of some empirically discovered truths of nature. The principle of energy conservation tolerates the energy requirements for processes to be calculated. The theory of increasing entropy (and the following Gibbs free energy minimisation) allows estimates to be produced of the degree to which those processes may proceed [34].

4.1 Free Energy

The term "free energy" is used to describe "available energy" that can be converted to "do work". Gibbs free energy can be obtained from the first law of thermodynamics, the conservation of energy, and the second law of thermodynamics, that states that an isolated system will always naturally strive towards maximum entropy. The changes for a phase "*i*" in an isolated system, can be expressed by the combination of 1st and 2nd law of thermodynamics as follows:

$$d\underline{U}^i \leq T^i d\underline{S}^i - pd\underline{V}^i + \sum_i^n \mu_j^i dN_j^i \qquad (4.1)$$

Where U is the internal energy [joule], μ is the chemical potential [joule/mole], T is the temperature [K], P is the pressure [Pa] and V is the volume [m^3]. S is the entropy [joule/K], N_j is the number of particles of a component, "*j*" is the component. The "*i*" is the phase represented, *i*=1,2,3…n (gas, liquid or solid). The last term in equation 4.1, $\sum_i^n \mu_j^i dN_j^i$, is the chemical work, the work necessary to put a molecule from one phase into the other phase. For all real and irreversible changes, we have less than (<) sign. Gibbs free energy is by definition:

$$\underline{G}^i = \underline{H}^i - T^i \underline{S}^i \qquad (4.2)$$

And since the expression for enthalpy is,

$$\underline{H}^i = \underline{U}^i + p^i \underline{V}^i \tag{4.3}$$

By combining eq.4.2 and 4.3, Gibbs free energy can be expressed as,

$$\underline{G}^i = \underline{U}^i + p^i \underline{V}^i - T^i \underline{S}^i \tag{4.4}$$

By using Legendre transforms and applying total derivative natural variables for equation 4.4;

$$d\underline{G}^i \leq \underline{V}^i dP - \underline{S}^i dT^i + \sum_i^n \mu_j^i dN_j^i \tag{4.5}$$

Equation 4.5 indicates that a system will always strive towards a minimum when exposed to changes in P, T or N. In this project, systems are considered both reversible and irreversible processes, the process continues until the total free energy achieves a minimum. This implies that we can use the change in Gibbs free energy to state which reaction or phase transition will be favoured and ensure spontaneously. If $\Delta G \leq 0$, then phase transition is thermodynamically favoured and will develop, if $\Delta G \geq 0$, then the phase transition is not favoured and phase transition will not occur [35].

4.2 Equilibrium thermodynamics

To accomplish thermodynamic equilibrium, the temperatures, pressures, and chemical potentials of all components must be the same in all coexisting phases, as given by the expressions below:

$$T^{(I)} = T^{(II)} = T^{(III)} = T \qquad \text{Thermal equilibrium (no net heat transport)} \tag{4.6}$$

$$P^{(I)} = P^{(II)} = P^{(III)} = P \qquad \text{Mechanical equilibrium, Newton's law} \tag{4.7}$$

$$\mu^{(I)} = \mu^{(II)} = \mu^{(III)} = \mu \qquad \text{Chemical equilibrium (no net chemical work)} \tag{4.8}$$

The superscripts, (I), (II) and (III) correspond to the phase index for all the co-existing phases in consideration. Although it is not possible to reach equilibrium, using a quasi-equilibrium method allows evaluating the thermodynamic advantages of various routes of either formation or dissociation of hydrates via equation 4.6 to 4.8. as asymptotic limits of inherent stability for each given phase transition [36].

4.3 Residual thermodynamics

Thermodynamic deviations from the ideal gas behaviour are represented as residual thermodynamics (fluid thermodynamics). Combining the 1st and the 2nd law of thermodynamics with the ideal gas law will yield for ideal gas [15]:

$$d\mu_i = RTd\ln x_i P \tag{4.9}$$

At constant temperature, where μ_i is the ideal gas chemical potential of component *i* with mole fraction x_i. To simplify, a new function *f* named the fugacity is presented to find a general representation for the chemical potential of component *i*.

$$d\mu_i = RTd\ln f_i \tag{4.10}$$

The fugacity can be interpreted as the corrected pressure. For a mixture of ideal gasses, the fugacity equals the partial pressure $x_i P$ of the component, where x_i is the mole fraction. For convenience, we also characterise the fugacity coefficient $\phi = f_i/(x_i P)$, which is the deviation factor from ideal gas partial pressure over to real fluid fugacity.

$$\ln\phi(T,P,\vec{x}) = \frac{\partial\left(\frac{NG^{\text{Residual}}}{RT}\right)_{T,P,N_{j\neq i}}}{\partial N_i} = \frac{\partial\left(\frac{NA^{\text{Residual}}}{RT}\right)_{T,V,N_{j\neq i}}}{\partial N_i} \tag{4.11}$$

The compressibility coefficient $Z = PV/RT$ and the corresponding equation for an ideal gas can now be inserted into Helmholtz (A) or Gibbs (G) free energy on the form of the equation of state. The final result is as shown;

$$\ln\phi(T,P,\vec{x}) = -\frac{1}{RT}\int_{\infty}^{\underline{V}}\left[\left(\frac{\partial P}{\partial N_i}\right)_{T,\underline{V},N_{j\neq i}} - \frac{RT}{\underline{V}}\right]d\underline{V} - \ln Z \tag{4.12}$$

The compressibility coefficient Z for the mixture is given by the specific equation of state used for the model calculations. For residual thermodynamics, Soave-Redlich-Kwong (SRK) equation of state [37] has been used for each hydrate forming components in all phases.

At a provided temperature and pressure for a specific mixture with constant composition,

$$\frac{G}{RT} = \sum_i x_i \frac{\mu_i^0(T,P)}{RT} + \sum_i x_i \ln x_i \phi_i(T,P,\vec{x}) \tag{4.13}$$

The chemical potential for an ideal gas, μ_i^0, is used as the reference state. This can be determined from Helmholtz free energy by using the real molar volume, which relates to the specific condition of temperature and pressure. For this reason, methane is considered as an approximately spherical atom, and the carbon dioxide molecule is treated as a line with a specific angular momentum provided by the bond lengths and masses. The molar volume and partial molar volumes of each component are calculated from the solution of the equation of state for every temperature, pressure and composition [15].

4.4 Excess thermodynamics

An ideal gas is not a suitable reference state for a condensed phase, but as an alternative, we choose an ideal solution. In a liquid solution, the molecules apply forces upon each other, in contrast to an ideal gas. All the intermolecular forces, independent of species, are equal.

Equation of state (EOS) is readily available for gas mixtures, and many of these are based on the van der Waals equation:

$$P = \frac{RT}{v_m - b} - \frac{a}{v_m^2} \tag{4.14}$$

Where the $RT/(v_m - b)$ is the correction to take account for the volume that a real gas molecule takes up, and a/v_m is to take to accounts for the fact that gas molecules attract each other and that real gases are consequently more compressible than ideal gases [38]. This was proposed in 1873 by van der Waals and was the first equation of state to perform better than the ideal gas law for liquid/vapour equilibrium. He believed that fluid was homogeneous and that the molecules were solid spheres with pair wise attraction [39]. The most common equation of state in the oil and gas industry is the Soave-Redlich-Kwong (SRK) and Peng-Robinson (PR). They use a more precise suited constant for the attractive forces among non-polar molecules in a fluid and is basically simple extensions of the van der Waals equation. Therefore excess thermodynamics is an alternative formulation to the residual thermodynamics for liquid mixture, and there are two different types; Symmetric and

asymmetric, dependent of what is chosen as the reference state of liquid [39]. The chemical potential for an ideal solution can be expressed as

$$\mu_i = \mu_i^0 + RT \ln x_i \tag{4.15}$$

Where the chemical potential of the pure liquid is shown as μ_i^0, and x_i is the mole fraction. Activity "*a*" which is defined as the ratio f / f^0 and the activity coefficient, which can be expressed in terms of the activity and the mole fraction as $\gamma_i = a_i / x_i$. This will result in an expression for fugacity as $f_i = \gamma_i x_i f_i^0$ where the ideal solution at a reference state is the f_i^0. Due to various cross-contact among different molecules and additional non-ideal mixtures, properties of mixtures changes are incorporated in the excess stage expressed as [15],

$$\mu_i^{excess} = RT \ln\left(\frac{x_i f_i^0 \gamma_i}{x_i f_i^0}\right) = RT \ln \gamma_i \tag{4.16}$$

Equation 4.16 shows the excess expression for the chemical potential of a real liquid. The pure liquid reference is termed symmetric convention. Symmetric excess thermodynamic uses pure liquid components as a reference state with the ideal mixing term derived from the statistical mechanic, where the activity coefficient approaches unity $\gamma_i \to 1$ as the mole fraction of the solute approaches unity $x_i \to 1$. However, for low solubility components in solvents, electrolyte solutions and super-critical components, we use another reference state. When a mixture is made infinitely dilute in a component, $x_i \to 0$, the activity coefficient will asymptotically approach a value,

$$\lim_{x_i \to 0} \gamma_i^{\infty} \equiv 1 \tag{4.17}$$

The superscript "∞" is used for quantities at infinite dilution and defines the asymmetrical convention. The activity coefficient can be relapsed by using the model for equilibrium to fit experimental data at high pressures and mole fractions. The advantage is that chemical potential at infinite dilution can be estimated by Molecular Dynamics (MD) simulations [39].

$$\mu_i = \mu_i^{\infty} + RT \ln(x_i \gamma_i^{\infty}) \tag{4.18}$$

The equation 4.18 express the chemical potential at infinite dilution.

4.5 Hydrate thermodynamics

For evaluating the chemical potential of water in hydrates, a statistical mechanical model such as a Langmuir type of adsorption model is conventionally used. However, this work is based on the extended theory by Kvamme and Tanaka [40] from 1995. Their method does not rely on empirical fitting to find the Langmuir constant [39] and allows to account for lattice movements and related impacts of different guest molecules:

$$\mu_{H_2O}^{H} = \mu_{H_2O}^{0,H} - \sum_{k=1,2} RTv_k \ln(1+\sum_i h_{ik}) \tag{4.19}$$

The expression above expresses the chemical potential of water in the hydrate $\mu_{H_2O}^{H}$. The $\mu_{H_2O}^{0,H}$ is the chemical potential of water in an empty hydrate structure, v_k is the fraction of cavity-type *k* per water molecule, and h_{ik} is the canonical cavity partition function of component *i* in cavity type *k*. To illustrate this in an example; structure I hydrate consists of 3 large cavities and one small cavity per 23 water molecules, so $v_{Large} = 3/23$ and $v_{Small} = 1/23$. If carbon dioxide were the only guest, *i* would be 1 in the sum over the canonical partial functions that are expressed as [36];

$$h_{ik} = e^{\beta\left(\mu_i^H - \Delta g_{ik}^{inclusion}\right)} \tag{4.20}$$

Where the inverse of the gas constant times the temperature($1/RT$) is represented by β and $\Delta g_{ik}^{inclusion}$ is the impact on hydrate water from the presence of the guest molecules *i* in cavity *k*. The chemical potential for a guest in the hydrate can be written as:

$$\mu_i^H = \Delta g_{ik}^{inc} + RT \ln h_{ik} \tag{4.21}$$

The corresponding filling fractions and mole-fraction and cavity of guest in the hydrate are expressed as:

$$\theta_{ik} = \frac{x_{ik}^H}{v_k(1-x_{Total})} = \frac{h_{ik}}{1+\sum_i h_{ik}} \tag{4.22}$$

θ_{ik} stand for the filling fraction of component *i* in cavity *k* where $\theta_{ik} < 1$, x_{ik}^{H} is the mole fraction of component *i* in cavity *k*. x_{Total} is the total mole fraction of all the guests in the hydrate.

$$x_i^H = \frac{\theta_{Large,i} v_{Large} + \theta_{Small,i} v_{Small}}{1 + \theta_{Large,i} v_{Large} + \theta_{Small,i} v_{Small}} \tag{4.23}$$

The corresponding mole fraction of water in the hydrate is then expressed as:

$$x_{H_2O}^H = 1 - \sum_i x_i^H \tag{4.24}$$

And the combined Gibbs free energy is then,

$$G^H = x_{H_2O}^H \mu_{H_2O}^H + \sum_i x_i^H \mu_i^H \tag{4.25}$$

The expression above is used in equation 3.2 - 3.4 to find the change in Gibbs free energy for different hydrates routes. The chemical potential for water in hydrate, the chemical potential for CH_4 in hydrate and the molar Gibbs free energy along the equilibrium curve is plotted as an example in Figure 3.2.

4.6 Enthalpy: The heat of formation and dissociation of hydrates

The next chapter involves the different approaches to determining the enthalpy of hydrate formation and dissociation. This is a short introduction of what the definition and uses of enthalpy are.

Enthalpy is a thermodynamic property of a substance and is defined as the sum of its internal energy and the product of its pressure and volume [41]. The expression of enthalpy previous shown in equation 4.3 is an extensive property [J], the expression for specific enthalpy, [J/mol] is given as:

$$H = U + pV \tag{4.26}$$

Introducing the 1st law of thermodynamics:

$$\Delta U = Q - W \tag{4.27}$$

Where the change in internal energy of a closed system is ΔU. Q is the amount of heat supplied to the system, and the W is the work done by the system on its surroundings.

For a body at a constant pressure process,

$$W = \int_1^2 pdV = p(V_2 - V_1) \tag{4.28}$$

Apply this to the 1st law, equation 4.27, and it gives

$$\Delta U = U_2 - U_1 = Q - p(V_2 - V_1) \tag{4.29}$$

By rearranging the equation;

$$\begin{aligned} &Q = U_2 - U_1 + p(V_2 - V_1) \rightarrow (U_2 + pV_2) - (U_1 + pV_1) \rightarrow H_2 - H_1 \\ &Q = \Delta H \end{aligned} \tag{4.30}$$

Therefore for a constant pressure process, the amount of heat given to a body equals the change in its enthalpy [41].

The heat of dissociation is described as the enthalpy change to dissociate the hydrate phase to vapour and aqueous liquid, with values given at temperatures just directly above the ice point [19]. In the case of hydrate formation, it is just the opposite. In the formation of hydrates, heat is released to the surroundings and results in a negative enthalpy value, so the different terms in comparing enthalpy values of either formation or dissociation are not crucial if the values from the different literature (positive or negative) are the same.

Hydration number, also known as occupation number, shown as “n”, is the ratio between the number of water molecules and the number of cavities occupied by guests at a given condition. Higher “n” means more empty cavities. In theory, if all the cavities in a structure (I) hydrate was occupied, the hydration number could get as low as n =5.75 (46 water molecules/ 8 filled cavities), but this is very unlikely.

4.7 Methods for determining the enthalpy of hydrate formation and dissociation

Most of the next chapters are based on previous work published by our research group, Kvamme et al. [42] and is based on the different approaches available for determining the heat of formation/dissociation of hydrates. There are two main categories; directly and indirectly, methods, which depends on the approaches used. The most straightforward and most popular indirect methods out there include the use of the Clausius-Clapeyron equation along with measured or calculated (T and P) data for hydrate formation but are limited to higher pressures, due to simplifications. However, using the original Clapeyron equation with various models for the volume changes has been proven more accurate than the Clausius-Clapeyron equation. This is according to Gupta et al. [43], who compared experimental data with Clapeyron data calculated by Anderson [44].

If the reader is further interested, the calculation of enthalpy and hydration number by Anderson [44] is explained and simplified in our recently published work [42]. Still, the next subsection contains a short explanation of how the Clapeyron equation is defined and used, additionally to the Clausius-Clapeyron equation. There is plenty of publications involving experimental measurements of enthalpy for methane hydrate formation, yet the lack of useful information in most of them is vast.

Experimental data is the preferred method compared to the Clapeyron or Clausius-Clapeyron because it's a directly measured, but again, this is determined by their approach. For instance, Handa [45] used an indirect approach for calculating the heat of dissociation, even though it involved experimental work.

Consequently, for comparing enthalpy values in this work, leaving only a few publications using calorimetry that is regarded as good enough and are reviewed in its own subsection. The method used for calculating the enthalpy of hydrate formation/dissociation in this work, residual thermodynamics, is a direct approach because Gibbs free energy is directly linked to the enthalpy. Values such as hydration numbers, densities and volume can be calculated and not estimated.

4.7.1 The Clapeyron equation

In determining thermodynamic properties such as enthalpy or entropy in positions of other properties that can be measured, the calculations fall into two distinct categories: changes in properties among two different phases and changes contained by a single homogeneous phase [46].

In section 3.4, the Gibbs phase rule stated that for a pure component that occurs in two phases at equilibrium, pressure and temperature could not be independent. Nevertheless, there is a way to find an expression involving the pressure at which two phases be able to coexist to the temperature of the system. As an example, this allows calculating how the saturation pressure shifts with temperature. Saturation pressure is defined as the distinctive pressure at which pure components boil at a given temperature [47]. The principle for equilibrium between two phases is:

$$G_i^{\alpha} = G_i^{\psi} \tag{4.31}$$

Where the superscript α and ψ in Gibbs free energy represents phases (vapour, liquid or solid) for the component i. Since two intensive variables entirely specify the state of the system, the value of G for each phase is limited at a given temperature and pressure. Therefore, by plotting the surfaces of Gibbs free energy for both phases, then the intersection of the two surfaces creates the so-called coexisting line. This characterises the conditions where equation 4.31 is pleased, and the two phases are in equilibrium.

Since equation 4.31 must be valid alongside both points on the coexisting line, the change in pressure, dP, can be calculated for every change in temperature, dT, at equilibrium. Therefore both $G_i^{\alpha} + \Delta G_i^{\alpha} = G_i^{\psi} + \Delta G_i^{\psi}$ and $G_i^{\alpha} = G_i^{\psi}$, Subtraction gives:

$$\Delta G_i^{\alpha} = \Delta G_i^{\psi} \tag{4.32}$$

Equation 3.1 can be changed to:

$$\Delta G = \Delta H - \Delta TS = V\Delta P - S\Delta T \tag{4.33}$$

That is the fundamental property relation for Gibbs energy, and by applying this to equation 4.32 for each phase, gives:

$$V_i^{\alpha}\Delta P - S_i^{\alpha}\Delta T = V_i^{\psi}\Delta P - S_i^{\Psi}\Delta T \tag{4.34}$$

$$\frac{dP}{dT} = \frac{S_i^{\alpha} - S_i^{\Psi}}{V_i^{\alpha} - V_i^{\psi}} \tag{4.35}$$

By introducing equation 4.31 and using the definition of Gibbs energy, gives

$$H_i^{\alpha} - TS_i^{\alpha} = H_i^{\Psi} - TS_i^{\Psi} \tag{4.36}$$

And by solving for the difference in entropy,

$$S_i^{\alpha} - S_i^{\Psi} = \frac{H_i^{\alpha} - H_i^{\Psi}}{T} \tag{4.37}$$

By swapping the entropy difference in equation 4.35 with the expression in equation 4.37, yields the Clapeyron equation:

$$\frac{dP}{dT} = \frac{H_i^{\alpha} - H_i^{\Psi}}{T(V_i^{\alpha} - V_i^{\psi})} \rightarrow \frac{\Delta H}{T\Delta V} \tag{4.38}$$

This is a very simple relation and yet a mighty one. It connects the slope of the coexistence curve to the enthalpy and volume variations of phase transition, both experimentally accessible properties [47]. Let us assume that the two phases are liquid and vapour. The left-hand side of the equation gives the slope of the vapour pressure as a function of temperature. It is also possible to determine the specific volumes of saturated vapour and liquid at the provided temperature. This implies that the enthalpy change and entropy change of vaporisation can both be calculated.

The same steps apply for changes in other phases, such as solid to liquid or solid to vapour. In each scenario, the outcome is the Clapeyron equation, and in every one of them involves the saturation pressure, specific volumes, entropy change and enthalpy change [46].

For hydrate equilibrium, it may seem somewhat bizarre to apply it to binary systems (water + one guest) of three-phase (Liquid $_{water}$ - Hydrate – Vapor) equilibrium to achieve the heats of dissociation. In the argument of simple hydrates, as long as the system is univariant(one degree of freedom), according to van der Waals and Platteeuw [48], the use of the Clapeyron equation is thermodynamically correct [19].

Unlike other publication that uses Clapeyron equation to determine the enthalpy, Anderson [44] [49] included volumes of the condensed phases for both carbon dioxide and methane hydrates and also calculated the hydration number.

4.7.2 The Clausius-Clapeyron equation

For hydrate formation reaction (L_w + V ↔ H), if we assume that the volume of the hydrate is approximate the same as for liquid water (or ice), then $\Delta V \approx V_g = RT/Pz$, where the z is the compressibility factor. Inserting this expression for ΔV into the Clapeyron equation (equation 4.38), converts it into a more practical form, the Clausius-Clapeyron equation [19]:

$$\frac{d \ln P}{d\left(1/T\right)} = -\frac{\Delta H}{zR} \tag{4.39}$$

For hydrate formation, semi-logarithmic plots of pressure versus reciprocal temperature generate straight lines, over restricted spans of temperature, from either liquid water or ice. Such linear plots in equation 4.39 either imply (1) reasonably constant values of the 3 factors:

(a) Enthalpy, (b) compressibility factor, (c) stoichiometry or (2) abandoning of curvilinear behaviour in these three factors.

4.7.3 Available experimental enthalpy values for CH_4 and CO_2 hydrates

Only experimental values can confirm whether a theory is correct or is in the proximity since the data represent the physical reality, and they have been carefully obtained. To assemble an experiment and its apparatus can typically take numerous months or even years. It is not unusual to achieve only one pressure/temperature data point per 1 or 2 days of experimental work due to long metastable periods [19].

There are numerous methods used for direct measurement; calorimetry, pressure drop, Raman, NMR, X-ray diffraction or DSC. However, calorimetry appears to be favoured by the experimentalists. It is not possible to measure the heat of dissociation directly with an apparatus at precisely equilibrium conditions as it would take infinite time. Experiments have consequently been done outside the equilibrium conditions, typically with various degrees of superheating. Experiments from Handa [45], Nakagawa et al. [50], Lievois et al. [23] and Gupta et al. [43] are some of those who used calorimetry for clarification of the enthalpy of dissociation of methane hydrate.

These four are examples of the typical incompleteness of experimental data using calorimetry. Some reported data sets missing complete thermodynamic conditions that can tell how much the sample is heated above equilibrium temperature and pressure, and likewise how much of the quantified heat consumption is truly dissociation heat. The lack of information on hydrate composition is an additional limitation in the stability in the understanding of how much water and hydrate former the number really relates to. For simplification, the occupation number, also known as the hydration number, is often reported as an average value and often not including details on the precision of the number. Sometimes it is even just described as an assumed number.

Handa [45] used a Tian-Calvet heat-flow calorimeter in the 1980s to quantify the enthalpy of dissociation and heat capacities of hydrates under low temperatures and pressure. The experiment was evaluated in the temperature range 85K to 270K for methane (CH_4) and 85K to 260K for ethane (C_2H_6). To make sure that no gas was condensed inside the apparatus cell, a surplus of gas was inserted to generate a higher pressure than the dissociation pressure over the entire temperature scale of interest. Still, the standard enthalpy of dissociation from

hydrate to gas and water were found by a summation of the enthalpy of ice and the dissociation heat from hydrate to ice and gas, in another expression, an indirect method for interpretation the of heats of dissociation. Nakagawa et al. [50] performed a related experiment but obtained the specific heat of hydrates in the temperature spans of 264-276 K for methane and 264-282K for ethane. The dissociation heat was calculated by a temperature range of 279 K to 282 K. They portrayed a dissociation enthalpy of 55.3 kJ/mol gas for methane and a value of 71.1 kJ/mol gas for ethane, without any informed values of hydration number.

Lievois et al. [23] prepared an experiment with a heat flux calorimeter at a higher pressure for methane. The result was an enthalpy of 57.65 kJ/mol gas at 278K and 4.2 MPa, and 53.24 kJ/mol gas at 283.15K at 7.1 MPa. These values were calculated using an average occupation number. Only a few have done experiments for methane hydrate at pressures and temperatures which can simulate hydrate reservoir conditions. Gupta et al. [43] applied a high-pressure differential scanning calorimeter (DSC) to quantify the heat of dissociation up to 20 MPa and 292K for methane hydrate. The enthalpy value was reported to be constant for pressures up to 20 MPa and with no temperature dependence up to 292K.

Their results demonstrated that calculations from the Clausius-Clapeyron equation do not agree with measurements at high pressures. Yet, a constant hydration number (n) equal to 6.0 were used in their interpretation of the measured data. Even though there are several reported values of enthalpy published over the years, no one has ever given all the information necessary to compare values correctly. The experiments that were reviewed in this section is also shown in Table 4.1 but is also used in the “results and discussion” chapter for comparison.

Evaluating the amount of available calorimetry data for CH_4 hydrates to the amount for CO_2 hydrates, there isn’t much to look for. Still, there are some published data that can be used for this evaluation. Although the lack of some valuable information and conditions way out of equilibrium, it is the best ones out there. Kang et al. [51] did manage to define the enthalpy of dissociation and also the occupation number for a simple CO2 hydrate. They used an isothermal microcalorimeter, but this was at low pressure.

As mention beforehand, there are other methods besides calorimetry to determine the enthalpy. DTA, differential thermal analysis was used by Delahaye et al. [52], but they did not specify the occupation numbers (n). Table 4.2 shows the experimental enthalpy value of dissociation for CO_2 hydrate and its conditions but also used for comparing results.

Table 4.1: Capabilities and limitations of the different experimental data for CH_4 hydrate enthalpy by different literature [43] [23] [50] [51] [45].

Author	Conditions and available data on thermodynamic variables	Limitation	Pressure (MPa)	Temperature (K)
Gupta et al.	High pressures	Constant occupation number	< 20	< 292
Lievois et al.	High (P and T)	Average occupation number	4.2-7.1	278-283
Nakagawa et al.	Temperature	Occupation number not specified	5.0	264-276
Kang et al.	Temperature and hydration number	Low pressure	n/a	274.15
Handa	Heat capacities	Low temperature and pressure. An indirect method to determine enthalpy.	n/a	85-270

Table 4.2: Enthalpy of dissociation and the occupation number of simple CO2 hydrates by Kang et al. [51]

Arthur	Temperature (K)	Pressure (MPa)	Occupation number (n)	ΔH (kJ/mol)	Method
Kang et al.	273.65	0.1	7.23	65.22	Calorimetry

4.7.4 Enthalpy of hydrate formation via residual thermodynamics

Since the residual energy approach is going directly to the real thermodynamics, the actual limited effect of pressure on enthalpy for hydrate formation is more accurate and smaller than what the Clapeyron equation would predict. The free energy change of hydrate formation from water and separate hydrate former phase is shown in equation 3.2 (H_1). The chemical potential for liquid water is evaluated using symmetric excess conventions, as explained in chapter 4.4, the $\lim_{x_{H_2O}\to 1}\gamma_{H_2O}=1$ when x_{H_2O} approaches unity

$$\begin{aligned}\mu_{H_2O}^{water}(T,P,\vec{x}) &= \mu_{H_2O}^{pure,H_2O}(T,P)+RT\,ln\left[x_{H_2O}\gamma_{H_2O}(T,P,\vec{x})\right]\\ \mu_{H_2O}^{water}(T,P,\vec{x}) &\approx \mu_{H_2O}^{pure,H_2O}(T,P)+RT\,ln\left[x_{H_2O}\right]\end{aligned} \tag{4.40}$$

Since the aim is to explain the complexity of numerous hydrate formation in systems of water and hydrate former such as CO_2, a simpler kinetic model such as classical nucleation theory is used. This is more observable in terms of the different contributions to the hydrate phase transition dynamics, so the approximation in equation 4.40 is strictly needless, as it is accurate enough for this purpose.

The solubility of methane in water is exceptionally poor, so the right-hand side of equation 4.40 will be very close to the chemical potential of pure water. The chemical potential of water in a hydrate is expressed in equation 4.19 and are accessible from model water simulations(TIP4P) made by Kuznetsova and Kvamme [53].

The chemical potential for a guest molecule, "*i*", in this work what would be either CH_4 or CO_2, which enters equations 3.2 and 4.20 at equilibrium, is according to residual thermodynamics:

$$\mu_i(T,P,\vec{y}) = \mu_i^{pure,ideal\ gas}(T,P,\vec{y})+RT\,ln\left[y_i\phi_i(T,P,\vec{y})\right] \tag{4.41}$$

The mole fraction of component i in the gas mixture is referred to as y_i, and the fugacity coefficient for component i as ϕ_i. By using statistical mechanics from mass and intramolecular structures (bond angles and lengths), the chemical potential for a pure ideal gas can be calculated for every model molecule. The ideal gas chemical potential, together with density and temperature, is accessible from the momentum space canonical partial function.

Calculation of the ideal gas free energy requires density and fugacity coefficient, which is evaluated by the use of the SRK [37] equation of state.

The change in enthalpy is associated with the equivalent free energy change by the following thermodynamic relationship.

$$\frac{\partial\left[\frac{\Delta G^{Total}}{RT}\right]_{P,\vec{N}}}{\partial T} = -\left[\frac{\Delta H^{Total}}{RT^2}\right] \tag{4.42}$$

The superscript Total is introduced to include the penalty of pushing away the old phases, which is explained in chapter 3 and expressed in equation 3.6. The fact that critical nuclei sizes are tiny [54] [7], the whole grain can be regarded as coated with water due to capillary forces.

$$\frac{\partial\left[\frac{\mu^{H}_{H_2O}}{RT}\right]_{P,\vec{N}}}{\partial T} = \frac{\partial\left[\frac{\mu^{0,H}_{H_2O}}{RT}\right]_{P,\vec{N}}}{\partial T} - \left[\frac{\partial}{\partial T}\right]_{P,\vec{N}}\left[\sum_{k=1,2} v_k \, ln\left(1+\sum_i h_{ki}\right)\right] \tag{4.43}$$

From the expression in equation 4.19 with the chemical potential of an empty hydrate on the right-hand side of equation 4.43, which are obtained from Kvamme & Tanaka [40], the second term on the right-hand side can be reorganized as:

$$\left[\frac{\partial}{\partial T}\right]_{P,\vec{N}}\left[\sum_{k=1,2} v_k \, ln\left(1+\sum_i h_{ki}\right)\right] = \left[\sum_{k=1,2} v_k \frac{\sum_i\left[\frac{\partial h_{ki}}{\partial T}\right]_{P\vec{N}}}{\left(1+\sum_i h_{ki}\right)}\right] \tag{4.44}$$

The derivatives of the cavity partition function, shown in equation 4.20, can be stated as:

$$\left[\frac{\partial h_{ki}}{\partial T}\right]_{P\vec{N}} = h_{ki}\left[-\frac{1}{RT^2}(\mu_{ki}-\Delta g_{ki})+\frac{1}{RT}\left(\frac{\partial \mu_{ki}}{\partial T}-\frac{\partial \Delta g_{ki}}{\partial T}\right)\right] \tag{4.45}$$

By introducing equation 4.45 into equation 4.44 gives:

$$\frac{\partial\left[\frac{\mu^{H}_{H_2O}}{RT}\right]_{P,\vec{N}}}{\partial T}=\frac{\partial\left[\frac{\mu^{0,H}_{H_2O}}{RT}\right]_{P,\vec{N}}}{\partial T}+\left[\sum_{k=1,2}\nu_k\frac{\sum_i h_{ki}\left[\frac{1}{RT^2}(\mu_{ki}-\Delta g_{ki})-\frac{1}{RT}(\frac{\partial\mu_{ki}}{\partial T}-\frac{\partial\Delta g_{ki}}{\partial T})\right]}{\left(1+\sum_i h_{ki}\right)}\right] \tag{4.46}$$

The partial derivation in the last term on the right-hand side is differentiated numerically using the polynomial fits [40]:

$$H^{H}_{H_2O}=-RT^2\frac{\partial\left[\frac{\mu^{0,H}_{H_2O}}{RT}\right]_{P,\vec{N}}}{\partial T}+\left[\sum_{k=1,2}\nu_k\frac{\sum_i h_{ki}\left[(\mu_{ki}-\Delta g_{ki})-T(\frac{\partial\mu_{ki}}{\partial T}-\frac{\partial\Delta g_{ki}}{\partial T})\right]}{\left(1+\sum_i h_{ki}\right)}\right] \tag{4.47}$$

In an equilibrium condition, the chemical potential of the identical hydrate former in the two cavity-types must be the same, and these must also be identical to the chemical potential of the same guest molecule in the phase that it comes from.

In the case of heterogeneous formation, that implies the chemical potential of the molecule in gas(or liquid) hydrate former phase. However, outside the equilibrium, gradients in chemical potentials as a function of temperature, pressure and mole fraction must reflect how the guest molecule behaves inside the cavity.

Monte Carlo simulations can calculate enthalpy values for various guest molecules in the two types of cavities by sampling guest/water interaction energies and efficient volumes from movements [9] [55] that is expressed as:

$$H^{Residual}_{ik}=U^{Residual}_{ik}+(z_{ik}-1)RT \tag{4.48}$$

U stands for the residual contribution of energy for the guest in molecule *i* inside the cavity *k*. z_{ik} is the compressibility factor for the guest molecule *i* inside the cavity *k*. Ideal gas values for the identical interaction models that were applied in the calculation of the residual values is trivial.

$$z_{ki} = \frac{PV_{ki}}{k_B T} \tag{4.49}$$

K_B is the Boltzmann's constant and V_{ik} are the excluded volume of a molecule *i* in cavity *k*. This volume can be calculated from the sampled volume of the centre of mass movements plus excluded volume because of water/guest occupation. Somewhat more complex sampling and calculation for molecules which are not monoatomic (or approximated as monoatomic such as CH_4) but still standard and explicit discussion on this are not required here.

For a relevant range of temperature (273-290K), the differences in enthalpies as evaluated from equation 4.48 using sampled data from Monte Carlo, do not significantly differ and could even be approximated as a constant for the purpose of this work. This is because the H_2O lattice of the hydrate is reasonably rigid, and the average movements are nearly the same for the restricted temperature range.

Sampled cavity partition functions will differ remarkably over the same range of temperature because of the direct exponential (Boltzmann factor) reliance. The interaction models for CH_4 and CO_2 used are the same used by Kvamme & Tanaka [40]. Even though there is an average attraction for CO_2, the sampled Langmuir constant is very tiny and not significant.

This is confirmed by molecular dynamics(MD) studies [40], where the movements of CO_2 in the small cavity interfere with various H_2O liberation frequencies. The resulting free energy of enclosure is not favourable for CO_2 in the small cavity. However, small cavity occupation of CO_2 has been discovered at extreme circumstances in the ice-range of temperatures in some studies [56], it remains uncertain if there would be any considerable small cavity filling at all for temperatures above 0 degree Celsius (Table 4.3).

Table 4.3: The sample energies and cavity occupation volumes for methane and carbon dioxide. The superscript R stands for residual interaction [42].

	CH_4		CO_2	
Property	Large cavity	Small cavity	Large cavity	Small cavity
$U_{ik}^{R}(kJ/mole)$	-16.53	-17.73	-27.65	-10.58
$V_{ik}(\AA^3)$	164.2	89.2	135.6	76.9

The energy for CO_2 in the small cavity was sampled once a structure I hydrate, including just CO_2 in large cavities was stabilised. When this was archived, small cavities were slowly filled, and simulations were operated up to the average fluctuations in sampled interaction energies were symmetrical and on average < 0.5 % of the average energy for the hydrate crystal. This energy does not have any effect on the enthalpy, is given that the canonical partition function for CO_2 is almost zero in the small cavities.

At pressures below 95 bars alongside the equilibrium line, it is zero to the 10^{-3} digit in mole fraction, while the highest filling fraction in the small cavity provides 0.006 to the mole fraction at (290.0 K and 403.0 bars). In compare, the approximated mole fraction of CH_4 in structure (I) fluctuated between 0.134 at (276.16 K and 25.2 bars) to 0.138 at (290.0K and 164.7 bars) along the equilibrium line.

The derivative of the chemical potential of the component i in cavity-type k with respect to temperature can be expressed as the negative of partial molar entropy for the same guest;

$$\left[\frac{\partial \mu_{ki}}{\partial T}\right]_{P\vec{N}} = -\left[\frac{\partial S_{ki}}{\partial N_i}\right]_{T,P,N_{j\neq i}} = \frac{\mu_{ki} - H_{ki}}{T} \tag{4.50}$$

By introducing equation 4.50 into equation 4.47 gives:

$$H^H_{H_2O} = -RT^2 \frac{\partial\left[\frac{\mu^{0,H}_{H_2O}}{RT}\right]_{P,\vec{N}}}{\partial T} + \left[\sum_{k=1,2} v_k \frac{\sum_i h_{ki}\left[(H_{ki} - \Delta g_{ki} + T\frac{\partial \Delta g_{ki}}{\partial T})\right]}{\left(1 + \sum_i h_{ki}\right)}\right] \tag{4.51}$$

Residual enthalpies for hydrate former in a distinct hydrate former phase are trivially given by:

$$H^R_i = -RT^2 \sum_i y_i \left[\frac{\partial \ln \phi^{gas}_i}{\partial T}\right]_{P,y_{j\neq i}} \tag{4.52}$$

In which the identical equation of state is used as the one used for evaluating the fugacity coefficient for the chemical potentials.

The free energy change of the homogeneous hydrate formation from water and dissolved hydrate former in liquid water, ΔG^{H_2}, is shown in equation 3.3. The solubility of hydrocarbons in water is very low, especially for methane, so the chemical potential for water as a solvent for methane would not be affected significantly. For carbon dioxide dissolved in water, the approximation in equation 4.40 is considered good enough.

The asymmetric excess convention can be used where the activity coefficient for methane in liquid water approaches unity when the mole fraction of methane in water approaches zero, $\lim_{x_{CH_4} \to 0} \gamma^{\infty}_{CH_4} = 1$.

The chemical potential for the dissolved methane in the liquid water can then be formulated as:

$$\mu^{\text{aqueous}}_{\text{CH}_4}(\text{T},\text{P},\vec{\text{x}}) = \mu^{\infty,\text{Residual}}_{\text{CH}_4}(\text{T},\text{P},\vec{\text{x}}) + \mu^{\text{ideal gas}}_{\text{CH}_4}(\text{T},\text{P},\vec{\text{x}}) + \text{RT}\ln\left[\text{x}_{\text{CH}_4}\gamma^{\infty}_{\text{CH}_4}(\text{T},\text{P},\vec{\text{x}})\right] \quad (4.53)$$

T_R in equation 4.54 – 4.56, is the temperature divided by the critical temperature for methane (190.6 K). The maximum temperature that is used in this fitting is 325 K [57].

$$\mu^{\infty,\text{Residual}}_{CH_4} = 3.665 + \frac{40.667}{T_R} - \frac{48.860}{T_R^2} \quad (4.54)$$

And,

$$\mu^{ideal\ gas}_{CH_4} = -73.901 + \frac{129.925}{T_R} - \frac{70.024}{T_R^2} \quad (4.55)$$

The activity coefficient for methane in liquid water has been fitted to the following expression:

$$\ln \gamma^{\infty}_{CH_4}(T,P,\vec{x}) = \sum_{i=1,2}^{39}\left[a_0(i) + \frac{a_1(i+1)}{T_R}\right](x_{CH_4})^{\left[0.05+\frac{i-1}{40}\right]} \quad (4.56)$$

The lower summation $i = 1, 2$ indicates beginning from 1 and counting in steps of two up to 39. The parameters a_0 and a_1 are given by Kvamme et al. [57] and adapted into Table 4.5.

For carbon dioxide, a vaguely different approach is utilized. The density of carbon dioxide in liquid water will correspond to the partial molar volume of CO_2 at infinite dilution. The chemical potential of the ideal gas at infinite dilution is not sensitive to pressures, so the following approximation to only temperature dependency is considered as acceptable:

$$\mu_{CO_2}^{\infty,ideal\ gas} = -130.006 + \frac{163.818}{T_{0,R}} - \frac{64.898}{T_{0,R}^2} \tag{4.57}$$

Where $T_{0,R}$ is $273.15\,K$ divided by the actual temperature. Equation 4.57 does not apply to temperatures above 303 Kelvin or below 273.16 Kelvin due to the limited range of temperatures for which infinite partial molar volumes are used. The fugacity coefficient for carbon dioxide in water is expressed as:

$$\ln \phi_{CO_2}^{water}(T,P,\vec{x}) = \sum_{i=1,2}^{39}\left[a_0(i) + \frac{a_1(i+1)}{T_R} \right](x_{CO_2})^{\left[0.05+\frac{i-1}{40}\right]} \tag{4.59}$$

Where T_R is the actual temperature divided by the critical temperature for carbon dioxide (304.35 K). The parameters a_0 and a_1 are given in Table 4.5. The chemical potential for carbon dioxide in liquid water is given as:

$$\mu_{CO_2}^{aqueous}(T,P,\vec{y}) = \mu_{CO_2}^{\infty,ideal\,gas}(T,P,\vec{y}) + RT\ln\left[x_{CO_2}\phi_{CO_2}(T,P,\vec{x}) \right] \tag{4.58}$$

In this case, the only change to equation 4.51 is in the cavity partition function, so that equation 4.20 is now with more specific notations:

$$h_{ki} = e^{\beta\left[\mu_i^{aqueous}(T,P,\vec{x}) - \Delta g_{ik}^{inclusion}(T) \right]} \tag{4.60}$$

$$\Delta g^{inclusion} = \sum_{i=0}^{5} k_i \left(\frac{T_c}{T} \right)^i \tag{4.61}$$

The computed free energies of guest inclusion can be calculated by the equation above by using the coefficients in Table 4.4. The chemical potential for methane (equation 4.53) or carbon dioxide (equation 4.58) can be applied since it is assumed that the chemical potential for the guest molecule has the same chemical potential in both cavities in the case of

equilibrium conditions, $\mu_{i,\text{large cavity}} = \mu_{i,small\ \text{cavity}}$. A difference, in relative to the case of separate phases for liquid water and hydrate former, sits in the enthalpy for the hydrate former that enters in the changes associated with the phase transition [58]:

$$H_{CO_2}^{Water} = -RT^2 \left[\frac{\partial \left(\frac{\mu_{CO_2}^{\infty,ideal\ gas}}{RT} \right)_{P,y_{j\neq CO_2}}}{\partial T} + \left[\frac{\partial \ln \phi_{CO_2}^{water}}{\partial T} \right]_{P,y_{j\neq CO_2}} \right] \tag{4.62}$$

And:

$$H_{CO_2}^{R} = -RT^2 \left[\frac{\partial \ln \phi_{CO_2}^{water}}{\partial T} \right]_{P,y_{j\neq CO_2}} \tag{4.63}$$

For non-equilibrium cases, the only phase that needs attention is the hydrate phase, because the description of all fluids phase is continuous, while the theory for hydrate is based on a Langmuir type of equilibrium theory [58]. The chemical potentials of guest molecules in hydrates are not directly available from models and may be approached using a Taylor expansion around the equilibrium:

$$G_{non-equilibrium}^{H}(T,P,\vec{x}) = \left[\begin{array}{l} G^{H,eq}(T^{eq},P^{eq},\vec{x}^{eq}) + \left.\frac{\partial G^H}{\partial T}\right|_{P,\vec{x}} (T-T^{eq}) \\ + \left.\frac{\partial G^H}{\partial P}\right|_{T,\vec{x}} (P-P^{eq}) + \sum_r \left.\frac{\partial G^H}{\partial x_r}\right|_{P,T,x_{i\neq r}} (x_r - x_r^{eq}) \end{array} \right] \tag{4.64}$$

Where "eq" in the superscript denotes the equilibrium values, with all the derivatives evaluated at equilibrium. The chemical potentials needed for equation 4.25 in a non-equilibrium case is given by:

$$\mu_m^H = \left. \frac{\partial \left(N G_{non-equilibrium}^{H}(T,P,\vec{x}) \right)}{\partial N_m} \right|_{T,P,N_{k\neq m}} \tag{4.65}$$

Where "m" denotes a hydrate former or water.

Table 4.4: Coefficients for $\Delta g^{inclusion}$ series expansion in case of methane inclusion in both large and small cavities. Coefficients for inverse-temperature expansion in case of carbon dioxide inclusion, if no CO_2 enters the small cavities. Adapted from ref [59].

	CH_4		CO_2	
$k_i(kJ/mol)$	Small cavity	Large cavity	Small cavity	Large cavity
0	−42.47683	17.97150	0	14.85234
1	119.24124	−23.440123	0	2.70758
2	−183.19565	−161.81535	0	−92.74317
3	128.39252	45.20561	0	$-5.07768 \times 10^{-001}$
4	−54.98784	36.67261	0	9.40264
5	−78.55671	138.00217	0	21.65244

Table 4.5: Parameters for equations 4.56 and 4.59. Adapted from ref. [57]

	CH_4		CO_2	
i	a_0	a_1	a_0	a_1
1	1.360608	3.796962	−139.137483	−138.899061
3	0.033630	-0.703216	−76.549658	−72.397006
5	0.656974	-12.441339	−20.868725	−14.715982
7	1.763890	-21.119318	18.030987	24.548835
9	5.337858	-33.298760	44.210433	52.904238
11	-0.024750	12.387276	63.353037	71.596515
13	48.353808	17.261174	74.713278	82.605791
15	-11.580192	16.384626	80.411175	88.536302
17	-0.087295	13.171333	82.710575	90.262518
19	-0.558793	13.556732	82.017332	89.094887
21	-23.753020	16.573197	79.373137	85.956670
23	-10.128675	13.591099	75.429910	81.519167
25	-41.212178	5.060082	70.680932	76.270320
27	-31.279868	31.289978	65.490785	70.551406
29	-23.855418	31.720767	60.126698	64.683147
31	-35.125907	37.064849	54.782421	58.865478
33	-33.675110	41.544360	49.592998	53.235844
35	-27.027285	57.609882	44.500001	47.728622
37	-19.026786	54.961702	39.869990	42.730831
39	-37.872252	57.204781	35.597488	38.125674

5 Results and discussion

The estimated equilibrium curves for both methane and carbon dioxide are presented in Figure 5.1 and Figure 5.2. The other data points are the conditions used to conduct experiments or calculation of enthalpy in Table 4.1 and Table 4.2 by the other authors to show that there exists an agreement about this.

The rapid steep change for CO_2 in Figure 5.2 is due to the phase change that occurs at around 283 K and 46.9 bars, where the SRK EOS is not that accurate.

It seems that the bulk of published research, either measure or calculate equilibrium pressures for CO_2 to the point of phase change and no further, or they skip the whole section below the phase change. This phase change will, of course, affect other calculations at the same pressure and temperature region and therefore makes it easier to see which plots are related to methane and which is related to carbon dioxide in the result figures.

However, the phase change and its effect are explained in more substantial details in an article published by Kvamme and Aromada [60].

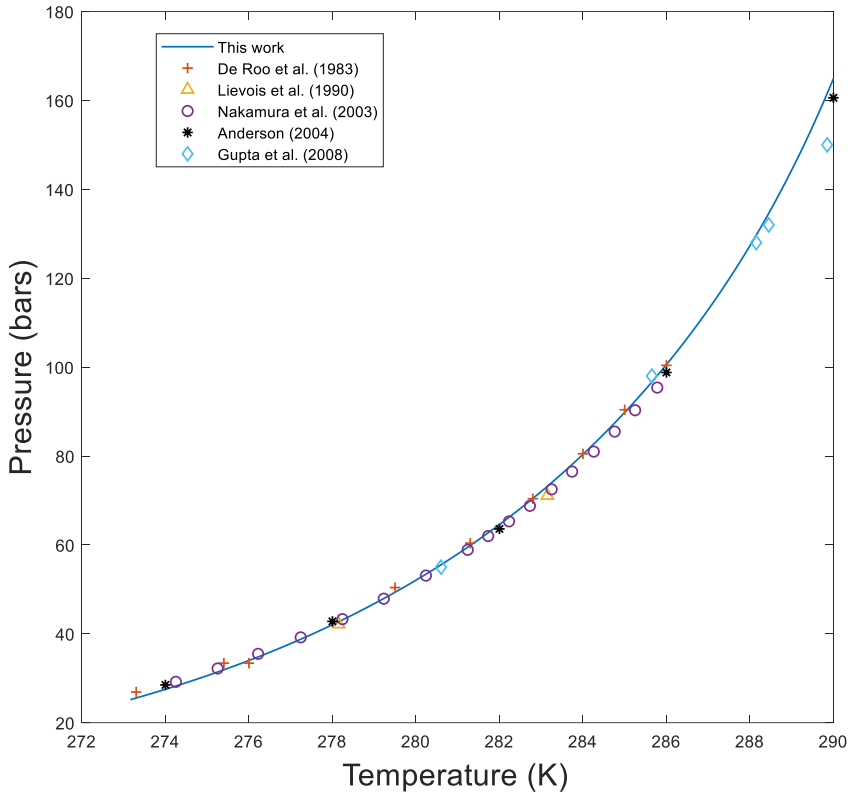

Figure 5.1: Equilibrium curve for methane from the residual thermodynamics shown as a solid line compared with pressure and temperature plots used from other literature [61] [23] [62] [49] [43] such as in Table 4.1.

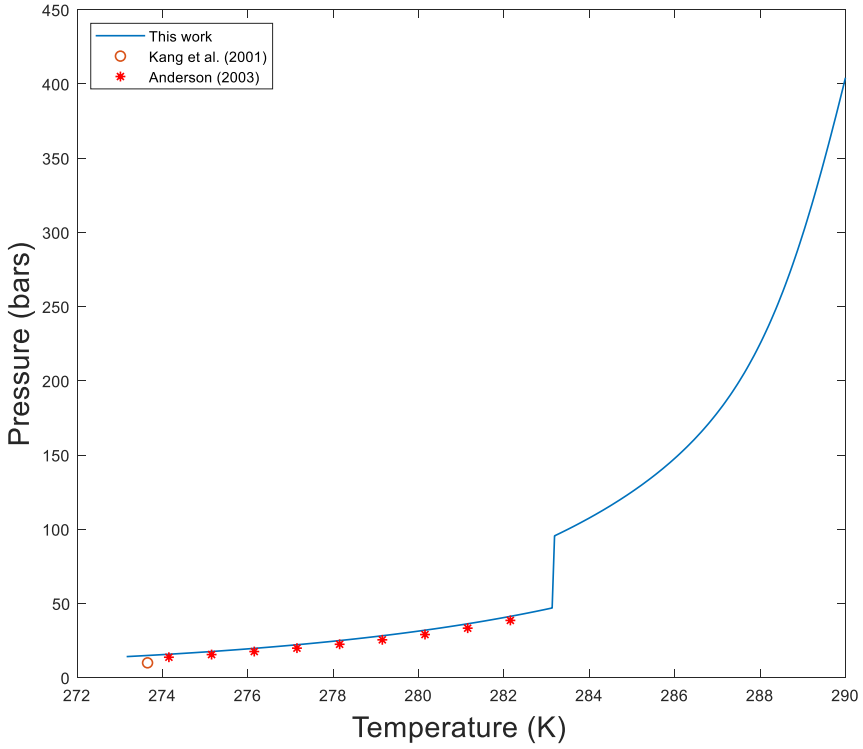

Figure 5.2: Equilibrium curve for carbon dioxide from the residual thermodynamics shown as a solid line compared with pressure and temperature data used from other literature [51] [44] such as in Table 4.2.

5.1 Evaluating the chemical potential, free energy, and mole fraction in hydrates by means of residual thermodynamics

By using the mole fraction of guest in the hydrate along with the chemical potential of water and guest in the hydrate makes it possible to calculate the molar free energy. The calculated mole fractions of both methane and carbon dioxide in the hydrate is presented in Figure 5.3. The calculated chemical potential of guests in hydrates and water in the hydrate is plotted in Figure 5.4 and Figure 5.5. An example of the calculation of the molar free energy for a methane hydrate at goes as follows: The mole fractions of methane inside the hydrate, formed from a saturated solution, was calculated by using the expression in equation 4.23, and the results are plotted in Figure 5.3. The mole fraction of water in the hydrate can now be calculated by using the expression in equation 4.24.

At T = 273.16 K and P = 25.19 bars:

$$x_{H_2O}^H = 1 - \sum_i x_i^H$$

$$\downarrow$$

$$x_{H_2O}^H = 1 - x_{CH_4}^H$$

$$\downarrow$$

$$x_{H_2O}^H = 1 - 0.134$$

$$\downarrow$$

$$x_{H_2O}^H = 0.866$$

The chemical potential of water in hydrate was found using the expression in equation 4.19, and the chemical potential of methane in hydrate was found using the expression in equation 4.21. These values are plotted in Figure 5.4.

Table 5.1: Calculated mole fractions and chemical potentials for water and methane in hydrate at equilibrium condition.

$T(K)$	$P(bars)$	$X_{CH_4}^H$	$X_{H_2O}^H$	$\mu_{CH_4}^H (kJ/mole)$	$\mu_{H_2O}^H (kJ/mole)$
273.16	25.19	0.134	0.866	-25.683	-49.311

The values in Table 5.1 can now be applied to equation 4.25 for calculating the molar free energy of the methane hydrate.

$$G^H(T,P) = x^H_{H_2O}\mu^H_{H_2O} + \sum_i x^H_i \mu^H_i$$

$$\Downarrow$$

$$G^H(T,P) = x^H_{H_2O}\mu^H_{H_2O} + x^H_{CH_4}\mu^H_{CH_4}$$

$$\Downarrow$$

$$G^H(273.16K,\ 25.19bar) = \left(0.866\cdot(-49.311) + 0.134\cdot(-25.683)\right) kJ/mole$$

$$\Downarrow$$

$$G^H(273.16K,\ 25.19bar) = -46.145\ kJ/mole$$

The calculated molar free energy for both CH_4 and CO_2 hydrates along the equilibrium curves is plotted in Figure 5.4 and Figure 5.5. These values are essential for further calculation involving the enthalpies of hydrate formation.

If we approximate that the hydrate former guest reaches equilibrium, or close to equilibrium, then:

$$\mu_i^{Hydrate} = \mu_i^{liquid\ water} = \mu_i^{gas}$$

Where i is the guest component. For example, in the case of methane, since the chemical potential of the hydrate former at non-equilibrium is:

$$\mu_{CH_4}^{Hydrate} \neq \mu_{CH_4}^{liquid\ water} \neq \mu_{CH_4}^{gas}$$

then $h_{CH_4,k}^{gas} \neq h_{CH_4,k}^{liquid\ water}$ and $\theta_{CH_4,k}^{gas} \neq \theta_{CH_4,k}^{liquid\ water}$

Different composition and different free energy define different phases [63]. This is the reason there are three different hydrate formation (H_1, H_2, and H_3) which is explained in chapter 3. The dynamic development of the system is controlled by the minimum free energy under constrains of conservation of mass and energy. For stable hydrate formation, the chemical potential for water and guest in the hydrate phase must be lower than in the separated phase. This means that the water prefers to be in a hydrate phase and not in a liquid phase (or gas). The same thing goes for the guest molecules. In the case of hydrate condition, the CH_4 and CO_2 molecules prefer to be in a hydrate phase, not in an aqueous solution, gas or a supercritical fluid.

For water: For hydrate former:

$$\mu_{H_2O}^{Hydrate} < \mu_{H_2O}^{Liquid} < \mu_{H_2O}^{vapour} \qquad \mu_{CH_4}^{Hydrate} < \mu_{CH_4}^{liquid\ water} < \mu_{CH_4}^{Gas}$$

Hydrate phase is the lowest free energy phase for water and will control the possible remaining hydrocarbons of each type in the presence of hydrate. Take note that the molar free energy of CO_2 hydrate in Figure 5.5 is lower than the molar free energy of CH_4 in Figure 5.4 with a difference of approximately 1-2 kJ/mole. This implies that the CO_2 hydrate is more stable than the CH_4 hydrate and is an important factor for cases where "swapping" methane guests with carbon dioxide in hydrate reservoirs for natural gas production and CO_2 storing.

The solubility of hydrocarbons in water is limited. The solubility of methane in liquid water is shown in Figure 5.6 as a function of temperature and pressure. Each of those blue lines represents the saturated $x_{CH_4}^{liquid\ water}$ at different constant pressure (48 bars to 200 bars) with increasing temperature (273.16 K – 290.0 K). The other solid lines, which is coloured black, is the minimum mole fraction of CH_4 in water that is required to maintain hydrate stability. If the concentration of hydrate formers in the surrounding water is below the black lines, then hydrate will start to dissociate. The free energy of a hydrate is controlled by the pressure, temperature and the concentration in the system, and so does the stability as equation 4.5 shows: $d\underline{G}^i \leq \underline{V}^i dP - \underline{S}^i dT^i + \sum_i^n \mu_j^i dN_j^i$

The pressure change shows a significant impact on the solubility of methane. The solubility of CO_2 and the minimum mole fraction of CO_2 in water for hydrate stability is plotted in Figure 5.7. Carbon dioxide is significantly more soluble in water than methane is. By comparing the two different figures, shows that the solubility of CO_2 in liquid water at 48 bars and 273.16 K, is between 17-18 times higher compared to methane at the same pressure and temperature. This massive difference will be reduced as the temperature and pressure increase. The supersaturation is the difference between the hydrate stability limit, as given in Figure 5.6 and Figure 5.7. The hydrate can grow from an initial liquid solubility until the liquid mole fraction of hydrate former has reached the stability limit. The mole fraction of guest in hydrate varies considerably from very low supersaturation near the stability limit of the hydrate up to the maximum driving force for the solubility limit [57]. For homogeneous hydrate formation, there will be an infinite number of hydrate phases corresponding to concentrations spanning the range between guest solubility in liquid water and its hydrate stability limit.

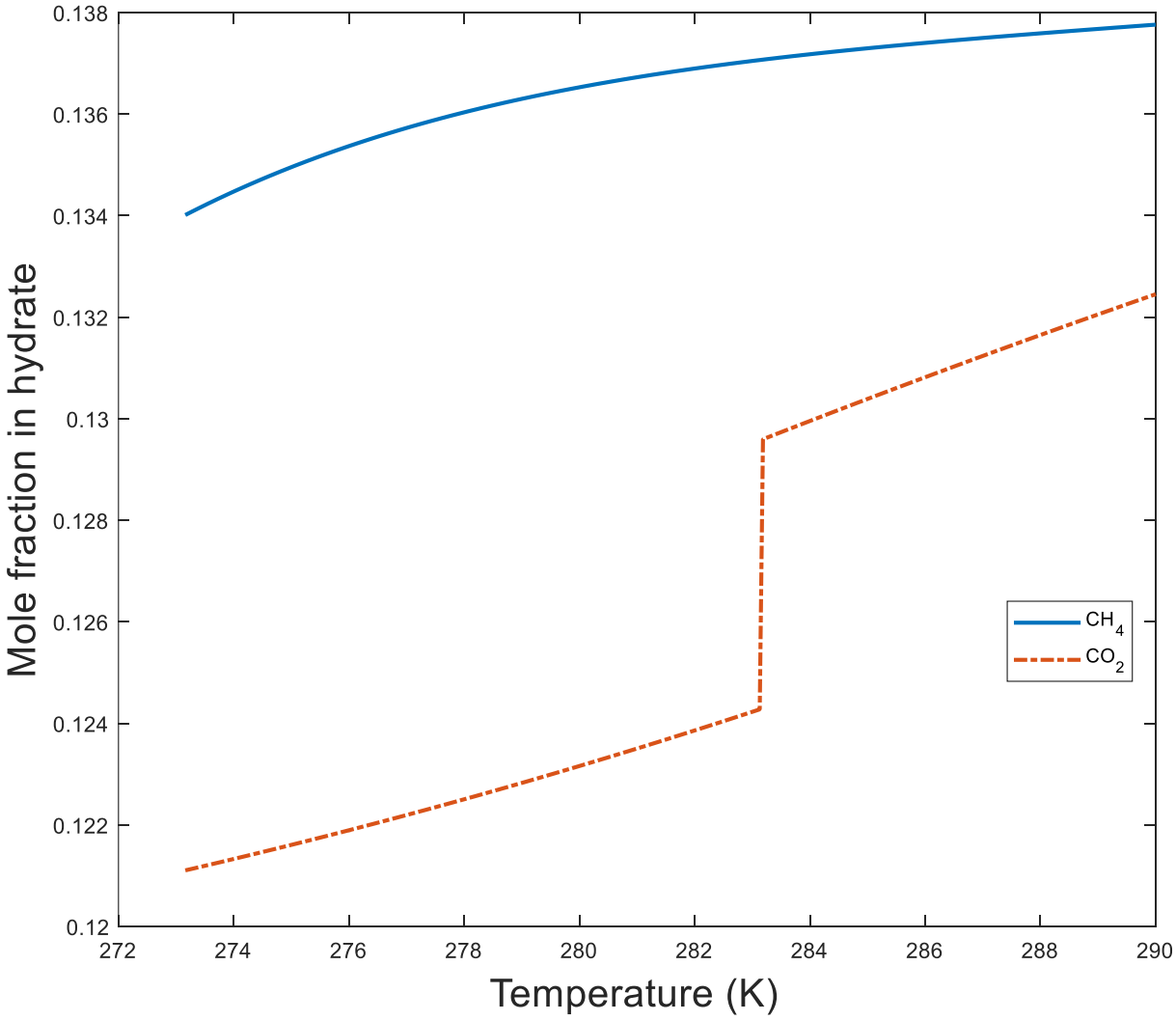

Figure 5.3: Mole fraction of guest component in hydrate formed from saturated aqueous solutions as a function of temperature. The solid line is for methane hydrate, and the dashed line is for carbon dioxide hydrate.

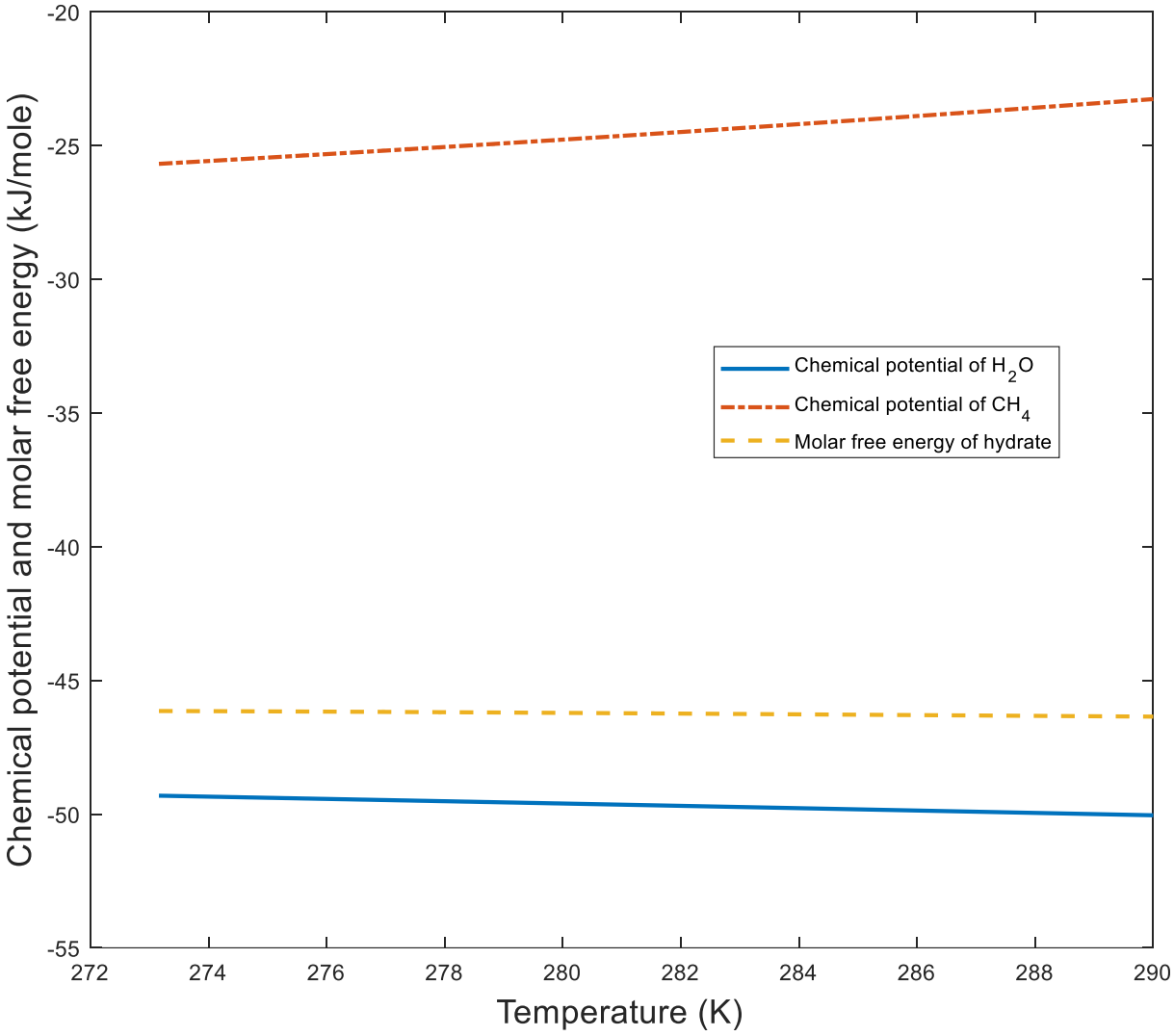

Figure 5.4: The chemical potential for methane and water in the clathrate hydrate along the equilibrium line, respectfully. The dashed line in the middle is the molar free energy for the gas hydrate.

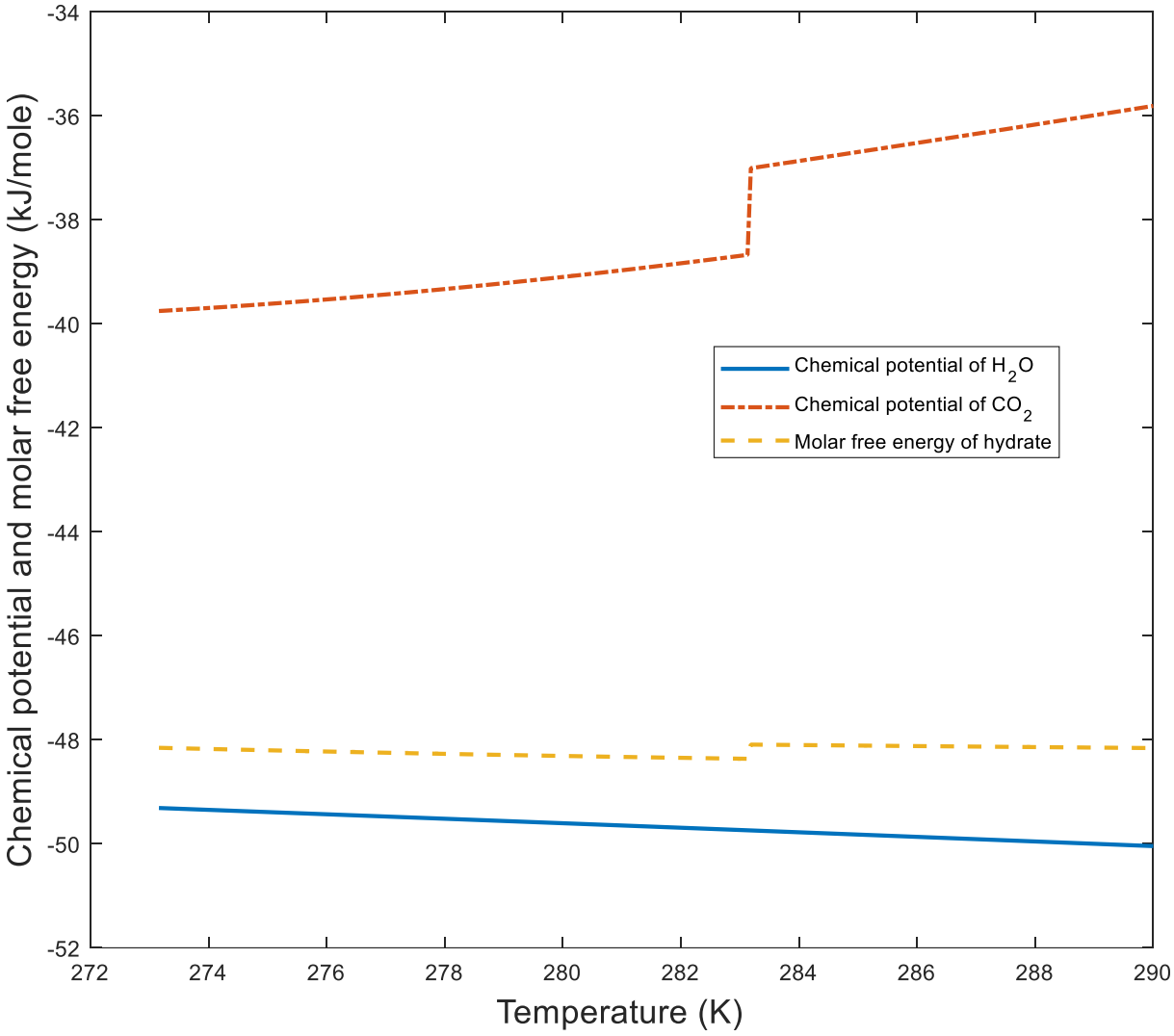

Figure 5.5: The chemical potential for carbon dioxide and water in the clathrate hydrate along the equilibrium line, respectfully. The dashed line in the middle is the molar free energy for the gas hydrate.

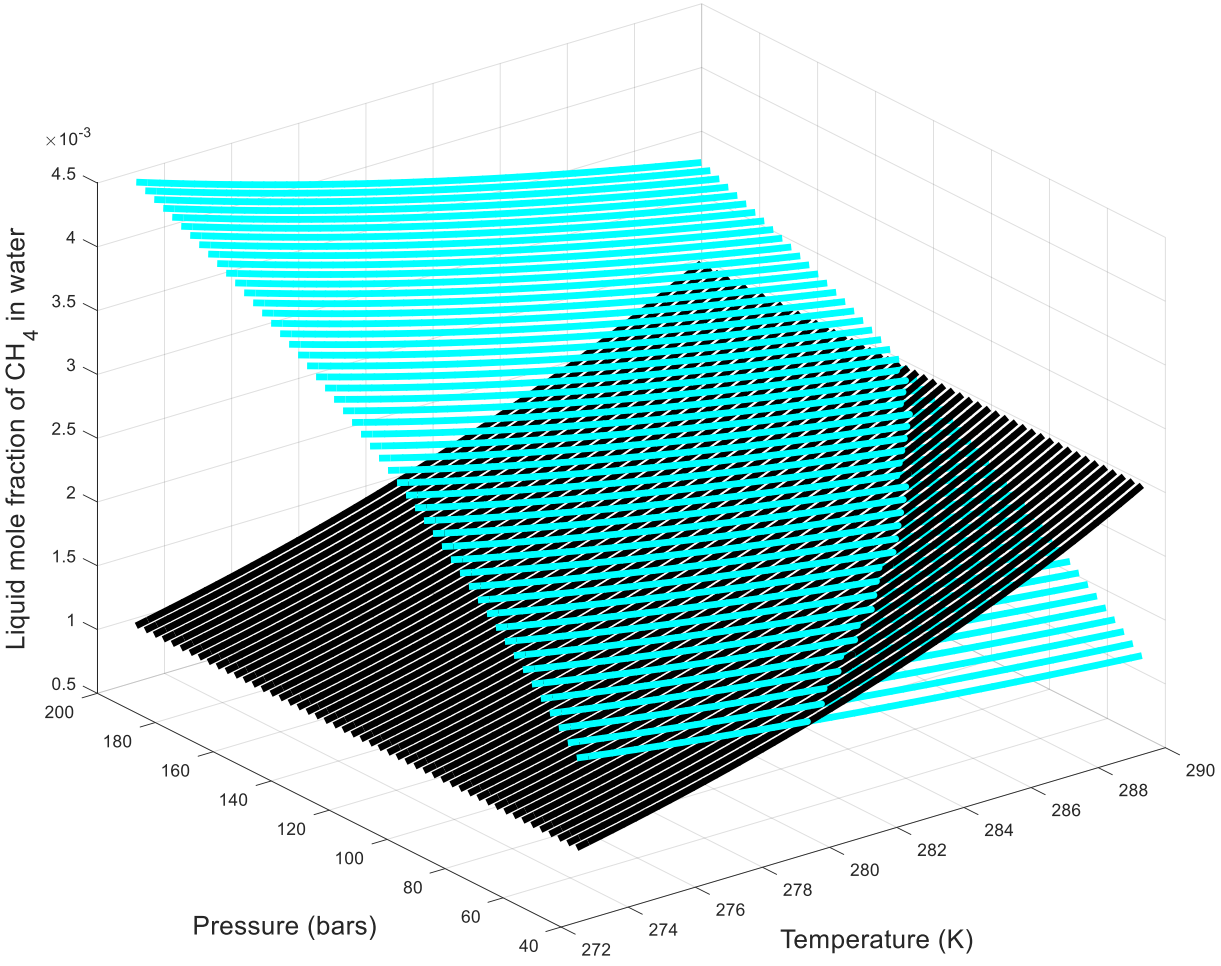

Figure 5.6: The solid black lines are the minimum mole fraction of methane in liquid water for hydrate stability. The solid blue lines are the solubility of methane in liquid water.

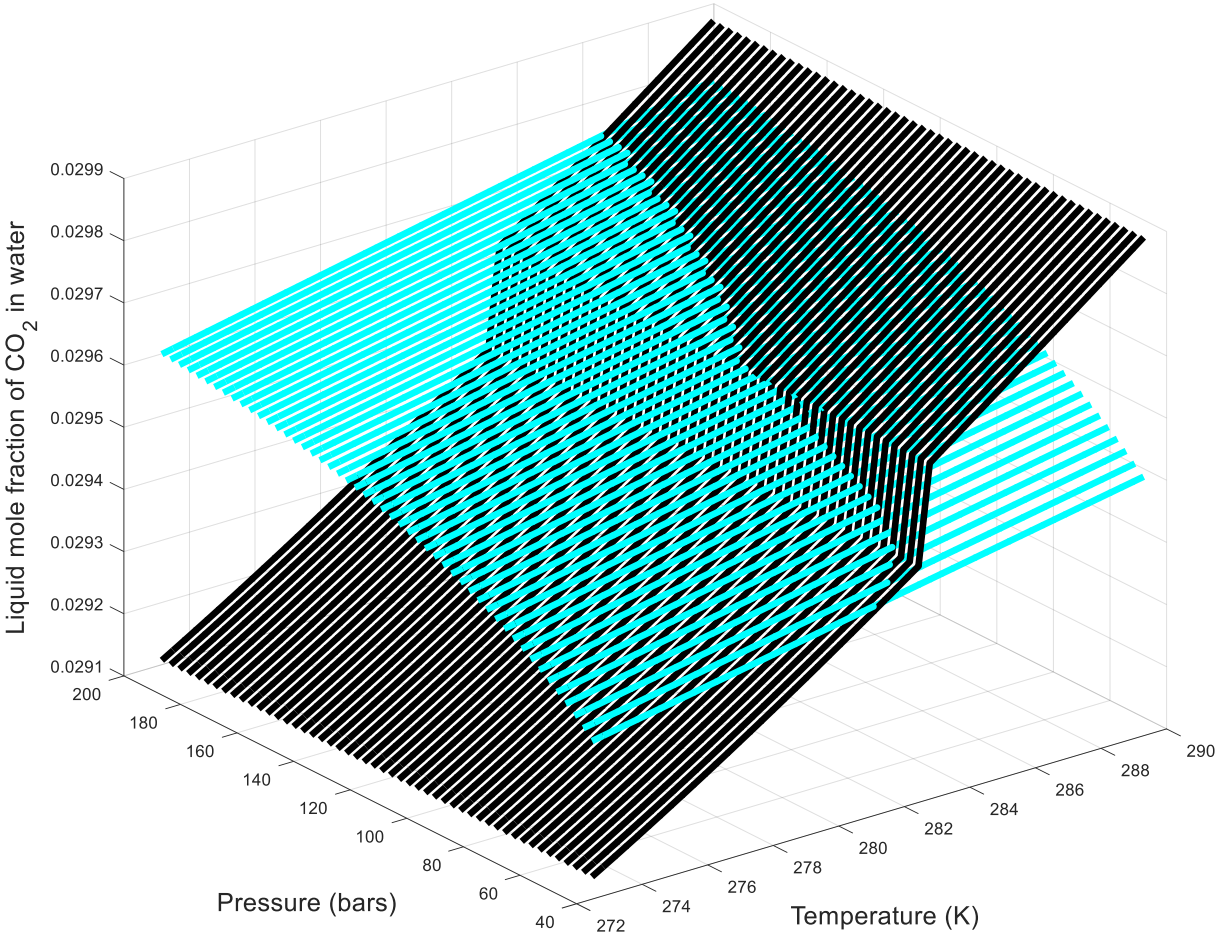

Figure 5.7: The solid black lines are the minimum mole fraction of carbon dioxide in liquid water for hydrate stability. The solid blue lines are the solubility of carbon dioxide in liquid water.

5.2 Evaluating the enthalpies of hydrate formation using residual thermodynamics

The enthalpy changes of hydrate formation from pure CH_4, CO_2, and liquid H_2O along the equilibrium line, the three-phase co-existing conditions (L-H-V), have been estimated using residual thermodynamics, as shown in Figure 5.8 and Figure 5.9. The enthalpy values for hydrate formation is presented as a function of pressure and temperature in Figure 5.10.

This figure illustrates how different the enthalpy change is for the different hydrate formers. The sharp change in curvature of the CO_2 hydrate tells us that it requires increasing high pressure to maintain hydrate equilibrium as the temperature increases.

This occurs at around 282 K and up. Such extreme conditions are not likely for reservoir conditions and therefore not worth discussing. The difference in enthalpy change, however, is noteworthy. It is difficult to see the difference in Figure 5.10 unless we plot the enthalpy of hydrate formation along the equilibrium curve for both CH_4 and CO_2 as a function of temperature, as shown in Figure 5.11.

The formation of CO_2 hydrate releases approximately 9-11 kJ/mole more energy than the energy required to dissociate CH_4 hydrate. The benefit is that not only is CO_2 hydrate thermodynamically more stable than CH_4 hydrate, but by injecting CO_2 gas into CH_4 hydrate reservoirs, the heat of formation is enough to dissociate more CH_4 hydrate than the amount of CO2 injected.

Another benefit of this is that this is a noteworthy alternative to capture the greenhouse gas instead of releasing it into the atmosphere. Carbon capture and hydrates have been Kvamme's primary research over many years, and he has published several papers within this subject.

For instance, a recent study of his shows how methanol inhibitor affects the enthalpy of hydrate formation for CH_4 and CO_2 hydrates [4]. This theory of production is still under development and have some constraint. The nucleation of the carbon dioxide/pore water interface hydrate is extremely fast and rapidly blocks the pore space for further mass transport.

By adding surfactants to the injected carbon dioxide will reduce the hydrate formation on the interface and consequently make it possible to control combined methane production and carbon dioxide storage [64].

From Figure 5.8 and Figure 5.9, we can see that the enthalpy change for hydrate formation decreases (note the negative sign) as the pressure and temperature conditions increases. As explained before, the negative enthalpy value for hydrate formation is because it is exothermic, for hydrate dissociation it is the opposite.

During hydrate crystallisation, heat must be transported out of the system. When all the other conditions for hydrate formation is encountered, the heat transport is still a significant factor. It is about 2 to 3 times [65] the amount of mass transport, which is more rapid, so a restriction of heat transport can lead to hydrate dissociation.

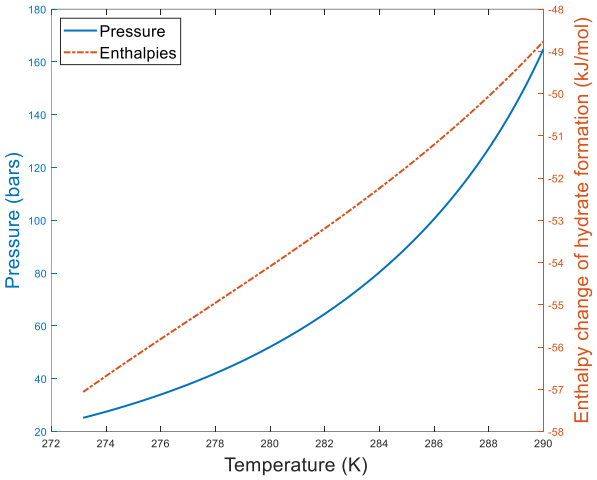

Figure 5.8: Enthalpy change of methane (CH_4) hydrate formation with hydrate equilibrium.

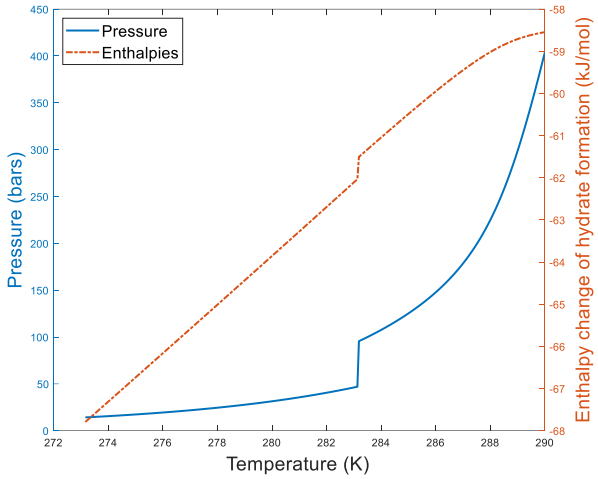

Figure 5.9: Enthalpy change of carbon dioxide (CO_2) hydrate formation with hydrate equilibrium.

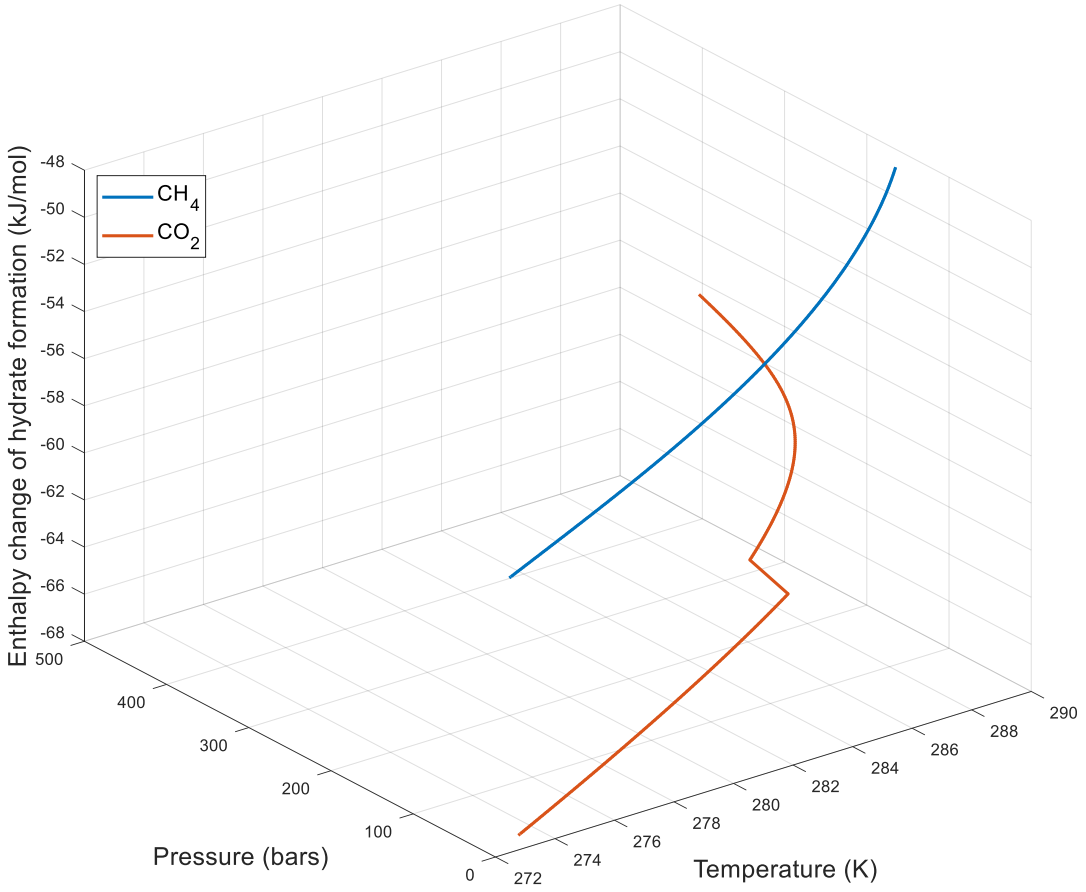

Figure 5.10: Three-dimensional plot of the enthalpy change of hydrate formation as a function of temperature and pressure. The solid lines are for different hydrate former, the smooth curve on the left is for CH_4 hydrate, the more twisted curve on the right is for CO_2 hydrate.

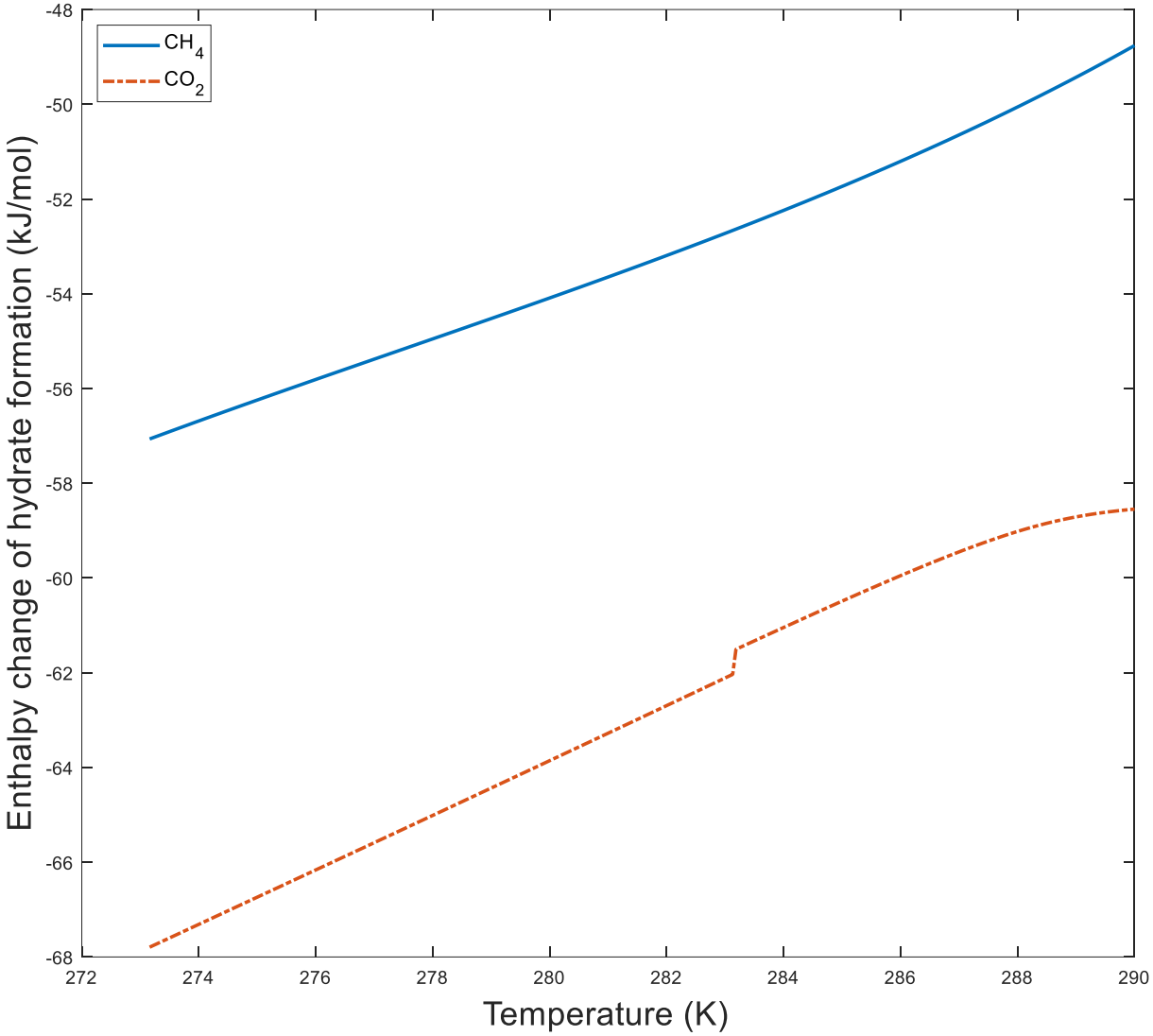

Figure 5.11: Enthalpy change of hydrate formation as a function of temperature. The solid curve at the top is for methane (CH_4) hydrate, the dashed curve with a slight steep change at the bottom is for carbon dioxide (CO_2) hydrate.

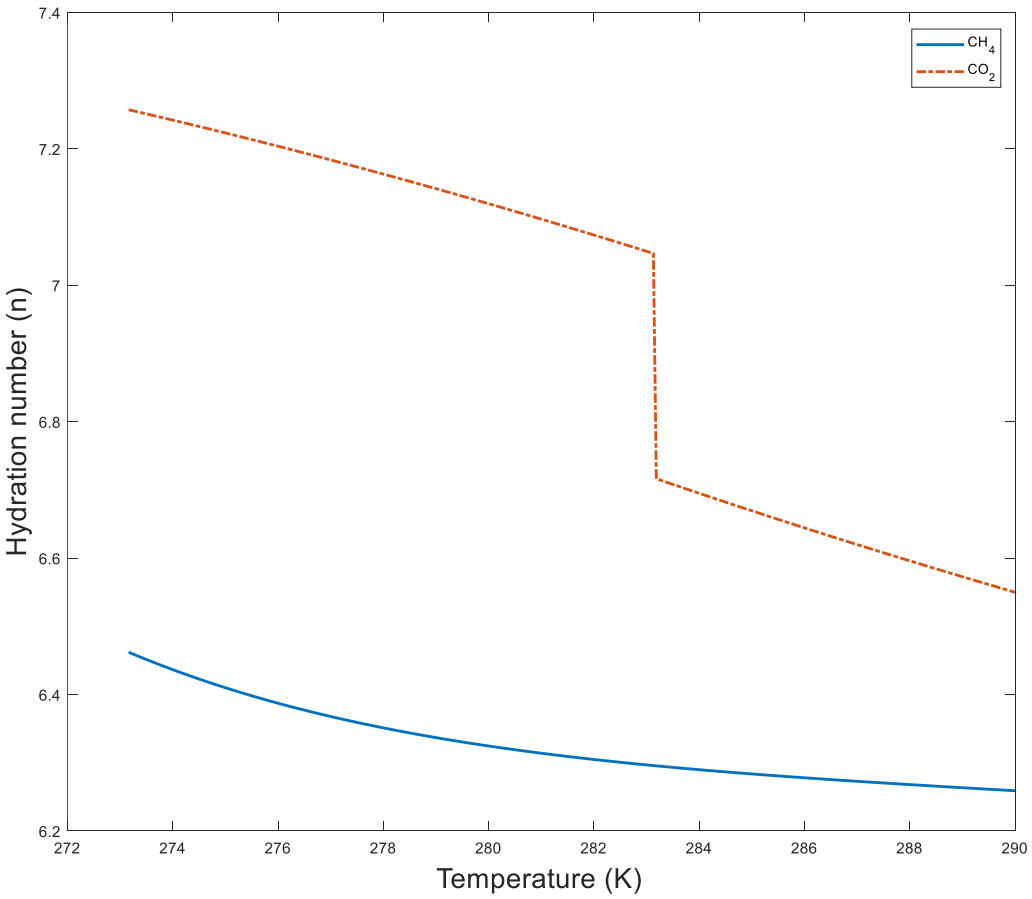

Figure 5.12: Hydration/Occupation number for different hydrates as a function of temperature. At the top with a dashed line and a sharp change in curvature (due to change in density) is for carbon dioxide (CO_2) hydrate. At the bottom with a solid smooth line is for methane hydrate (CH_4).

Table 5.2: Hydration number and heat of formation for carbon dioxide and methane hydrates computed using residual thermodynamics, respectively. These values are based on the equilibrium pressure and temperature, which is listed with a step of approximately one Kelvin in each row.

Temperature (K)	**CO_2**			**CH_4**		
	Pressure (*bars*)	*Hydration number* (n)	ΔH (kJ / mol)	Pressure (*bars*)	*Hydration number* (n)	ΔH (kJ / mol)
273.16	14.19	7.26	-67.79	25.19	6.46	-57.07
274.17	15.73	7.24	-67.24	27.87	6.43	-56.63
275.19	17.70	7.22	-66.63	31.20	6.40	-56.16
276.15	19.73	7.20	-66.08	34.53	6.38	-55.75
277.16	22.21	7.18	-65.50	38.45	6.37	-55.31
278.17	25.06	7.16	-64.91	42.83	6.35	-54.88
279.19	28.37	7.14	-64.33	47.72	6.33	-54.44
280.14	31.96	7.11	-63.77	52.87	6.32	-54.03
281.16	36.34	7.09	-63.18	58.97	6.31	-53.57
282.17	41.42	7.07	-62.59	65.80	6.30	-53.11
283.19	95.55	6.72	-61.50	73.48	6.29	-52.64
284.14	109.88	6.69	-60.96	81.64	6.29	-52.17
285.15	128.38	6.67	-60.40	91.41	6.28	-51.65
286.17	152.24	6.64	-59.86	102.55	6.28	-51.11
287.18	185.60	6.62	-59.36	115.41	6.27	-50.54
288.14	233.44	6.59	-58.96	129.55	6.27	-49.97
289.16	313.22	6.57	-58.68	147.28	6.26	-49.33
290.00	404.15	6.55	-58.55	164.94	6.26	-48.76

5.3 Evaluating the various approaches: Clapeyron, Clausius-Clapeyron, experimental and residual thermodynamics

Even though there are plenty of different theories for hydrates formation/dissociation, one of the main concepts for this thesis is to give an overview of the considerable uncertainty in hydrate literature, but also to compare the heat of formation for hydrates using residual thermodynamics with other approaches. Kvamme and his research team usually present their values in graphic plot and not in tables. Since this work is reviewing other works of literature and their limitation of information, then we should also specify our data in the form of a table.

The equilibrium pressures in Table 5.2 were used to calculate the change in enthalpy of CH_4 and CO_2 hydrate formation, but also hydration number at a given temperature using residual thermodynamics. The table presents the values calculated from 273.16 K to 290 K, with a change in temperature at around one kelvin for each step. The heat of dissociation/formation (enthalpy) and hydration number for both methane and carbon dioxide hydrate obtained from different literature is presented in Figure 5.13 to Figure 5.16, along with the results using residual thermodynamics.

The result from Nakagawa et al. [50] are not entirely relevant here due to their value being determined at a constant pressure of 5 MPa over a temperature range of 279 K to 282 K, so the 4 data points plotted in Figure 5.13 are the same enthalpy value. They did not give any information about the hydration number.

Most of the approaches are indirect methods that are obtained at equilibrium. This means that non-equilibrium conditions are overlooked, such as superheating, the amount of heat to dissociate above the equilibrium. Several of those do not even provide information about the pressure and temperature conditions used for their evaluation [66].

The lack of information concerning the equation of state or compressibility factors used for their calculation is not always described. A short brief of the literature data plotted in the figures is given here. Some of it will be a repetition of the experimental literature reviewed in section 4.7.3, but this includes the literature that used Clapeyron and Clausius-Clapeyron.

The enthalpies of hydrate dissociation were calculated by Nakamura et al. [62] by applying the Clapeyron equation on equilibrium (T, P) data they measured experimentally with a high-pressure cell apparatus. The volumetric fluid properties of methane were evaluated using IUPAC recommendation equation in Angus et al. [67], and the molar volume for methane hydrate was estimated from a lattice constant of the structure (I) hydrate [68]. They assumed ideal hydration for their work, and their results are plotted in Figure 5.13.

The change in enthalpy for dissociation of formation does not show any significant dependence on temperature. De Roo et al. [61] used the Clapeyron equation for their approach to determining the enthalpy dissociation of methane hydrate. Their value stands out compared to the other literature with a value of 67.85 kJ/mol. They also calculated the hydration number at the quadruple point (ice - liquid water – hydrate – vapour) at 2.523 MPa and 272.95 K. This resulted in hydration number of 7.4, but after using the Mille and Strong method, their hydration number was reduced to 6.3 as shown in Figure 5.15.

The evaluation of hydrate dissociation enthalpies using Clapeyron equation was also done by Anderson [44] [49]. He calculated for both methane and carbon dioxide along the equilibrium curve, respectively, and his results are plotted in Figure 5.13 and Figure 5.14. For his calculation, he considered the finite volumes of all the phases, methane solubility in liquid water and the nonideality of the gas phase. The equilibrium data used for his calculation were obtained from Sloan [69] in a temperature range of 273 K to 290 K. The change in enthalpy for hydrate dissociation did not show any remarkable temperature dependency, especially for methane hydrate.

In the 1940s, Robert et al. [70] evaluated the enthalpy change for methane hydrate dissociation along the three-phase equilibrium line using the Clapeyron equation. The results plotted in Figure 5.13, was found in Glew [71], but information regarding the equation of state used for their calculation is not available. Their results do not show any significant dependence on temperature. In fact, their results show a negative slope as the temperature increases.

Another literature from the 1940s is Deaton and Frost [72]. They evaluated the dissociation enthalpy for methane hydrate but used the simplified Clausius-Clapeyron equation. Their result did not show any particular dependency on temperature and is plotted in Figure 5.13.

These data were found in Glew [71], but details of the equation of state used were not given. The Soave-Redlich-Kwang equation of state was not available before 1972, and the work of both Robert et al. [70], Deaton and Frost [72] were done up till 1971.

As mentioned in section 4.7.3, Kang et al. [51] used an isothermal microcalorimeter to directly measure the enthalpy change for both methane and carbon dioxide hydrate dissociation. However, the experiment was performed at low pressures, 1.0 bar (0.1 MPa) at 273.65 K (for CO_2 hydrate) which is way below the equilibrium pressure.

Gupta et al. [43] used experiments, Clapeyron and Clausius-Clapeyron equation to determine the enthalpy of methane hydrate dissociation. Unlike Kang et al. [51], Gupta and his team used high pressures for their calorimeter experiments. The pressures and temperatures used in the experiments were also used to calculate enthalpy values using the other approaches; Clapeyron and Clausius-Clapeyron equation. This was done for comparing the different methods. They assumed a constant hydration number, based on Circone et al. [73]. For the Clausius-Clapeyron approach, they assumed that molar volumes of methane hydrate were equal to water, which is based on Dickens et al. [74]. The use of Clausius-Clapeyron is described in section 4.7.2. Their Clapeyron approach was based on a method proposed by Anderson [44] [49]. All three different approaches are plotted in Figure 5.13.

Lievois et al. [23] used a calorimeter for their experiments on methane hydrates. To determine the hydration number, they measured the pressure change in the system to track the guest molecules, and their result is plotted in Figure 5.15. Most of the different works of literature within the field of methane hydrate enthalpies compare their values with the work of Handa [45]. For his experiments with a calorimeter, he considered corrections for the nonideality of the gas phase, impact of pressure on condensed phase volumes and the solubility of a gas in water.

The fugacity of methane was obtained from Angus et al. [67], and the fugacity of propane, iso-butane and ethane was with the use of second virial coefficients [75]. The solubility and standard thermodynamic functions for the solution process were from Wilhelm et al. [76].

Lirio and Pessoa [66] published their work in 2013 using the Clausius-Clapeyron equation. They calculated the enthalpy of dissociation for pure CO_2 hydrate, but also various mixed systems of sodium dodecyl sulphate, tetrahydrofuran and CO_2. The equilibrium conditions were measured using the closed-loop method at a constant cooling rate. They also stated in their work that they used equilibrium data from the literature, so both their generated values and other literature data were used to indirectly evaluate both the hydration/occupation number and the heat of dissociation.

A very steep slope can be observed in both Figure 5.14 and Figure 5.16, and to compensate they used an average value for both hydration number and for the enthalpy of dissociation to compare with other kinds of literature.

Sabil et al. [77] also first directly measured the 3 phase hydrate equilibrium conditions of pure CO_2 and mixtures with tetrahydrofuran and used the Clausius-Clapeyron equation to calculate the enthalpy of dissociation. Their work highlights that the compressibility faction has a significant impact on the enthalpy value.

A modified version of Clausius-Clapeyron, a theory proposed by Sloan and Fleyfel [78] was used by Skovborg and Rasmussen [29] in which a more detailed P and T relation for the liquid water/hydrate/vapour equilibrium than the regular Clausius-Clapeyron equation. They considered the total amounts of water going into the hydrate structure for a unit mole of the different gases.

Udachin et al. [79] used X-ray to evaluate the hydration number of CO_2 hydrate. Yoon et al. [80] used a modified Clausius-Clapeyron equation to determine the enthalpy of hydrate dissociation and hydration number that considers the change in compressibility by phase transition and the guest molecules solubility in the liquid phase. They also stated that the impact of two correction factors on the valuation of the hydrate enthalpy is significant.

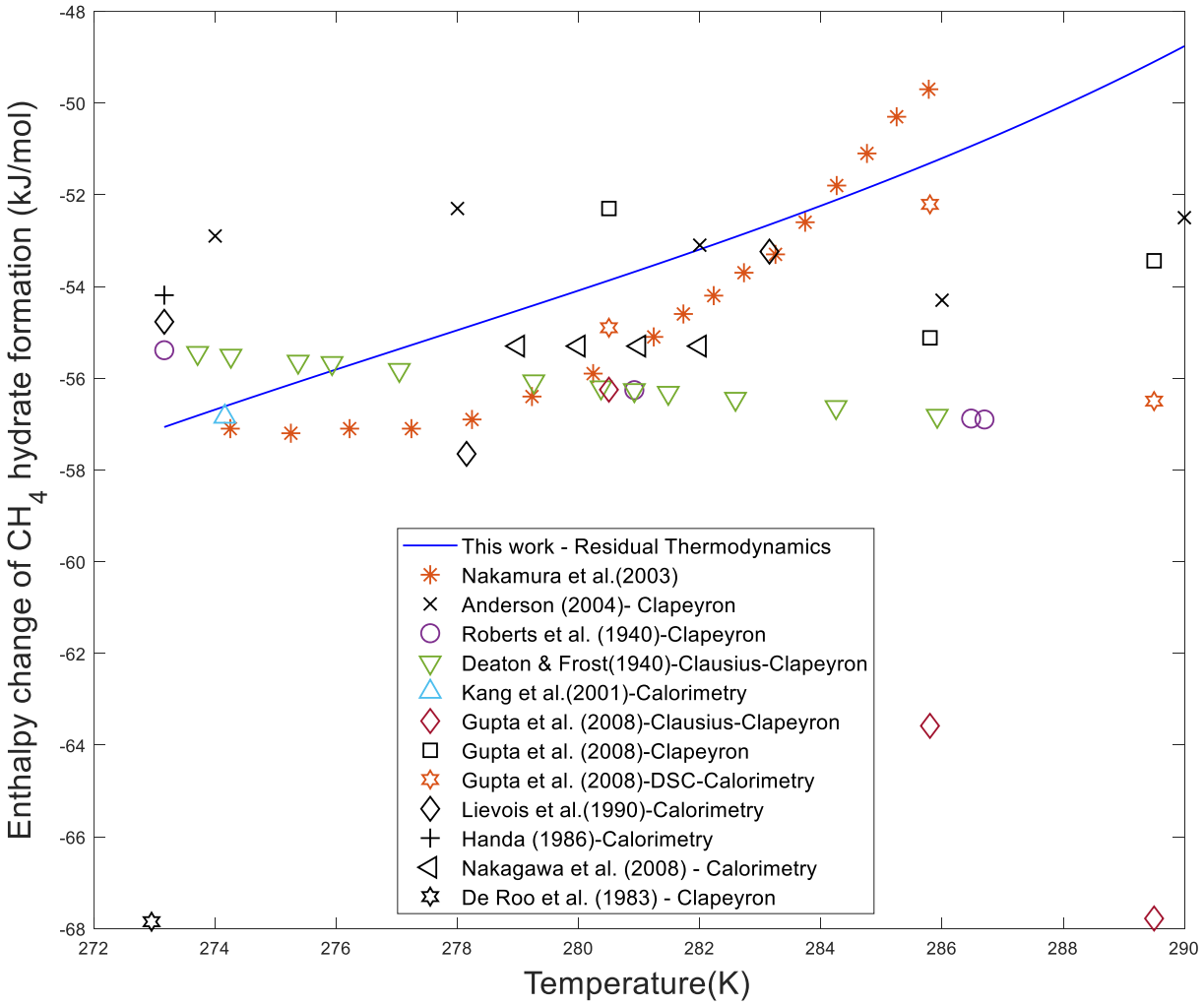

Figure 5.13: Enthalpy of methane (CH_4) hydrate formation calculated using residual thermodynamics shown as a solid line. The other data points are different literatures plotted for comparing enthalpy values at certain temperatures [62] [49] [70] [72] [51] [43] [23] [45] [50] [61].

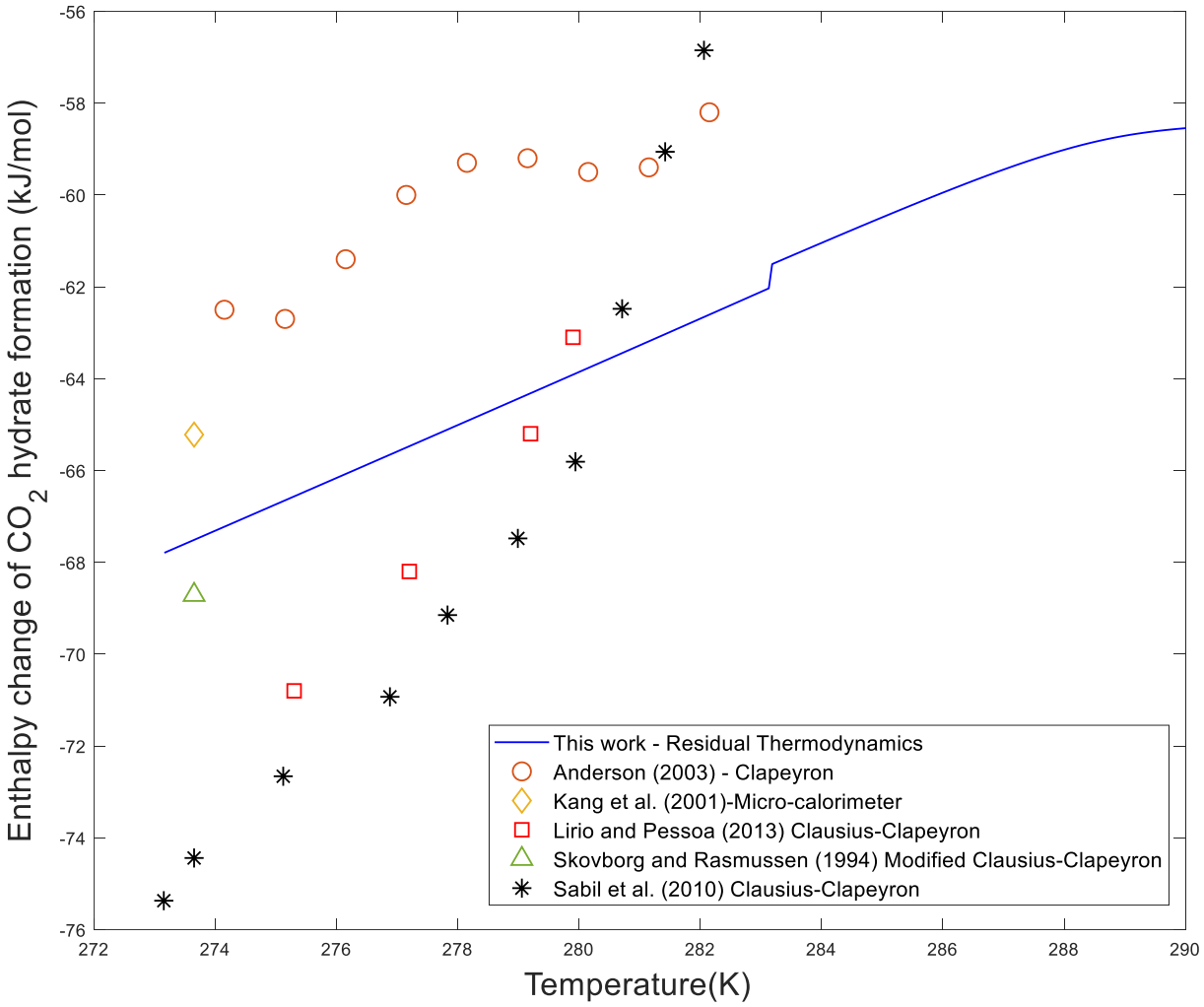

Figure 5.14: Enthalpy of carbon dioxide (CO_2) hydrate formation calculated using residual thermodynamics shown as a solid line. The other data points are different works of literature plotted for comparing enthalpy values at certain temperatures [44] [51] [66] [29] [77].

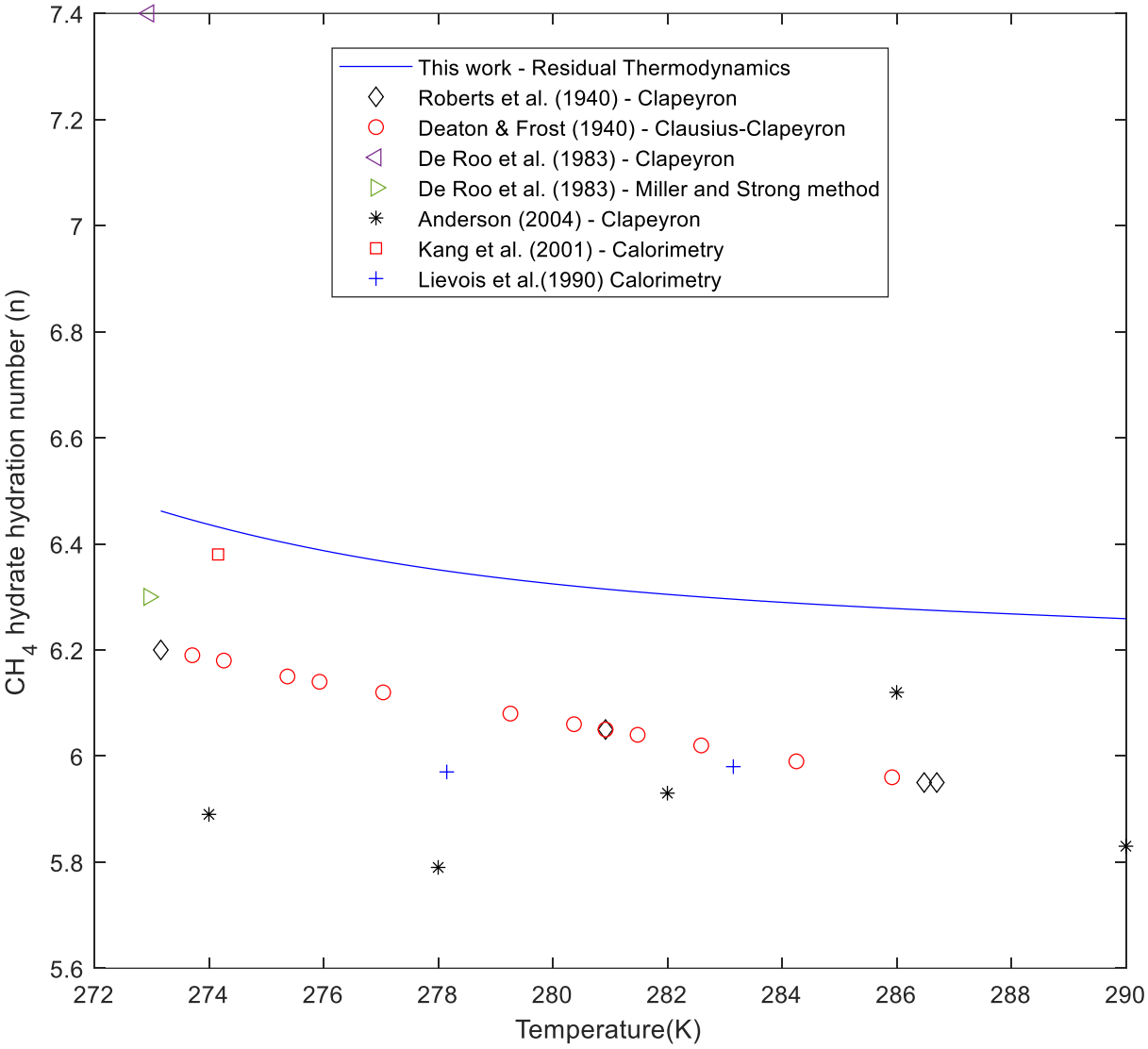

Figure 5.15: Hydration number for methane (CH_4) hydrate as a function of temperature calculated using residual thermodynamic, shown as a solid line. The other data points are different literatures plotted for comparison [70] [72] [61] [49] [51] [23].

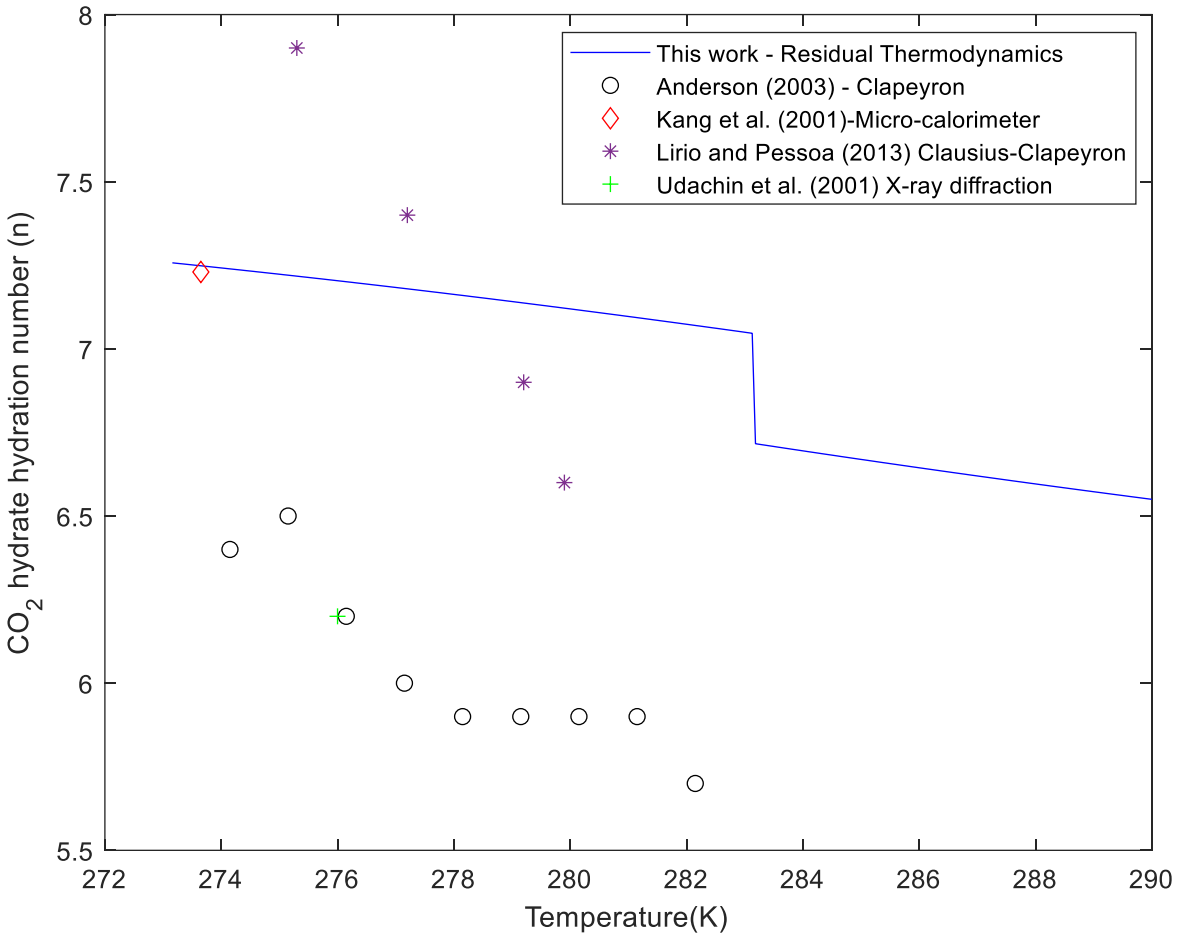

Figure 5.16: Hydration number for carbon dioxide (CO_2) hydrate as a function of temperature calculated using residual thermodynamic, shown as a solid line. The other data points are different literatures plotted for comparison [44] [51] [66] [79].

6 General Discussion

Most of the available experimental data for enthalpies of hydrate formation/dissociation for methane or carbon dioxide are limited. Methane hydrate is far the most popular hydrate former compared to CO_2 hydrate or other gases in works of literature. Some are determined directly using apparatus such as calorimetry, and some of the data is indirect that they first measured the hydrate equilibrium curve and then apply the Clausius-Clapeyron approach. For pure components, such as methane and carbon dioxide, the chemical potential of the particular component must be equal along the equilibrium curve, but for a complex structure like hydrate, it is not quite as insignificant, but can be done for pure hydrate former [44].

The incline in the free energy for different hydrate formers is different for mixtures of hydrate formers (such as CH_4 + CO_2, CH_4 + C_2H_6), and the different hydrate formers will have various attractions to water and different thermodynamic preferences for condensing on the surface of liquid water. So for mixtures of carbon dioxide and supercritical methane, the carbon dioxide will adsorb on the liquid water which will have a thermodynamic driving force for condensing on the water surface. Examples of this can be found in the work of Kvamme [81] where 10 mol per cent of carbon dioxide in the air result in 30 per cent of the carbon dioxide to adsorbed on the liquid water (at 30 bars and 274 K).

The concentration of carbon dioxide at the gas side interface will also suggest in super-saturation of carbon dioxide at the liquid water interface. As a result, the formed hydrate will be dominated by carbon dioxide, with small amounts of nitrogen in the small cavities. This will also be in the case of mixtures of carbon dioxide and methane.

It is the adsorbed concentrations and the chemical potentials which will determine the concentration at the liquid interface and the composition of the hydrate. For closed systems of primary composition, the most stable hydrate will form, following the 1^{st} and 2^{nd} law of thermodynamics.

These characteristics can not be calculated using the Clapeyron equation on its own. However, it can be applied in combination with a free-energy minimisation scheme. The approach using residual thermodynamic can efficiently be used for any simple or mixtures of hydrates that will form during a free-energy analysis of hydrate formation.

Anderson [44] used an equilibrium approach based on the difference in chemical potential between liquid water and empty hydrate clathrate for the calculation of the equilibrium curve, hence could not calculate outside of the equilibrium conditions.

Residual thermodynamics do not have these types of limitations and can be applied for all phases and components in all phases. Many publications use the simplified Clausius-Clapeyron equation together with experimental or calculated hydrate equilibrium curve. These approaches fail at the conditions where the condensed phase volumes become significant. Even if the temperature is presented, the missing information about the pressure makes it impossible to characterise the degree of superheating, relative to the hydrate equilibrium pressure at the provided temperature.

A conventional example can be found in the work of Kang et al. [51], who stated that the pressure was kept above the dissociation equilibrium pressure. Information regarding the level of superheating is critical in understanding how much heat is used into heating the hydrate sample and how much heat is actually being used to dissociate the sample. This is important as it is definitely not possible to dissociate a sample exactly at equilibrium conditions since that will require infinite time.

As long as both the temperature and pressure in the experiment are defined, we know for a fact that it is a non-equilibrium system. The typical equilibrium conditions are not bounded to the chemical potentials of the components in different phases (liquid, hydrate, gas), that other factors can influence the phase transitions. During hydrate dissociation, it can dissociate towards a liquid water phase that contains a lower concentration of CO_2 than the required minimum concentration for hydrate stability.

It is also possible for hydrate to dissociate towards a gas phase, which is undersaturated with water molecules. Information regarding the stirring rate is crucial since it affects the ratio of hydrate formed from gas and water vs the hydrate formed from dissolved hydrate formers in the liquid water. It can also promote supersaturation and distribution of nano and microsized bubbles of hydrate formers that have other properties than a bulk gas phase, because of the influence of shape, size and interaction with bubble walls (water).

For systems where carbon dioxide is in contact with THF enriched water, this is even more crucial. The combination of heterogeneous and homogeneous hydrates is a complex issue that makes it difficult to understand their experimental data. Even for simple, pure carbon dioxide, a huge variety of hydrates will form from gas and water, and dissolved carbon dioxide in the liquid water. The calculated solubility of carbon dioxide is plotted in Figure 5.7 on page 66, but a more detailed description can be found in the work of Kvamme et al. [57].

From each hydrate formed from a given mole fraction of carbon dioxide in the water solution, and since the filling fraction is unique, it produces a unique hydrate. These results and similar calculation can be found in the work of Kvamme [82] [25] [83].

The work of Delahaye et al. [52] is difficult to understand since they use as up to 30 wt % (weight per cent) of THF and only presents hydrate pressure and temperature curves, while much of the hydrate may form in the liquid water solution.

The composition of hydrates from these solutions might vary significantly due to the rate of stirring and the concentration of carbon dioxide and THF in the water at all times.

Because of this and the other causes of inaccuracy, their results were not used for this work, and the same goes for their work from 2004 [84] at which they reported a constant hydration number over a wide range of thermodynamic conditions.

7 Conclusions

The available experimental data of enthalpies of hydrate formation and dissociation in works of literature are minimal and commonly lack critical information necessary for interpretation. In most of the cases, the hydration number, which gives valuable information about the hydrate composition is either missing, estimated or hold constant. The degree of superheating during hydrate dissociation is also frequently missing.

Models based on the Clausius-Clapeyron approach seems to be the most popular and favourable for evaluation enthalpies of hydrate dissociation. These methods have several limitations, which have been debated in this work. The proposed method in this work is built on residual thermodynamics. Because the enthalpy change of hydrate phase change is directly connected to the change in free-energy, the enthalpy of hydrate formation and dissociation can be calculated directly.

Although this work only considered simple CH_4 and CO_2 hydrates at equilibrium conditions, there are no limitations for this approach, and it can be used for all mixtures, all components, in all phases at every condition. This implies that it can be used for non-equilibrium purposes, which is conditions outside the equilibrium. Calculation based on non-equilibrium conditions is more suitable and realistic since hydrates can never reach equilibrium in nature.

Unlike the Clapeyron approach, which is locked to equilibrium conditions, residual thermodynamics would be the best choice for calculating hydrate phase transitions. This is relevant for industries where realistic thermodynamically properties will be necessary. Production of natural gas from hydrates using CO_2 swapping requires a better understanding of the theory and is already proposed using residual thermodynamics. Transport of natural gas in pipelines is also relevant, due to nucleation of hydrate toward mineral surfaces that can cause plugging or damage to pieces of equipment.

8 Suggestion for further work

Just before working on this thesis, our research group was already working on a paper for a scientific journal. I was supposed to look for some experimental data we could use for comparison, and it was not meant to be a significant focus. That was easier said than done, but that created the objective for this master thesis. Most of the time, working on this thesis went into doing research and examining experimental data. In fact, most of the articles found were not even mention in this work. There were several reasons for this:

Most of the experimental literature ended up using either Clapeyron or Clausius-Clapeyron to calculate the final enthalpy of hydrate dissociation. Many of the estimated values, such as hydration numbers were not mentioned at all. There were different apparatus and different approaches used, and the lack of useful information during their setup or experiments made it difficult to decide if this was good enough for comparison.

A suggestion for future work would be to do more experiments with calorimetry but conducting them more precisely. Hydrates require high pressure and low temperature to form, which was and still is a challenge when performing precise measurements. Better information of the setup and the process during the experiment would be helpful, such as; Where the temperature is measured (Inside the hydrate core, just underneath the hydrate surface, in the liquid water, in the gas phase), at what pressure, concentration and time, the list goes on. Even though hydrates can never reach equilibrium, conducting these experiments close to these conditions would be a challenge, time-consuming and expensive but not impossible. Another suggestion for future work is to calculate the enthalpy changes of hydrate phase transition for mixtures of different hydrate formers.

References

1. Kvenvolden, K. A. "Gas hydrates-geological perspective and global change", *Rev.Geophys,* **1993,** *31* (2), pp: 173-187.

2. Makogon, Y. F. "Natural gas hydrates – A promising source of energy", *Journal of Natural Gas Science and Engineering,* **2010,** *2* (1), pp: 49-59.

3. Mienert, J.; Posewang, J.; Lukas, D. "Changes in the Hydrate Stability Zone on the Norwegian Margin and their Consequence for Methane and Carbon Releases Into the Oceanosphere", In *The Northern North Atlantic;* Springer: Berlin, Heidelberg, **2001**; pp 259-280.

4. Kvamme, B. "Environmentally Friendly Production of Methane from Natural Gas Hydrate Using Carbon Dioxide", *Sustainability,* **2019,** *11* (7), pp: 1964.

5. Ripmeester, J. A. "Hydrate Research-From Correlations to a Knowledge-based Discipline: The Importance of Structure", *Annals of the New York Academy of Sciences,* **2000,** *912* (1), pp: 1-16.

6. Wikipedia, Molecular dynamics: https://en.wikipedia.org/wiki/Molecular_dynamics (accessed Sept 30, 2019).

7. Tegze, G.; Pusztai, T.; Tóth, G.; Gránásy, L.; Svandal, A.; Buanes, T.; Kuznetsova, T.; Kvamme, B. "Multiscale approach to CO2 hydrate formation in aqueous solution: Phase field theory and molecular dynamics. Nucleation and growth", *J. Chem. Phys.,* **2006,** *124* (23), pp: 23410.

8. Baig, K. "Phase Field Theory Modeling of CH4 and CO2 Fluxes from Exposed Natural Gas Hydrate Reservoirs" Master of Science Thesis; University of Bergen, **2009**.

9. Kvamme, B.; Lund, A.; Hertzberg, T. "The influence of gas-gas interactions on the Langmuir-constants for some natural gas hydrates", *Fluid Phase Equilib,* **1993,** *90* (1), pp: 15-44.

10. Koh, A. C.; Sloan, E. D.; Sum, K. A.; Wu, T. D. "Fundamentals and Applications of Gas Hydrates", *Annual review of chemical and biomolecular engineering*, **2011,** *2*, pp: 237-257.

11. Speight, G. J. "Handbook of industrial hydrocarbon processes", Gulf Professional Publishing, **2011**; pp 43-83.

12. Song, Y.; Yang, L.; Zhao, J.; Liu, W.; Yang, M.; Li, Y.; Li, Q. "The status of natural gas hydrate research in China: A review", *Renewable and Sustainable Energy Reviews*, **2014,** *31*, pp: 778-791.

13. Kvamme, B.; Aromada, S. A.; Kuznetsova, T.; Gjerstad, P. B.; Canonge, P. C.; Zarifi, M. "Maximum tolerance for water content at various stages of a natuna production", *Heat and Mass Transfer*, **2018,** *55*, pp: 1059-1079.

14. Collett, T. "Natural Gas Hydrates: Vast Resource, Uncertain Future" U.S. Geological Survey, **2001**.

15. Svandal, A. "Modeling hydrate phase transitions using mean-field approaches" PhD dissertation for the Degree Philosophiae Doctor; University of Bergen, **2006**.

16. Sloan, D. E. "Natural Gas Hydrates in Flow Assurance", Gulf Professional Publishing, **2011**; pp 1-11.

17. Geomar, Why did gas hydrates melt at the end of the last ice age?: https://www.geomar.de/en/news/article/was-loeste-gashydrate-am-ende-der-letzten-eiszeit-auf/ (accessed Aug 05, 2019).

18. Aman, Z. M.; Brown, E. P.; Sloan, E. D.; Sum, A. K.; and Koh, C. A. "Interfacial mechanisms governing cyclopentane clathrate hydrate adhesion/cohesion", *Physical Chemistry Chemical Physics*, **2011,** *13* (44), pp: 19796-19806.

19. Sloan, E. D.; Koh, C. A. "Clathrate Hydrates of Natural Gases" 3rd ed., **2007**.

20. Aromada, S. A.; Kvamme, B. "Impacts of CO2 and H2S on the risk of hydrate formation during pipeline transport of natural gas", *Frontiers of Chemical Science and Engineering,* **2019,** *13* (3), pp: 616-627.

21. Kvamme, B.; Aromada, S.; Saeidi, N.; Hustache, T.; Gjerstad, P. "Hydrate nucleation, growth and induction", *ACS Omega*, **2019,** Submitted, waiting for acceptation.

22. Chejara, A. K. "Gas hydrates in Porous Media:CO2 Storage and CH4 Production" PhD dissertation for the Degree Philosophiae Doctor; University of Bergen, **2014**.

23. Lievois, J. S.; Perkins, R.; Martin, R. J.; Kobayashi, R. "Development of an Automated, High Pressure Heat Flux Calorimeter and its application to measure the heat of dissociation and Hydrate Number of Methane Hydrate", *Fluid Phase Equilib.,* **1990,** *59,* pp: 73-97.

24. Polte, J. "Fundamental growth principles of colloidal metal nanoparticles – a new perspective", *CrystEngComm,* **2015,** *17* (48), pp: 6809-6830.

25. Kvamme, B. "Kinetics of Hydrate Formation From Nucleation Theory", *International Journal of Offshore and Polar Engineering,* **2002,** *12* (4).

26. Christiansen, R. L.; Sloan, E. D. "Mechanisms and Kinetics of Hydrate Formation", *Annals of the New York Academy of Sciences,* **1994,** *715,* pp: 283-305.

27. Kvamme, B. "A new Theory for The Kinetics of Hydrate Formation", *2nd International Conference on Natural Gas Hydrates,* **1996,** pp: 131-146.

28. Englezos, P.; Kalogerakis, N.; Dholabhai, P. D.; Bishnoi, P. R. "Kinetics of formation of methane and ethane gas hydrates", *Chemical Engineering Science,* **1987,** *42,* pp: 2647-2658.

29. Skovborg, P.; Rasmussen, P. "A mass transport limited model for the growth of methane and ethane gas hydrates", *Chemical Engineering Science,* **1994,** *49,* pp: 1131-1143.

30. Kvamme, B.; Graue, A.; Buanes, T.; Kuznetsova, T.; Ersland, G. "Storage of CO2 in natural gas hydrate reservoirs and the effect of hydrate as an extra sealing in cold aquifers.", *Int. J. Greenhouse Gas Control*, **2007,** *1*, pp: 236-246.

31. Kvamme, B.; Coffin, R. B.; Zhao, J.; Wei, N.; Zhou, S.; Li, Q.; Saeidi, N.; Chien, Y.; Dunn-Rankin, D.; Sun, W.; Zarifi, M. "Stages in the Dynamics of Hydrate Formation and Consequences for Design of Experiments for Hydrate Formation in Sediments", *Energies*, **2019,** *12*.

32. Wikipedia, Phase (matter): https://en.wikipedia.org/wiki/Phase_(matter) (accessed Sept 05, 2019).

33. Tester, J. W.; Modell, M. "Thermodynamics and Its Applications" 3rd ed. Prentice Hall, **1997**.

34. Modell, M.; Reid, R. "Thermodynamics and Its Applications" 2nd ed. Prentice Hall, **1983**.

35. Aromada, S. "New concept for Evaluating the Risk of Hydrate Formation during Processing and Transport of Hydrocarbons" Master of Science Thesis; University of Bergen, **2017**.

36. Kvamme, B.; Aromada, S. A. "Risk of Hydrate Formation during the Processing and Transport of Troll Gas from the North Sea", *J. Chem. Eng. Data*, **2017,** *62* (7), pp: 2163-2177.

37. Soave, G. "Equilibrium constants from a modified Redlich-Kwong equation of state", *Chem. Eng. Sci*, **1972,** *27*, pp: 1192-1203.

38. Wikipedia, Van der Waals equation: https://en.wikipedia.org/wiki/Van_der_Waals_equation (accessed Sept 09, 2019).

39. Bauman, J. M. "Kinetic Modelling of Hydrate Formation, Dissociation, and Reformation" PhD; University of Bergen, **2015**.

40. Kvamme, B.; Tanaka, H. "Thermodynamic Stability of Hydrates for Ethane, Ethylene, and Carbon Dioxide", *J. Phys. Chem.*, **1995,** *99*, pp: 7114-7119.

41. Karlekar, B. V. "Thermodynamics for engineers", Englewood Cliffs, N.J. : Prentice-Hall, **1983**.

42. Kvamme, B.; Aromada, S. A.; Gjerstad, P. B. "Consistent enthalpies of hydrate formation and dissociation using residual thermodynamics", *Chem.Eng.Data,* **2019,** *64,* pp: 3493-3504.

43. Gupta, A.; Lachance, J.; Sloan, E. D.; Koh, C. A. "Measurements of methane hydrate heat of dissociation using high pressure differential scanning calorimetry", *Chem. Eng. Sci.,* **2008,** *63,* pp: 5848-5853.

44. Anderson, G. K. "Enthalpy of dissociation and hydration number of carbon dioxide hydrate from the Clapeyron equation", *J. Chem. Therm,* **2003,** *35,* pp: 1171-1183.

45. Handa, Y. P. "Compositions, enthalpies of dissociation, and heat capacities in the range 85 to 270 K for clathrate hydrates of methane, ethane and propane, and enthalpy of dissociation of isobutene hydrate, as determined by a heat-flow calorimeter", *J. Chem. Therm.,* **1986,** *18,* pp: 915-921.

46. Borgnakke, C.; Sonntag, R. E. "Fundamental of Thermodynamics" 8th ed. Wiley, **2013**.

47. Koretsky, M. D. "Engineering and Chemical Thermodynamics" 2nd ed. Wiley, **2013**.

48. van der Waals, J. H.; Platteeuw, J. C. "Validity of Clapeyron's Equation for Phase Equilibria involving Clathrates", *Nature,* **1959,** *183,* pp: 462.

49. Anderson, G. K. "Enthalpy of dissociation and hydration number of methane hydrate from the Clapeyron equation", *J. Chem. Thermo.,* **2004,** *36,* pp: 1119-1127.

50. Nakagawa, R.; Hachikubo, A.; Shoji, H. "Dissociation and specific heats of gas hydrates under submarine and sublacustrine enviroments", *The 6th International Conference on Gas Hydrates (ICGH),* Vancouver, Canada, **2008**.

51. Kang, S. P.; Lee, H.; Ryu, B. J. "Enthalpies of Dissociation of Clathrate Hydrates of Carbon Dioxide, Nitrogen, (Carbon Dioxide + Nitrogen), and (Carbon Dioxide + Nitrogen + Tetrahydrofuran)", *J. Chem. Therm,* **2001,** *33,* pp: 513-521.

52. Delahaye, A.; Fournaison, L.; Marinhas, S.; Chatti, I.; Petitet, J.- P.; Dalmazzone, D.; Fürst, W. "Effect of THF on Equilibrium Pressure and Dissociation Enthalpy of CO2 Hydrates Applied to Secondary Refrigeration", *Ind. Eng. Chem. Res.*, **2006,** *45*, pp: 391-397.

53. Kuznetsova, T.; Kvamme, B. "Grand canonical molecular dynamics for TIP4P water systems", *Molecular Phys.,* **1999,** *97*, pp: 423-431.

54. Kvamme, B.; Graue, A.; Aspenes, E.; Kuznetsova, T.; Gránásy, L.; Tóth, G.; Pusztai, T.; Tegze, G. "Kinetics of solid hydrate formation by carbon dioxide: Phase field theory of hydrate nucleation and magnetic resonance imaging", *Phys. Chem. Chem. Phys.,* **2004,** *6,* pp: 2327-2334.

55. Kvamme, B.; Førrisdahl, O. K. "Polar guest-molecules in natural gas hydrates", *Fluid Phase Equilib,* **1993,** *83*, pp: 427-435.

56. Kuhs, W. F.; Chazallon, B.; Klapproth, A.; Pauer, F. "Filling isotherms in clathrate hydrates", *The Review of High Pressure Science and Technology,* **1998,** *7,* pp: 1147-1149.

57. Kvamme, B.; Selvåg, J.; Saeidi, N.; Kuznetsova, T. "Methanol as hydrate inhibitor and hydrate activator", *Phys.Chem.Chem.Phys,* **2018,** *20* (34), pp: 21968-21987.

58. Kvamme, B. "Enthalpies of Hydrate Formation from Hydrate Formers Dissolved in Water", *Energies*, **2019,** *12* (6), pp: 1039.

59. Kvamme, B.; Kuznetsova, T.; Bauman, J. M.; Sjöblom, S.; and Kulkarni, A. A. "Hydrate Formation during Transport of Natural Gas ContainingWater and Impurities", *Journal of Chemical & Engineering Data,* **2016,** *61,* pp: 936-649.

60. Kvamme, B.; Aromada, S. A. "Alternative Routes to Hydrate Formation during Processing and Transport of Natural Gas with a Significant Amount of CO2:Sleipner Gas as a Case Study.", *J.Chem.Eng.Data,* **2018,** *63,* pp: 832-844.

61. De Roo, J.; Peters, C.; Lichtenthaler, R.; Diepen, G. "Occurrence of methane hydrate in saturated and unsaturated solutions of sodium chloride and water in dependence of temperature and pressure", *AIChE J,* **1983,** *29*, pp: 651-657.

62. Nakamura, T.; Makino, T.; Sugahara, T.; Ohgaki, K. "Stability boundaries of gas hydrates helped by methane—structure-H hydrates of methylcyclohexane and cis-1, 2-dimethylcyclohexane", *Chem. Eng. Sci,* **2003,** *58,* pp: 269-273.

63. Kvamme, B. "Fundamentals of Natural Gas Hydrates and Practical Implications" Unpublished Work: PTEK 232, Course Material; Department of Physics and Technology, University of Bergen, Norway: Bergen, **2018,** spring semester.

64. Saeidi, N.; Kvamme, B.; Rankin, D. D. "Strategies for Energy Production from Natural Gas Hydrates and Safe Long Terms Storage of CO2", *Conference: 12th International Methane Hydrate Research and Development Conference*, Chengdu Shi, Sichuan Sheng, China, **2018**.

65. Buanes, T.; Kvamme, B.; Svandal, A. "Computer simulation of CO2 hydrate growth", *Journal of Crystal Growth,* **2006,** *287,* pp: 491-494.

66. Lirio, C.; Pessoa, F. "Enthalpy of dissociation of simple and mixed carbon dioxide clathrate hydrate", *Chem.Eng.Trans*, **2013,** *32,* pp: 577-582.

67. Angus, S.; Armstrong, B.; de Reuck, K. M. "International Thermodynamic Tables of the Fluid State-5 Methane", Pergamon Press: Oxford, New York, **1978**.

68. Parrish, W. R.; Prausnitz, J. M. "Dissociation pressures of gas hydrates formed by gas mixtures", *Ind.Eng.Chem.Process Des.Dev.,* **1972,** *11,* pp: 26-35.

69. Sloan, E. D. "Clathrate Hydrates of Natural Gases", Marcel Dekker: New York, **1998**; pp 314-318.

70. Roberts, O. L.; Brownscombe, E. R.; Howe, L. S.; Ramser, H. "Constitution diagrams and composition of methane and ethane hydrates", *Oil Gas J,* **1940,** *39,* pp: 37-43.

71. Glew, D. N. "Aqueous nonelectrolyte solutions. Part XVIII.Equilibrium pressures of two methane hydrates with water. Formulae and dissociation thermo-dynamic functions for the structures I and II methane hydrates", *Can.J.Chem.,* **2002,** *80,* pp: 418-439.

72. Deaton, W. M.; Frost, E. M. . J. "Gas hydrate composition and equilibrium data", *Oil Gas J.,* **1946,** *45,* pp: 170-178.

73. Circone, S.; Kirby, S. H. "Direct measurement of methane hydrate composition along the hydrate equilibrium boundary ", *J.Phys.Chem.B,* **2005,** *109,* pp: 9468-9475.

74. Dickens, G. R.; O'Neil, J. R.; Rea, D. K.; Owen, R. M. "Dissociation of oceanic methane hydrates as a cause of the carbon isotope excursion at the end of the paleocene", *Paleoceanography,* **1995,** *10* (6), pp: 965-971.

75. Dymond, J. H.; Smith, E. B. "The Virial Coefficients of Pure Gases and Mixtures", Clarendon Press: London, **1980**.

76. Wilhelm, E.; Battino, R.; Wilcock, R. J. "Low-pressure solubility of gases in liquid water", *Chem.Rev.,* **1977,** *77,* pp: 219-262.

77. Sabil, K. M.; Witkamp, G. J.; Peters, C. J. "Estimations of enthalpies of dissociation of simple and mixed carbon dioxide hydrates from phase equilibrium data", *Fluid Phase Equilib.,* **2010,** *290,* pp: 109-114.

78. Sloan, E. D.; Fleyfel, F. "Hydrate dissociation enthalpy and guest size", *Fluid.Phase.Equilib,* **1992,** *76,* pp: 123-140.

79. Udachin, K. A.; Ratcliffe, C. I.; Ripmeester, J. A. "Structure, composition, and thermal expansion of CO2 hydrate from single crystal X-ray diffraction measurements", *J.Phys.Chem. B,* **2001,** *105,* pp: 4200-4204.

80. Yoon, J. H.; Yamamoto, Y.; Komai, T.; Haneda, H.; Kawamura, T. "Rigorous approach to the prediction of the heat of dissociation of gas hydrates", *Ind.Eng.Chem.Res,* **2003,** *42,* pp: 1111-1114.

81. Kvamme, B. "Thermodynamic limitations of the CO2/N2 mixture injected into CH4 hydrate in the Ignik Sikumi field trial", *J.Chem.Eng.Data,* **2016,** *61* (3), pp: 1280-1295.

82. Kvamme, B. "Droplets of Dry Ice and Cold Liquid CO2 for Self-Transport of CO2 to Large Depths", *Int.J.Offshore Polar Eng,* **2003,** *13,* pp: 139-146.

83. Kvamme, B. "Initiation and Growth of Hydrate", *Ann.N.Y.Acad.Sci,* **2000,** pp: 496-501.

84. Fournaison, L.; Delahaye, A.; Chatti, I.; Petitet, J. P. "CO2 Hydrates in Refrigeration processes", *Ind.Eng.Chem.Res,* **2004,** *43,* pp: 6521-6526.

Appendix A:

Maximum tolerance for water content at various stages of a natuna production

Bjørn Kvamme, Solomon Aforkoghene Aromada, Tatiana Kuznetsova, Petter Berge Gjerstad, Pablo Charles Canonge, Mojdeh Zarifi.

Heat and Mass Transfer, 2018

Heat and Mass Transfer (2019) 55:1059–1079
https://doi.org/10.1007/s00231-018-2490-4

ORIGINAL

Maximum tolerance for water content at various stages of a natuna production

Bjørn Kvamme[1] · Solomon Aforkoghene Aromada[1] · Tatiana Kuznetsova[1] · Petter Berge Gjerstad[1] · Pablo Charles Canonge[1] · Mojdeh Zarifi[1]

Received: 12 March 2018 / Accepted: 24 September 2018 / Published online: 3 October 2018

Abstract
Though the Natuna field in offshore Indonesia contains natural gas resources, its CO_2 content exceeds 70%. While existing technologies can handle the separation challenges, the question of CO_2 transport and storage will still remain due to the lack of aquifer storage sites with sufficient sealing integrity in this part of South Asia. Substantial occurrences of natural gas hydrates have been discovered in offshore Indonesia roughly 700 miles from Natuna, making the pipeline transport economically feasible. This work aimed to assess the risk of hydrate formation during this transport as evaluated by two different approaches: traditional method based on water dew-point versus evaluation accounting for alternative routes of hydrate formation. The hydrate risk analysis was also conducted for produced natural gas at transport conditions. We have investigated the case study involving using the separated CO_2 for simultaneous safe long-term storage of CO_2 and release of methane for in situ hydrates located at the North Makassar Basin in offshore Indonesia. Utilization of CO_2 will require additive gases to increase gas permeability and reduce the blocking of sediments by new CO_2-dominated hydrate. This analysis was conducted for variable content of nitrogen and H_2S. We have concluded that the water dew-point-based method appears to severely underestimate the risk of hydrate formation; the maximum water concentration it allows in gas will be larger by a factor of eighteen than the one permitted by approaches that used water adsorption on hematite (rust) as the criterion.

Nomenclature

T	Temperature [K]
T_c	Critical temperature [K]
P	Pressure [bar or kPa]
μ	Chemical potential [kJ/mol]
H	Hydrate phase
ΔG	Free energy change
G	Free energy change [kJ/mol]
P	Parent phase
R	Universal Gas Constant [kJ/(K mol)]
$\varnothing$	Fugacity coefficeint
γ	Activity coefficient
$\vec{x}$	Mole fraction of liquid
$\vec{y}$	Mole fraction of gas
h_{ij}	Canonical cavity partition function of component j in cavity type i
Δg_{ij}^{inc}	Free energy of inclusion of the guest molecules j in the cavity i
θ_{ij}	Filling fraction of component j in cavity type i
β	Inverse of gas constant times temperature
x_T	Total mole fraction of all guests in the hydrate

1 Introduction

Hydrocarbons being transported to the processing plant for treatment are always accompanied by reservoir water. Under certain conditions, the water presence in natural gas mixtures during processing and transport gives rise to serious hydrate formation concerns. At high pressures and low temperatures, it can be thermodynamically beneficial for water molecules to form ice-like lattices (three-dimensional structures) with cavities encaging molecules of hydrocarbons and volatile liquids as well as certain inorganics like carbon dioxide and hydrogen sulphide (guest molecules). The resulting nonstoichiometric crystalline compounds are often referred to as clathrate

✉ Tatiana Kuznetsova
tatyana.kuznetsova@uib.no

[1] Department of Physics and Technology, University of Bergen, Allegaten 55, 5007 Bergen, Norway

hydrates or natural gas hydrates. Hydrate can grow to plug processing equipment and transport pipeline. In this work, we have evaluated the risk of hydrate formation based on the upper limit of water content that can be permitted in a multicomponent natural gas mixture with substantial amount of carbon dioxide. The Natuna gas field contains more than 70% of CO_2 and as such makes for a good case study of hydrate formation risk during the transport of CO_2 and hydrocarbons. The potential for simultaneous utilization and safe long terms storage of CO_2 in the natural gas hydrate coastal fields of Indonesia is a fascinating opportunity.

Several unit operations commonly employed in natural gas processing involve thermodynamic conditions that could give rise lead to hydrate formation. Processes that lead to increasing pressure and/or decreasing temperature can in many cases bring the fluid phases (CO_2, hydrocarbons) into hydrate formation region if free water is either available outright or can drop out from the fluid. Examples are turbines where gas expands and cools down, as well as low-temperature separators and compressors. The Natuna field has the advantage of not being very far from mainland Indonesia. From a long-term production perspective, 700 miles of pipeline transport for utilization and storage of CO_2 is certainly economically feasible. Moreover, the presence of offshore methane hydrates fields provides a storage option for the excessive CO_2 produced by the gas field. The seafloor temperatures in the area between Natuna and mainland Indonesia typically vary between 274 K and 283 K, with the pipeline transport from Natuna to onshore Indonesia involving pressures between 50 and 300 bars. A substantial portion of this thermodynamic range will fall inside the hydrate formation zone if free water becomes available by either dropping out from as liquid water or being adsorbed on rusty pipeline walls. A direct hydrate formation from water dissolved in fluid is possible but highly unlikely due to substantial limitation in mass transport and transport of released heat. As will be discussed in more detail later, studies available in open literature indicate that the presence of hematite significantly lowers the level of water tolerated during transport without invoking the risk of hydrate formation.

Determining the maximum water tolerance for gas being processed or transported is one of the critical parameters when it comes to design of drying facilities, whether solvent based (glycols is most common) or adsorption based (zeolites for instance).

Hydrate formation occurring in a system composed of natural gas with substantial admixture of impurities, for example water and carbon dioxide, will be a complex process involving competition between different phase transition mechanisms and routes, with both kinetics and thermodynamics playing significant roles. Conventional techniques currently used in industry to evaluate the risk of hydrate formation assume that hydrate will form when water drops out of the gas stream during processing or transport. Therefore, this method involves estimating the dew-point temperature of natural gas mixtures in question. We refer to this approach as water drop-out or dew-point route to hydrate formation. However, the problem with this approach is that absolutely disregards that the presence of rust on the inside of pipeline walls and processing equipment will provide sites for water adsorption and consequently offer an alternative route for hydrate formation (the hematite route, hematite being the most dominant and one of the most thermodynamically stable forms of rust).

The problem grows in complexity [1] due to the fact that in an industrial setting like pipeline transport and processing, hydrate formation from natural gas cannot successfully attain equilibrium, as a result of limitations imposed by either Gibbs phase rule or mass and heat transport. The Gibbs phase rule is given as: $\tau = n - \pi + 2$. Here, τ refers to the degrees of freedom, which is the number of defined independent thermodynamic variables in the system, and π represents the number of actively coexisting phases, while n is the number of active components in terms of hydrate phase transitions. If we choose a simple scenario with only a single hydrate forming guest molecule present in the system containing bulk gas and water, say methane and water, with the existence of a hydrate nucleus, we will have three actively coexisting phases ($\pi = 3$) and two actively components ($n = 2$). And according to the Gibbs phase rule, the degrees of freedom should be just one ($\tau = 1$) for the system to reach equilibrium. But the system will never attain equilibrium because for a real industrial case involving flowing stream, hydrodynamics and hydrostatics including phase transitions which involves heat exchange, the fact that local pressure and temperature are specified. This means that even the simplest system with one guest molecule equilibrium (methane) can never achieve equilibrium. Furthermore, mass transport limitation and low concentration of water in methane could hinder hydrate crystal nucleus from ever attaining the critical size, thus preventing stable growth from even commencing.

Heat transport is yet another problem that can compound the issue of hydrate growth. Methane is a bad thermal conductor compared to liquid water clusters and hydrate before hydrate is formed [1], this means that transporting the exothermic heat of hydrate formation away from the system will become a challenge that could also critically restrict hydrate formation rate. Solid surfaces will also indirectly affect formation of hydrate; for instance, hydrate formation occurring on the interface between methane-rich gas and the aqueous phase adsorbed on solid wall surfaces covered with rust. This possible impact of water-wetting surfaces on the phase transitions should not be ignored just because the gas phase will dominate as far as the mass is concerned [1]. Hydrate nucleation and growth may take place either when both water and hydrate formers are adsorbed on the rusty surface or when water alone is present in the adsorbed phase, and hydrate former species are imported from the methane-rich phase. Hydrate formation will not occur directly on hematite surfaces due to

incompatibility between charge distribution in hydrate water lattice and hematite surface. Nevertheless, hematite will effectively function as a catalyst that removes water from the bulk gas via adsorption, thereby providing a separate water phase for hydrate formation, which will occur just outside the first two or three tightly structured water layers.

Thermodynamically, there exists a third possible pathway to hydrate formation. It involves hydrate forming directly from water dissolved in the natural gas stream. But the low concentration of water in the bulk gas combined with heat and mass transport limitations will make it highly improbable for hydrate to form via this pathway. Therefore, this alternative pathway has been left out of consideration in this work. Nevertheless, if surface stress from flow does not impact on water/hydrocarbon system at all, a quick formation of hydrate film on the water/hydrocarbon interface can take place, which will very rapidly block further transport of molecules of hydrate formers and waters through the hydrate film (extremely low diffusivity). Therefore, hydrate will form from the hydrate formers dissolved in water, and could also form from water dissolved in gas, which then would take advantage of nucleation on the hydrate surface. However, in case of flow with turbulent shear forces present, this situation is not feasible. Another difference between a flowing case and a case of a stationary constant volume and constant mass laboratory experiment is that new mass is supplied continuously. Consequently, the limiting situation where the water is completely consumed thus stopping hydrate formation will never happen.

This paper presents the application of our novel thermodynamic scheme for investigation of different routes to hydrate formation, utilizing ideal gas as reference state for all components in all phases including hydrate phase. We apply this scheme to determine the upper limit of water content that could be tolerated in a multicomponent natural gas with a substantial amount of CO_2 (Natuna gas as a case study) without the risk of hydrate formation during processing and transport. Two alternative pathways to hydrate formation, the traditional dew-point route approach and that facilitated by water adsorption on hematite-covered surfaces inside process equipment and pipeline are discussed below.

Using CO_2 for simultaneous safe long terms storage of CO_2 and release of methane from *in situ* hydrates is one alternative use for the substantial amount of CO_2 produced at the Natuna field. The conversion between methane hydrate and CO_2-dominated hydrate is made viable by two primary mechanisms. A solid-state exchange is possible but will be extremely slow and thus of limited practical importance. The second mechanism will involve the formation of new hydrate from injected CO_2, with heat released by the formation process assisting in dissociation of *in situ* methane hydrate. The formation of new hydrate from injected CO_2 will be an extremely fast process and can potentially plug the reservoir. In addition, the permeability of CO_2 injected into water wetting reservoir is quite low. One way to circumvent these limitations is to add nitrogen to the injection gas. For instance, injection gas used in the Ignik Sikumi experiment in Alaska [2] even consisted of 77.5% N_2 by volume. A drawback of adding such high fraction of N_2 is the dramatic impact it can have on the thermodynamics of new CO_2 hydrate formation. In the worst-case scenario, the injection mixture may become too lean in CO_2 to create a new hydrate. In this limit, the system will have to proceed via the very slow solid-state exchange process, while a number of other phase transitions contributing to dissociation of in-situ methane hydrate may occur in the meantime. These transitions include hydrate dissociation when exposed to a N_2 rich phase and water under-saturated with methane. A substantial portion of accumulated methane released in the above-mentioned pilot experiment was likely due to the pressure reduction period. It is therefore hard to extract from the data how much CH_4 that were converted due to CO_2. In view of the low concentrations of CO_2 in the injected gas and other phase transitions that consume CO_2 (solution in water, adsorption of CO_2 on minerals). Various laboratories around the world has also conducted experiments on the exchange process but experimental set-up and conditions are frequently far away from a real situation in nature, including the fact that most of these available experimental data were conducted in equipment with tight temperature control. Since the most efficient conversion mechanism involves the formation of a new hydrate and dissociation of the methane hydrate due to released heat from this new formation of CO_2 dominated hydrate. Heat exchange with an external cooling system will therefore interfere with the natural mechanism. On top of this there are all the usual limitations of imitating a natural hydrate system which exposed to flow (diffusion to hydrodynamics depending on connection to fracture systems),

Table 1 Composition of the original gas from Natuna gas-field

Gas	Mole fraction
CO_2	0.710
CH_4	0.270
C_2H_6	0.010
N_2	0.010

Table 2 Composition of the CH_4-rich gas stream

Gas	Mole fraction
CH_4	0.940
C_2H_6	0.035
CO_2	0.025

Table 3 Composition of the CO_2-rich gas stream

Gas	Mole fraction
CO_2	0.982
N_2	0.014
CH_4	0.004

geochemistry and fluid/hydrate/mineral interactions which are different from the experimental set-up. And since these hydrate systems can never reach thermodynamic equilibrium they exist in a stationary that has developed over geological time scales that is impossible to reproduce over limited time in a laboratory set-up.

The second part of this study has been therefore focused on the examination of thermodynamic stability limits governing the formation of hydrate from various mixtures of CO_2 and N_2 as related to a particular hydrate field example in offshore Indonesia. A comprehensive examination of all of the hydrate occurrences in that are lay well beyond the scope of this work; our choice of example also reflects the varying scope and quality of data available in the open literature.

2 Natuna gas reservoir

The gas composition of the Natuna Gas Reservoir is dominated by a very high content of CO_2. According to [3], the gas consists of approximately 71% carbon dioxide, 27% methane, 1% ethane and heavier hydrocarbons (approximated as ethane), and 1% nitrogen and hydrogen sulphide combined. While hydrogen sulphide is an aggressive hydrate former, a tiny fraction of H_2S (less than 1%) will have only a limited impact on either the water dew-point and the maximum water content before drop-out due to adsorption on hematite. Rough estimates of conditions relevant for transport from Natuna to onshore Indonesia indicate that temperatures (below 280 K for seafloor pipeline transport) and pressures (between 50 and 300 bar) will fall inside the hydrate formation region. A critical question thus arises concerning the lowest fraction of water that will trigger either water condensation or adsorption on rusty pipe walls. In view of this, Table 1 presents gas composition chosen to model the gas stream being transported to land for separation.

Typically, the maximum CO_2 content of sales gas is limited to 2.5%. The acceptable loss levels of hydrocarbons in the separated CO_2 stream will be highly dependent on the separation method and costs versus increased value per extra unit of methane recovered. It will be desirable to separate as much of the methane as possible from the other gasses. Assuming that all N_2 will follow CO_2, and all ethane will follow the CH_4-rich phase resulted in the model systems for separated phases given in Tables 2 and 3 below.

3 Fluid thermodynamics

In equilibrium, temperatures, pressures, and chemical potentials of all coexisting phases must be the same across all phase boundaries. Though the equilibrium is unattainable in practice, applying a quasi-equilibrium method will help us to evaluate the thermodynamic advantages of different pathways to formation/dissociation of hydrate as asymptotic stability limits for each given phase transition. The residual thermodynamics approach will be applied for all components and all phases (hydrate, liquid water, aqueous phases, ice) through the use of the Soave–Redlich–Kwong (SRK) equation of state [4]. Parameters required by the SRK have been mostly supplied by molecular dynamics simulations involving water in different phases (empty hydrates, liquid water, and ice) [5].

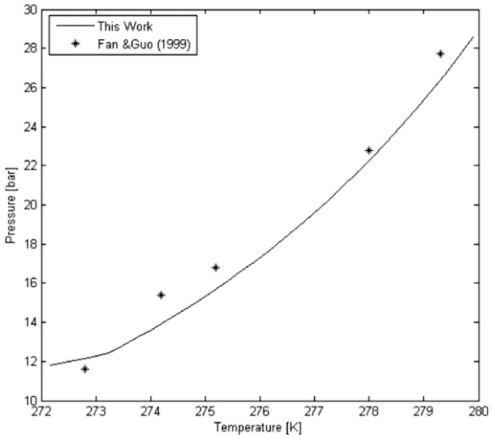

Fig. 1 Estimated equilibrium pressures for hydrate formed from a gas mixture containing 88.53 mol% of CO_2, 6.83 mol% of CH_4, 0.38 mol% C_2H_6 and 4.26 mol% of N_2 compared to experimental data [11] [

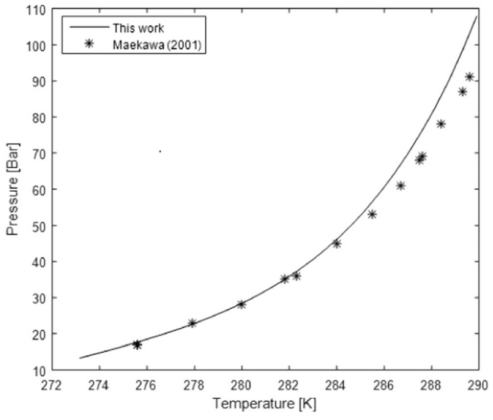

Fig. 2 Estimated equilibrium pressures for hydrate formed from a gas mixture containing 90.2 mol% of CH_4 and 9.8 mol% of C_2H_6 compared to experimental data [12]

In equilibrium systems, both phase distributions and compositions can be evaluated by means of free energy minimization. Provided that thermodynamic models are available, it is not a critical issue to choose a reference state for different components in different phases for equilibrium systems. However, in non-equilibrium systems, the most favourable local phase distributions, together with the thermodynamic driving forces encouraging each component to move across the phase boundaries from one phases to another can be determined by a free energy analysis. It is convenient in this case to use ideal gas as the reference state to ensure same reference values for free energy of every phase present in the estimation of the chemical potential of all components, irrespective of the phase as presented in Eq. (1):

$$\mu_j\left(T,P,\overrightarrow{y}\right)-\mu_j^{ideal\ gas}\left(T,P,\overrightarrow{y}\right)=R.T.ln\varnothing_j\left(T,P,\overrightarrow{y}\right)$$
$$\lim\left(\varnothing_i\right)\to 1.0\ldots\text{for ideal gas} \tag{1}$$

Where $\varnothing_i$ refers to the fugacity coefficient for component j in given phase; $\overrightarrow{y}$ is the gas mole fraction vector. The chemical potential of the ideal gas comprises the trivial mixing term since ideal gas mixing of gases at constant pressure.

Another reference state is used to evaluate the chemical potential of component j as an intermediate step for the liquid state. It is given in Eq. (2) below generally known as symmetric excess. This equation involves the ideal liquid term (chemical potential) as well including the trivial ideal mixing term together with the pure liquid value.

$$\mu_j\left(T,P,\overrightarrow{x}\right)+\mu_j^{ideal\ liquid}\left(T,P,\overrightarrow{x}\right)=R.T.ln\gamma_j\left(T,P,\overrightarrow{x}\right)$$
$$\lim\left(\gamma_j\right)\to 1.0\text{ when }xj\to 1.0 \tag{2}$$

where γ_j is the activity coefficient for component j in the liquid mixture. When applying Eq. (2) to water, the ideal gas reference state can suitably be applied too when the chemical potential of pure liquid water is evaluated from molecular interaction models by means of molecular dynamics (MD) simulations. In this work we have utilized data from [5].

In case of gas components with low solubility in water, like the hydrocarbons in consideration, the "infinite dilution" of gas in water will make for a more suitable liquid reference state. Therefore, the asymmetric excess formulation in Eq. (3) will be appropriate. It is called asymmetric excess because the activity coefficient limit of the component j tends to one as the mole fraction vanishes as shown below:

$$\mu_j^{H_2O}\left(T,P,\overrightarrow{x}\right)+\mu_j^{H_2O,\infty}\left(T,P,\overrightarrow{x}\right)$$
$$=R.T.ln\left[x_j^{H_2O}.\gamma_j^{H_2O,\infty}\left(T,P,\overrightarrow{x}\right)\right]\lim\left(\gamma_j^{H_2O,\infty}\right)\text{ when }xj\to 0 \tag{3}$$

Where $\mu_j^{H_2O}$ is the chemical potential of component j in water; ∞ stands for infinite dilution; $\gamma_j^{H_2O,\infty}$ is activity coefficient of component j in aqueous phase based on the same reference state; R is the universal gas constant. In practice, the evaluation of infinite dilution chemical potential with ideal gas as the reference state can be be achieved by means of molecular dynamics (MD) simulations and application of the Gibbs −Duhem relation [6, 7], contingent on thermodynamic properties of all phases can also be specified and evaluated outside of equilibrium. The combination of the first and the second laws of thermodynamics requires that both available mass of every component as well as the overall mass will have to be distributed over all possible phases coexisting under specific local pressure and temperature conditions. This evaluation is quite straightforward for most of the fluid phases of interest, with the hydrate phase being somewhat an exception and needing a special consideration; it has however been comprehensively evaluated in Kvamme et al. [7, 8]. Thus, the minimization of free energy and obtaining values for the local phase distributions becomes possible through combining thermodynamic formulations for fluids in Eqs. (1), (2) and (3) with hydrate nonequilibrium formulations from Kvamme et al. [7, 8]. A number of algorithms capable of implementing this approach are available in the open literature.

Except for the hydrate phases, all the relevant pressures and temperatures will refer to a liquid state. All the situations considered in this work involve very low mutual solubilities and/or low concentrations. The following approximation in Eq. (4) should therefore prove satisfactorily accurate for most industrial applications where hydrate formation is a risk factor:

$$\mu_j^i\left(T,P,\overrightarrow{x}\right)\approx\mu_j^{i,\infty}\left(T,P,\overrightarrow{x}\right)$$
$$+R.T.ln\left[x_j^i.\gamma_j^{i,\infty}\left(T,P,\overrightarrow{x}\right)\right] \tag{4}$$

Here the subscript i distinguish between different phases with low solubility and subscript j refers to different components.

4 Thermodynamics of hydrate: model description and verification

The chemical potential of water in hydrate can be evaluated using the statistical mechanical model for water in hydrate, which is a typical Langmuir type of adsorption model. We used the version presented in Kvamme & Tanaka [5] given in Eq. (5). Unlike that of van der Waal and Platteuw (1959) [9], the Kvamme & Tanaka [5] form considers the lattice movements and corresponding effects of different guest molecules; it takes into account collisions between guest

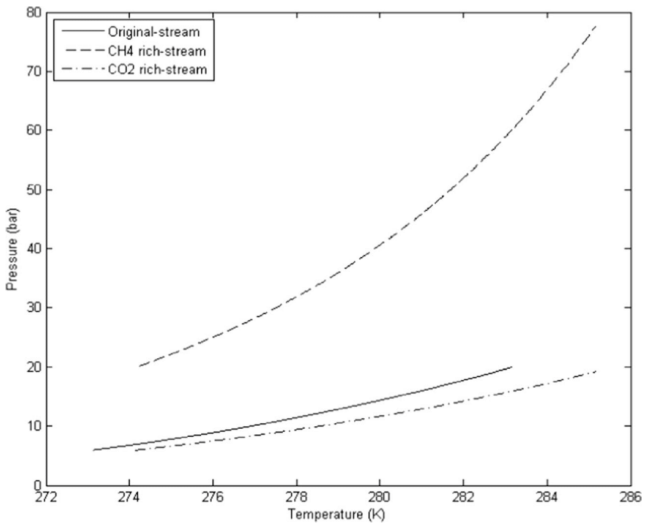

Fig. 3 Hydrate equilibrium pressures for the original Natuna gas mixture (solid), CH_4-rich gas (dash) and CO_2-rich gas (dash-dot) streams

molecules and water sufficiently strong to affect the water motion. A rigid lattice is presumed by the van der Waal and Platteuw (1959) [9] model, it assumes that the guest j does not affect water movements in the lattice.

$$\mu_{H_2O}^{(H)} = \mu_{H_2O}^{(0,H)} - \sum_{i=1}^{2} R.T.v_i.ln\left(1 + \sum_{j=1}^{n_{guest}} h_{ij}\right) \tag{5}$$

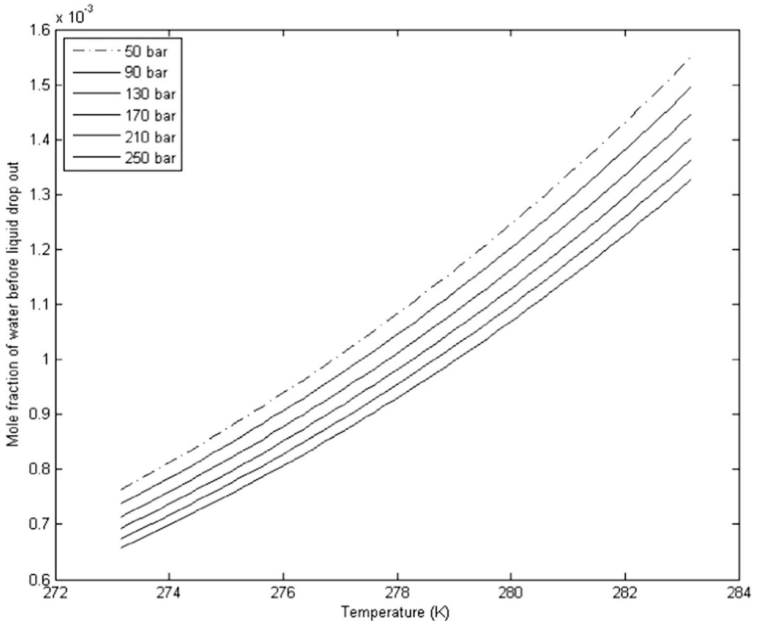

Fig. 4 Maximum concentration of water that can be permitted in Natuna gas before liquid water drops out. Curves from top to bottom correspond to pressure of 50 bar, 90 bar, 130 bar, 170 bar, 210 bar and 250 bar respectively

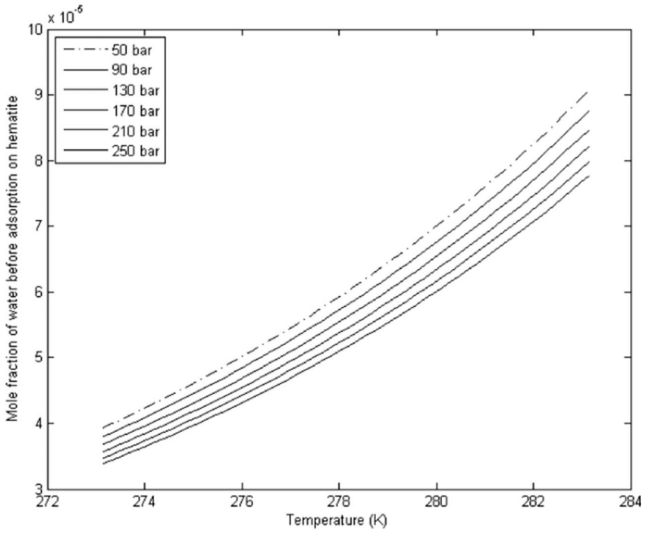

Fig. 5 Maximum concentration of water that can be permitted in Natuna gas before water is adsorbed on hematite. Curves from top to bottom correspond to pressure of 50 bar, 90 bar, 130 bar, 170 bar, 210 bar and 250 bar respectively

Where H denotes to hydrate phase; $\mu_{H_2O}^{(H)}$ refers to the chemical potential of water in hydrate; $\mu_{H_2O}^{(0,H)}$ is the chemical potential of water in empty clathrate structure; v_i refers to the fraction of cavity type i per water molecule. The unit cell of hydrate of structure I is composed of forty-six water molecules. Structure I hydrate has two small and six large cavities, consequently, $v_{small\ cavity} = 1/23$ and $v_{large\ cavity} = 3/23$. h_{ij} is the canonical cavity partition function of component j in cavity type i. n_{guest} stands for number of guest molecules in the system. Equation (6) is used to evaluate the canonical partition function:

$$h_{ij} = e^{-\beta\left(\mu_i^H - \Delta g_{ij}^{inc}\right)} \tag{6}$$

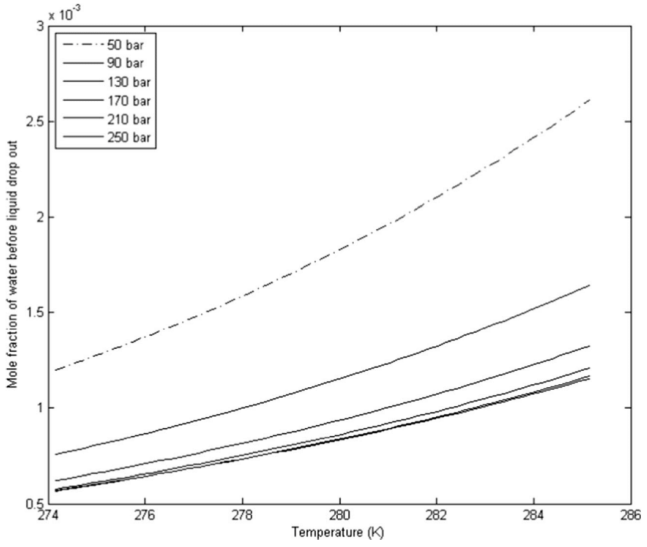

Fig. 6 Maximum concentration of water that can be permitted in the CH_4-rich gas before liquid water drops out. Curves from top to bottom correspond to pressure of 50 bar, 90 bar, 130 bar, 170 bar, 210 bar and 250 bar respectively

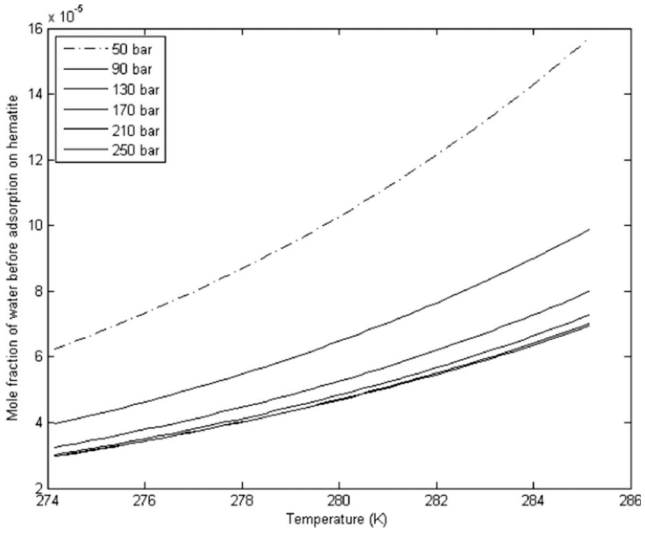

Fig. 7 Maximum concentration of water that can be permitted in the CH_4-rich gas before water is adsorbed on hematite. Curves from top to bottom correspond to pressure of 50 bar, 90 bar, 130 bar, 170 bar, 210 bar and 250 bar respectively

Here, β is the inverse of the product of gas constant and temperature, and Δg_{ij}^{inc} is the impact on hydrate water from inclusion of the guest molecules j in the cavity i [10]; its expansion coefficients are tabulated in Tables 4 and 5 below for carbon dioxide and hydrogen sulfide guests, respectively. In equilibrium, the chemical potential of component j in hydrate phase "H" must be identical to that in the (parent) phase from which it has been extracted [1]. Chemical potential of all gas components in hydrate are estimated by employing Eq. (1). The usual equilibrium approximation most hydrate simulators utilize is presented in Eq. (7) below assuming a free hydrate former phase (gas, liquid, fluid) in which every component's chemical potential is generally estimated by an equation of state and the resulting chemical potential required in Eq. (6) for the cavity.

$$\mu_{H_2O}^{(0,H)} - R.T\sum_{i=1}^{2} v_i ln\left(1+\sum_{j=1}^{n_{guest}} h_{ij}\right) = \mu_{i,H_2O}^{Pure\ water}(T,P) + RTln\left[x_{i,H_2O}\gamma_{i,H_2O}\left(T,P,\vec{x}\right)\right] \quad (7)$$

The estimation of the chemical potential of water in empty chlatrate (hydrate) structure has been implemented by means of Kvamme and Tanaka model [5]. This model has been proven to have predictive capabilities; consequently, it makes any empirical formulations for these chemical potentials unnecessary and possibly also nonphysical since chemical potential is a fundamental thermodynamic property. Given that the aqueous phase water lacks any ions and includes only limited amount of dissolved gases, the right-hand side of Eq. (7) has been approximated by the pure water value. This involves only a minor shift in chemical potential of liquid water. For instance, at 15000 kPa and 274 K

Table 4 Coefficients of $\Delta g_{inclusion}$ in the equation $\Delta g^{inclusion} = \sum_{i=0}^{5} k_i \left[\frac{T_c}{T}\right]^i$ in case of CO_2 inclusion in structure I hydrate. Subscript c on T in the equation denote critical temperature. Critical temperature for CO_2 is 304.13 K. Units on k are in kJ/mol

k	Large cavity	Small cavity
0	1.624892126738541	−0.001472006897812825
1	1.163780531566063	−55.894438257553600
2	−56.736684127967590	−5.622310021096491
3	−27.993674783103930	19.483488092203920
4	16.859513200395660	11.325243831207700
5	19.774626541207180	3.033541053649439

Table 5 Coefficients of $\Delta g_{inclusion}$ in the equation $\Delta g^{inclusion} = \sum_{i=0}^{5} k_i \left[\frac{T_c}{T}\right]^i$ for H_2S in structure I. Subscript c of T in the equation denote critical temperature. Critical temperature for H_2S is 373.0 K. Units of k are kJ/mol

k	Large cavity	Small cavity
0	16.016081922594900	−22.756290074587520
1	24.620388773936620	0.7857734898893513
2	−44.136111233969420	−33.910124845368450
3	−39.553535022042830	0.2509106251170165
4	2.362730250749388	−16.141504094980840
5	15.324247971160300	19.005383720423500

Table 6 The maximum concentration of water permitted in different gas-streams and comparing the two different routes to hydrate formation at a pressure of 250 bar

Pressure: 250 bar	Original gas		CH_4-rich gas		CO_2-rich gas	
	274 K	280 K	274 K	280 K	274 K	280 K
Maximum mole fraction of water before liquid drop out ($\times 10^{-3}$)	0.701	1.078	0.569	0.836	0.564	0.832
Maximum mole fraction of water before adsorption on hematite ($\times 10^{-3}$)	0.036	0.061	0.030	0.047	0.029	0.047

the correction will be as small as −0.07 kJ/mol. Though slightly greater for 20,000 kPa and 25,000 kPa, it is still not dramatic for the purpose of this study. However, Eq. (8) has been proven to be beneficial to estimate free energy change corresponding to a hydrate phase transition Δg^H.

$$\Delta g^H = \delta \sum_{j=1}^{n^H} x_j^H \left(\mu_j^H - \mu_j^P\right) \tag{8}$$

Where H is refers to the hydrate phase of molecule *j;* P is parent phase of molecule *j*. While Eq. (9) presents the relation between the filling fraction, the mole fractions and cavity partition function as shown below:

$$\theta_{ij} = \frac{x_{ij}^H}{v_j(1-x_T)} = \frac{h_{ij}}{1+\sum_j h_{ij}} \tag{9}$$

Where x_T refers to the total mole fraction of all guests in the hydrate; θ_{ij} stands for the filling fraction of component *j* in cavity type *I*; and x_{ij}^H is the mole fraction of component *j* in cavity type *i*.

Figures 1 and 2 present the comparison between the experimental data [11, 12] and hydrate equilibrium pressure-temperature curves estimated by our theoretical model for components relevant to this work: carbon dioxide, methane, ethane, and nitrogen. Rather that fitting the interaction parameters to replicate the experiment, our main goal was to ensure that the statistical-physics model of [5] was free of adjustable parameters in every term, including chemical potential of water in empty hydrate lattice, as liquid water, and in the form of ice. The comparison of our estimates with widely accepted experimental data demonstrates a quite satisfactory agreement without any empirical fitting required. The slight deviation observed in Fig. 1 is due to guest-guest interactions for a quaternary gas mixture like the one in question. Figure 2 exhibits a very good match, especially inside the relevant temperature ranges of 273–286 K, which is just a binary gas mixture of methane and ethane. Therefore, we have deemed the deviations to be acceptable for the purposes of this work.

Table 7 Recapitulative table of pressure temperature and composition dependency for CO_2 hydrates formation and substitution in CH_4 hydrates structure I

Pressure [bar]	Fraction range	Minimal temperature required for (0.1) CO_2 [K]
200	[0.1; 0.8]	277.0
210	[0.1; 0.8]	276.9
220	[0.1; 0.8]	276.7
230	[0.1; 0.8]	276.5
240	[0.1; 0.8]	276.3
250	[0.1; 0.8]	276.1

5 Hydrate risk analysis: alternative approaches for evaluating the risk of hydrate formation for Natuna gas from the reservoir

When hydrate risk under transport or processing is to be assessed for a particular gas mixture containing hydrate-forming hydrocarbons and inorganics (structure I components and CO_2 and in this study), the initial step is to evaluate the upper safe limit of water tolerated by the gas or liquid system before water will drop out as condensate. The classical approach to hydrate risk analysis involves evaluating the mole fraction of water in gas or liquid phase at the water dew-point. More recent analysis has been extended by considering two other alternative pathways [1, 7]. The first of these alternative pathways takes into account the process of water condensing out as adsorbed phase on the rusty (hematite) pipe walls. The other alternative route to hydrate formation considers hydrate forming directly from water dissolved in hydrate former phase. Despite the fact that the latter alternative route is thermodynamically feasible, it was associated with large mass- and heat-transport limitations in the hydrate forming systems examined in those studies [1, 7]. Thus, the route where hydrate forms directly from dissolved water will be extremely improbable compared to both the classical (dew-point) water drop-out approach and the alternative approach involving adsorption of water on hematite (rusty) surfaces. Therefore, our study ignored the third alternative and focused on the other two.

The produced gas transportation from Natuna gas-field will typically involve temperature 274 K to 283 K and pressures ranging from 50 to 300 bars. The processing conditions during separation onshore are not known since they are highly dependent on the separation methods. After the separation process on mainland, two new gas streams will be generated with compositions presented above in Tables 2 and 3. Both the CH_4-and CO_2-rich gas streams are expected to be transported

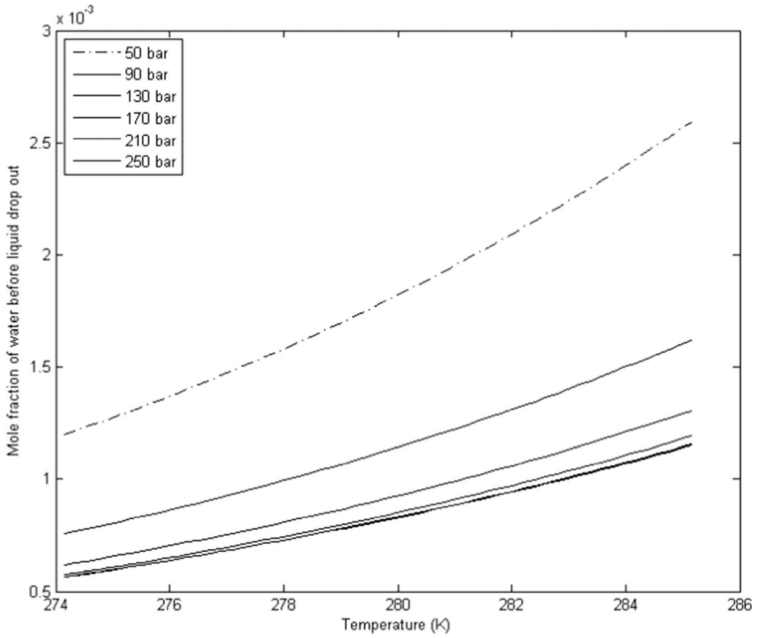

Fig. 8 Maximum concentration of water that can be permitted in the CO_2-rich gas before liquid water drops out. Curves from top to bottom correspond to pressure of 50 bar, 90 bar, 130 bar, 170 bar, 210 bar and 250 bar respectively

by pipeline operating at temperature and pressure ranging from 274 K to 285 K, and 50 bars to 250 bars, respectively.

Our novel thermodynamic scheme for investigation of different routes to hydrate formation, using ideal gas as reference state for all components in all phases including hydrate phase has been applied to investigate the maximum limit of water content that should be permitted in Natuna gas from the Greater Sarawak Basin. Figure 1 presents the hydrate

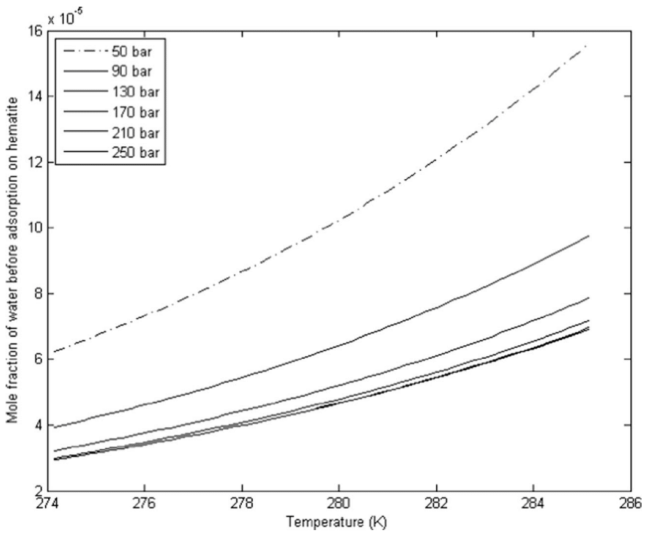

Fig. 9 Maximum concentration of water that can be permitted in the CO_2-rich gas before water is adsorbed on hematite. Curves from top to bottom correspond to pressure of 50 bar, 90 bar, 130 bar, 170 bar, 210 bar and 250 bar respectively

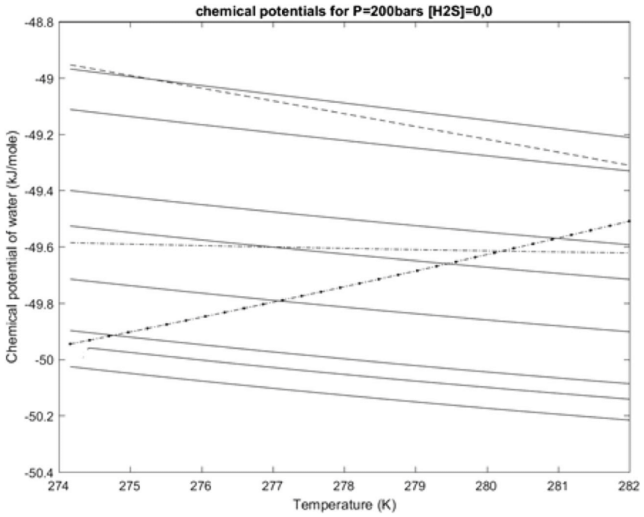

Fig. 10 Chemical potential as function of temperature of present components in the injection gas at $P = 200$ bar. The upper dashed curve is chemical potential of liquid water. The lower dashed curve is for chemical potential of water in methane hydrate. The dash-dot curve is the chemical potential of water in an artificial hydrate of structure II formed from a gas composition containing CH_4, C_2H_6 and C_3H_8. Solid curves are chemical potential for water in hydrate formed from various CO_2/N_2 ratios. Top curve is for a mole % of CO_2 of 1%. The following curves are for hydrate formed from a mole % of respectively 2, 5, 10, 20, 40, 60, 80% CO_2 from top to bottom

equilibrium curves for the three gas streams in question. Figures 2, 3, 4, 5, 6 and 7 illustrate qualitatively the safe limits of water content for Natuna gas before and after most of the CO_2 is separated out of the bulk, with both the classical dew-point liquid water drop-out approach and the alternative route involving adsorption of water on the rusty surfaces of process equipment and transport pipes. Maximum water level tolerated before water will start to drop out from the original gas from Natuna are plotted in Fig. 2. Levels calculated basing on adsorption on hematite is shown in Fig. 3 for the same gas.

Both the methane- and CO_2-rich gas exhibit similar trends for all pressures presented in Figs. 4 to 7. Only a tiny shift in absolute values of water drop-out mole fractions is present, with methane values being slightly higher compared to CO_2. Generally, both hydrate formation routes share a significant reduction in the gap/difference between the pressure curves between 50 bar and 90 bar, and between 90 bar and 130 bar. The curves for the two highest pressures, 210 bar and 250 bar, overlap for both methane and CO_2. In case of the CO_2 stream, the pressure curves overlap

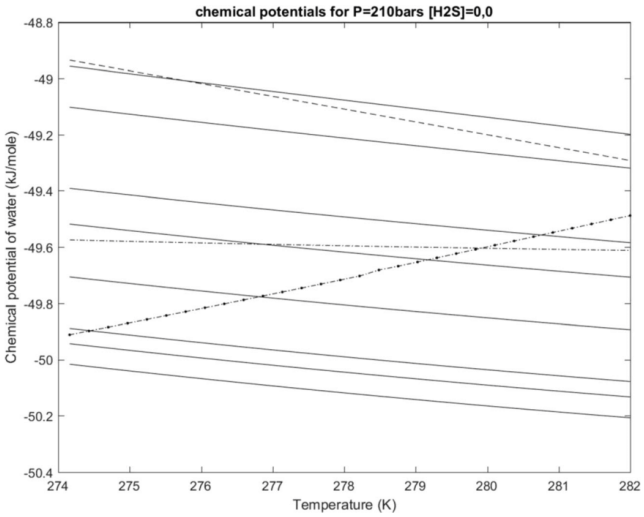

Fig. 11 Chemical potential as function of temperature of present components in the injection gas at $P = 210$ bar. The upper dashed curve is chemical potential of liquid water. The lower dashed curve is for chemical potential of water in methane hydrate. The dash-dot curve is the chemical potential of water in an artificial hydrate of structure II formed from a gas composition containing CH_4, C_2H_6 and C_3H_8. Solid curves are chemical potential for water in hydrate formed from various CO_2/N_2 ratios. Top curve is for a mole % of CO_2 of 1%. The following curves are for hydrate formed from a mole % of respectively 2, 5, 10, 20, 40, 60, 80% CO_2 from top to bottom

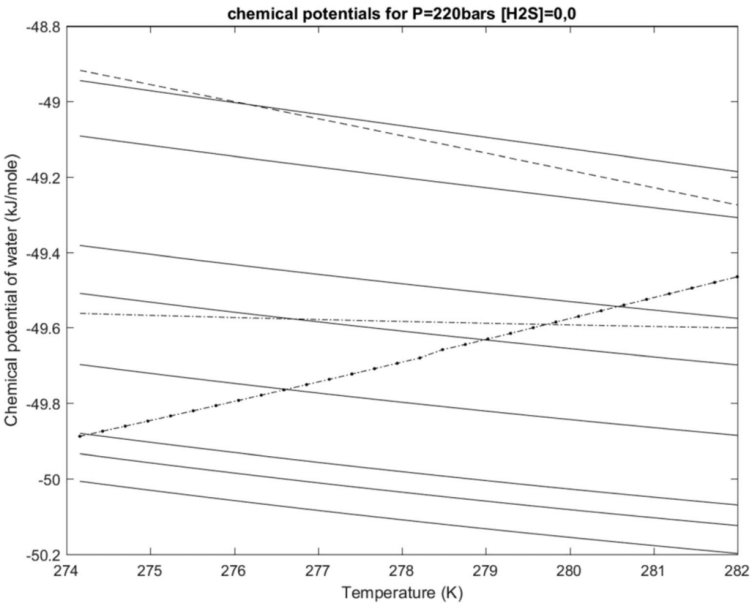

Fig. 12 Chemical potential as function of temperature of present components in the injection gas at $P = 220$ bar. The upper dashed curve is chemical potential of liquid water. The lower dashed curve is for chemical potential of water in methane hydrate. The dash-dot curve is the chemical potential of water in an artificial hydrate of structure II formed from a gas composition containing CH_4, C_2H_6 and C_3H_8. Solid curves are chemical potential for water in hydrate formed from various CO_2/N_2 ratios. Top curve is for a mole % of CO_2 of 1%. The following curves are for hydrate formed from a mole % of respectively 2, 5, 10, 20, 40, 60, 80% CO_2 from top to bottom

almost completely, indicating the higher density impact. The differences at the highest pressures are virtually insensitive to pressure due to the high density.

The safe-limit of water content decrease as the pressure increases for pure structure I hydrate components as methane and CO_2. This is also the case original CO_2-dominated Natuna

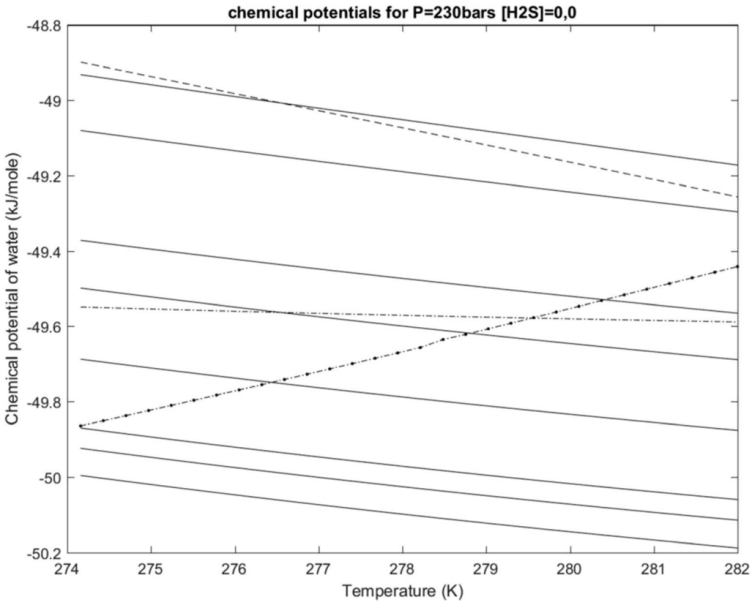

Fig. 13 Chemical potential as function of temperature of present components in the injection gas at $P = 230$ bar. The upper dashed curve is chemical potential of liquid water. The lower dashed curve is for chemical potential of water in methane hydrate. The dash-dot curve is the chemical potential of water in an artificial hydrate of structure II formed from a gas composition containing CH_4, C_2H_6 and C_3H_8. Solid curves are chemical potential for water in hydrate formed from various CO_2/N_2 ratios. Top curve is for a mole % of CO_2 of 1%. The following curves are for hydrate formed from a mole % of respectively 2, 5, 10, 20, 40, 60, 80% CO_2 from top to bottom

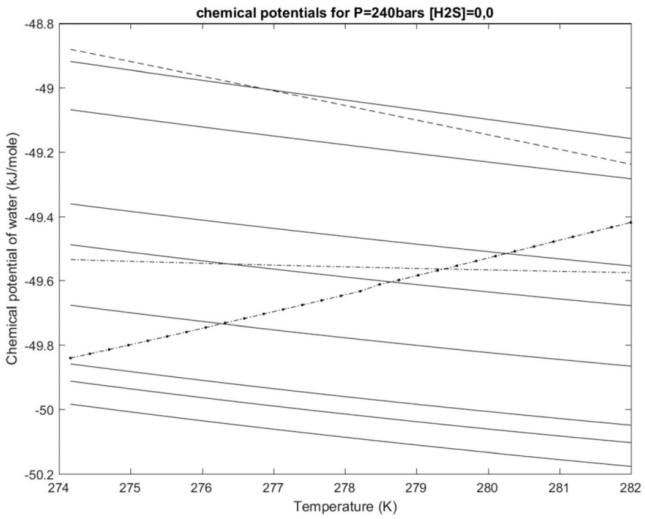

Fig. 14 Chemical potential as function of temperature of present components in the injection gas at $P = 240$ bar. The upper dashed curve is chemical potential of liquid water. The lower dashed curve is for chemical potential of water in methane hydrate. The dash-dot curve is the chemical potential of water in an artificial hydrate of structure II formed from a gas composition containing CH_4, C_2H_6 and C_3H_8. Solid curves are chemical potential for water in hydrate formed from various CO_2/N_2 ratios. Top curve is for a mole % of CO_2 of 1%. The following curves are for hydrate formed from a mole % of respectively 2, 5, 10, 20, 40, 60, 80% CO_2 from top to bottom

gas due to its lack of heavier hydrocarbons such as propane, and iso-butane etc.

When comparing safe water limit corresponding to the two hydrate formation routes in case of Natuna gas, the formation route that involves water adsorption on hematite yielded the water mole fraction which was by a factor of 19 smaller than value given by the classical dew-point approach currently used as industrial standard. This large difference underlines the risk that hydrates may still form in industrial processes if only the dew-point approach is used as the hydrate safety criterion measure. Therefore, this alternative route involving adsorption of water on rusty surfaces and providing a free water phase for hydrate nucleation should not be ignored if the risk of hydrate formation without addition of inhibitions or applying other costly measures during processing and pipeline transport of

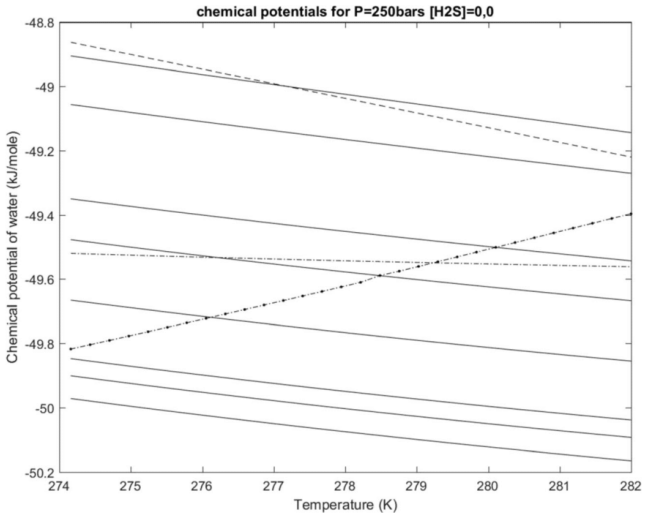

Fig. 15 Chemical potential as function of temperature of present components in the injection gas at $P = 250$ bar. The upper dashed curve is chemical potential of liquid water. The lower dashed curve is for chemical potential of water in methane hydrate. The dash-dot curve is the chemical potential of water in an artificial hydrate of structure II formed from a gas composition containing CH_4, C_2H_6 and C_3H_8. Solid curves are chemical potential for water in hydrate formed from various CO_2/N_2 ratios. Top curve is for a mole % of CO_2 of 1%. The following curves are for hydrate formed from a mole % of respectively 2, 5, 10, 20, 40, 60, 80% CO_2 from top to bottom

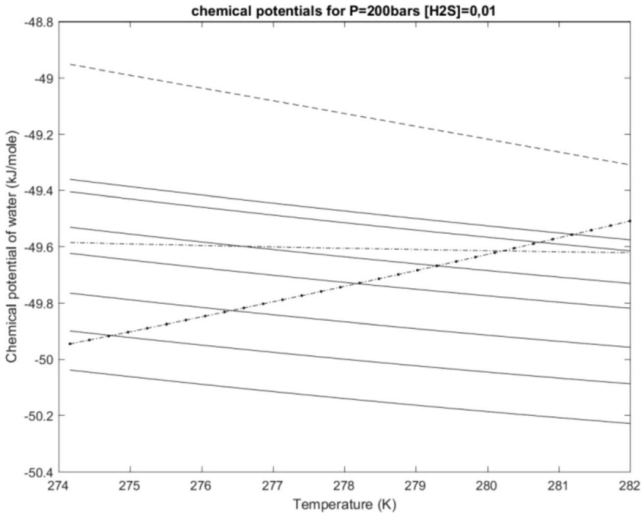

Fig. 16 Chemical potential as function of temperature of present components in the injection gas containing 1% H_2S at $P = 200$ bar. The upper dashed curve is chemical potential of liquid water. The lower dashed curve is for chemical potential of water in methane hydrate. The dash-dot curve is the chemical potential of water in an artificial hydrate of structure II formed from a gas composition containing CH_4, C_2H_6 and C_3H_8. Solid curves are chemical potential for water in hydrate formed from various CO_2/N_2 ratios. H_2S amount has been added directly as molar ratio and the composition has been normalized. Top curve is for a mole % of CO_2 of 1%. The following curves are for hydrate formed from a mole % of respectively 2, 5, 10, 20, 40, 60, 80% CO_2 from top to bottom

natural gas must be avoided. On the other hand, it is not possible for initial hydrate nuclei to attach directly to the rust surface due to the low chemical potential of adsorbed water. The hydrate formed will be bridged by at least three to four layers of structured water on the surface of the hematite. This alternative route to hydrate formation through adsorption on hematite absolutely dominates when it comes to the risk of water dropping out from gas mixture and pure components to form a separate water phase and ultimately resulting in hydrate formation. This can be understood from the fact that the average chemical potential of water adsorbed on hematite could be 3.4 kJ/mol lower than that of liquid water. And thermodynamics does favour minimum free energy.

Table 6 presents the maximum amount of water tolerated in various gas streams calculated using coefficients provided in Tables 4 and 5. With anticipated transport pressures varying between 50 and 250 bars and the highest seafloor

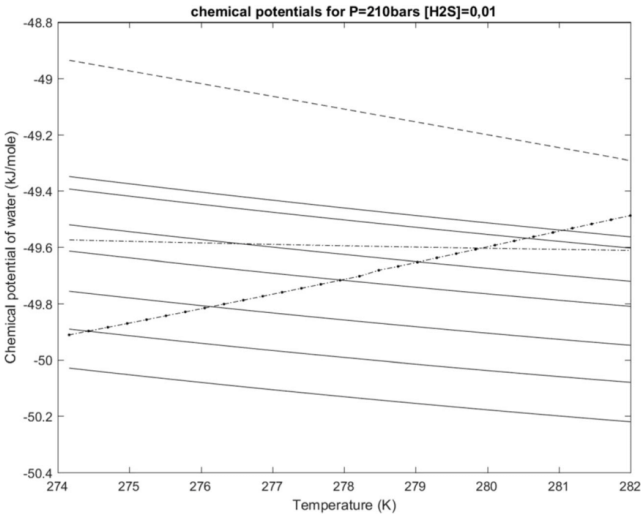

Fig. 17 Chemical potential as function of temperature of present components in the injection gas containing 1% H_2S at $P = 210$ bar. The upper dashed curve is chemical potential of liquid water. The lower dashed curve is for chemical potential of water in methane hydrate. The dash-dot curve is the chemical potential of water in an artificial hydrate of structure II formed from a gas composition containing CH_4, C_2H_6 and C_3H_8. Solid curves are chemical potential for water in hydrate formed from various CO_2/N_2 ratios. H_2S amount has been added directly as molar ratio and the composition has been normalized. Top curve is for a mole % of CO_2 of 1%. The following curves are for hydrate formed from a mole % of respectively 2, 5, 10, 20, 40, 60, 80% CO_2 from top to bottom

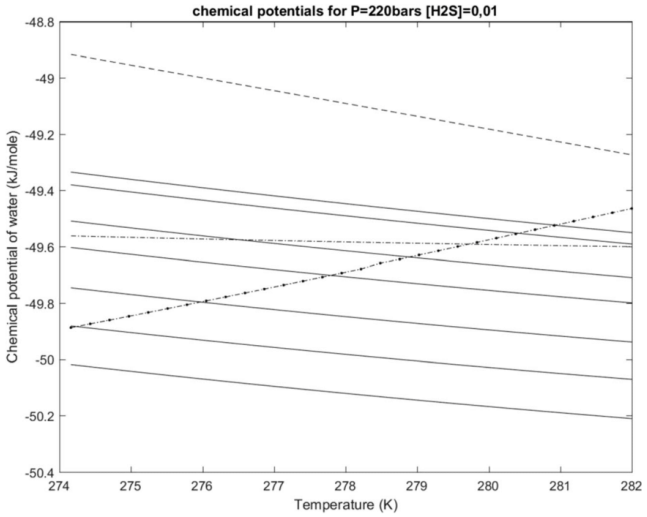

Fig. 18 Chemical potential as function of temperature of present components in the injection gas containing 1% H_2S at $P = 220$ bar. The upper dashed curve is chemical potential of liquid water. The lower dashed curve is for chemical potential of water in methane hydrate. The dash-dot curve is the chemical potential of water in an artificial hydrate of structure II formed from a gas composition containing CH_4, C_2H_6 and C_3H_8. Solid curves are chemical potential for water in hydrate formed from various CO_2/N_2 ratios. H_2S amount has been added directly as molar ratio and the composition has been normalized. Top curve is for a mole % of CO_2 of 1%. The following curves are for hydrate formed from a mole % of respectively 2, 5, 10, 20, 40, 60, 80% CO_2 from top to bottom

temperature around 6 degrees Celsius, it is obvious from Fig. 1 that all considered mixtures will exist inside the hydrate formation region. The question is therefore at which water concentrations in gas the water will drop out. Since the maximum pressure (Figs. 2 to 7) provides the estimate for the lowest of permitted gas in all systems, we have extracted some illustrative examples corresponding to that pressure. Table 6 lists the maximum safe water limits permitted at two temperatures 274 k and 280 K and 250 bars.

As expected from earlier studies, water solubility are quite similar for both methane-rich and carbon dioxide-rich gas mixtures. The maximum amounts of water before liquid water drop-out or adsorption respectively are also quite similar for the two mixtures, in contrast to the original Natuna

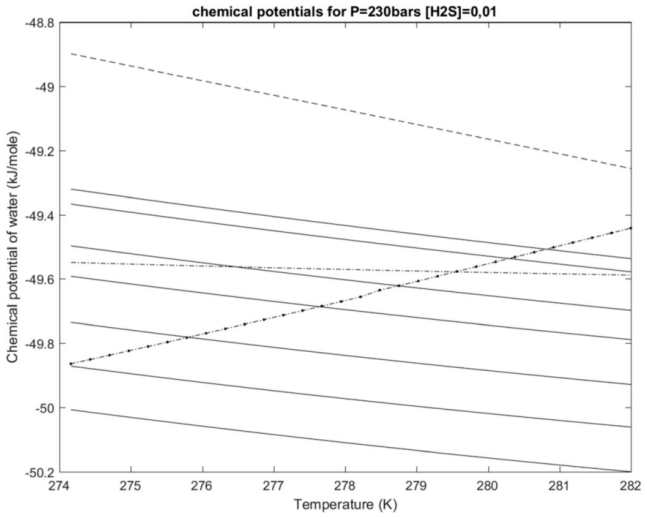

Fig. 19 Chemical potential as function of temperature of present components in the injection gas containing 1% H2S at $P =$ 230 bar. The upper dashed curve is chemical potential of liquid water. The lower dashed curve is for chemical potential of water in methane hydrate. The dash-dot curve is the chemical potential of water in an artificial hydrate of structure II formed from a gas composition containing CH_4, C_2H_6 and C_3H_8. Solid curves are chemical potential for water in hydrate formed from various CO_2/N_2 ratios. H_2S amount has been added directly as molar ratio and the composition has been normalized. Top curve is for a mole % of CO_2 of 1%. The following curves are for hydrate formed from a mole % of respectively 2, 5, 10, 20, 40, 60, 80% CO_2 from top to bottom

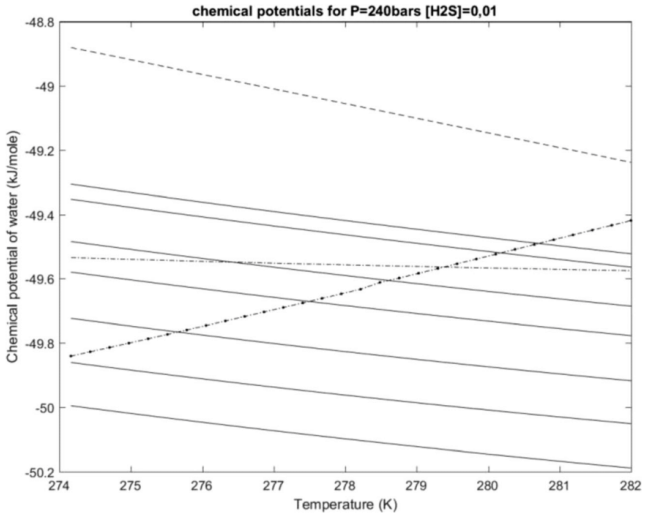

Fig. 20 Chemical potential as function of temperature of present components in the injection gas containing 1% H_2S at $P = 240$ bar. The upper dashed curve is chemical potential of liquid water. The lower dashed curve is for chemical potential of water in methane hydrate. The dash-dot curve is the chemical potential of water in an artificial hydrate of structure II formed from a gas composition containing CH_4, C_2H_6 and C_3H_8. Solid curves are chemical potential for water in hydrate formed from various CO_2/N_2 ratios. H_2S amount has been added directly as molar ratio and the composition has been normalized. Top curve is for a mole % of CO_2 of 1%. The following curves are for hydrate formed from a mole % of respectively 2, 5, 10, 20, 40, 60, 80% CO_2 from top to bottom

gas. In all cases, the maximum water tolerances based on the dew-point are in the order of 18 times higher that tolerance criteria based on Hematite adsorption.

6 A possible hydrate reservoir for CO_2 storage and utilization

While considering the production of natural gas from the Natuna field wells, it is extremely important to address the high fraction of CO_2 (71 mol%) that this field contains. Given the impact of global warming and the focus on sustainable industry, the storage alternatives for such a huge amount of CO_2 must be carefully considered. Luckily, Indonesia is fortunate to have several huge methane hydrates fields that could serve as perfect storage options for CO_2 and a viable intermediary for the EOR.

The North Makassar Basin hydrate field is one of them, with a reasonable collection of seismic data available [12], making it a good case study to address the storage and utilization of carbon

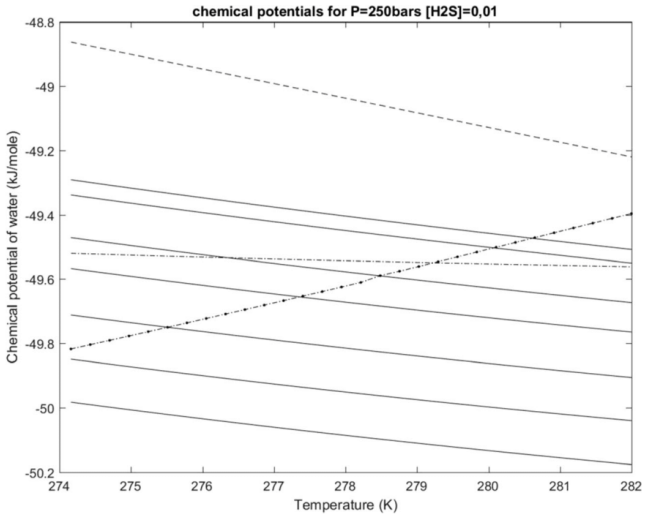

Fig. 21 Chemical potential as function of temperature of present components in the injection gas containing 1% H_2S at $P = 250$ bar. The upper dashed curve is chemical potential of liquid water. The lower dashed curve is for chemical potential of water in methane hydrate. The dash-dot curve is the chemical potential of water in an artificial hydrate of structure II formed from a gas composition containing CH_4, C_2H_6 and C_3H_8. Solid curves are chemical potential for water in hydrate formed from various CO_2/N_2 ratios. H_2S amount has been added directly as molar ratio and the composition has been normalized. Top curve is for a mole % of CO_2 of 1%. The following curves are for hydrate formed from a mole % of respectively 2, 5, 10, 20, 40, 60, 80% CO_2 from top to bottom

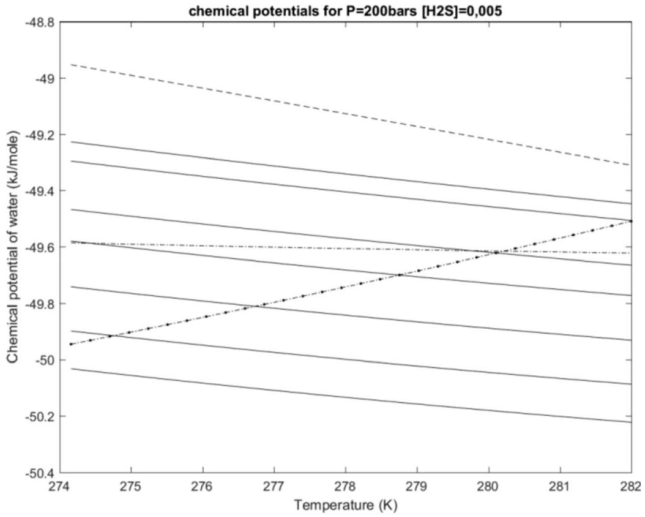

Fig. 22 Chemical potential as function of temperature of present components in the injection gas containing 0.5% H_2S at P = 200 bar. The upper dashed curve is chemical potential of liquid water. The lower dashed curve is for chemical potential of water in methane hydrate. The dash-dot curve is the chemical potential of water in an artificial hydrate of structure II formed from a gas composition containing CH_4, C_2H_6 and C_3H_8. Solid curves are chemical potential for water in hydrate formed from various CO_2/N_2 ratios. H_2S amount has been added directly as molar ratio and the composition has been normalized. Top curve is for a mole % of CO_2 of 1%. The following curves are for hydrate formed from a mole % of respectively 2, 5, 10, 20, 40, 60, 80% CO_2 from top to bottom

dioxide from Natuna. To be able to store CO_2 efficiently, CO_2 must be converted to hydrate. Indeed, in such a solid form, there are limited risks of leaks from the wells and pollution of the area.

Moreover, when it comes to EOR, combining the storage of CO_2 with recovery of almost pure methane is one of the best ways to go, provided that pressure and temperature of methane hydrate fields are suitable for CO_2 substitution in type I hydrate. The affinity of CO_2 for type I hydrate structures is greater than that of CH_4 over pressure and temperature ranges easily achievable in the hydrates fields, thus allowing us to seriously consider the possibility of CO_2 storage.

Data collected by B. A. Jackson [13] show an 8000 m^2 area where several indicators point to potential presence of hydrates at approximate depth of 2450 m. Given the provided properties of seafloor and crust, it is possible to calculate pressure and temperature gradient in the field. Our calculations

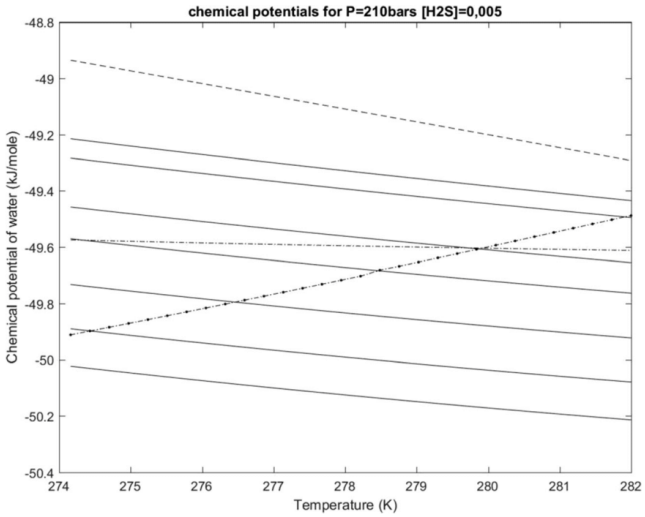

Fig. 23 Chemical potential as function of temperature of present components in the injection gas containing 0.5% H_2S at P = 210 bar. The upper dashed curve is chemical potential of liquid water. The lower dashed curve is for chemical potential of water in methane hydrate. The dash-dot curve is the chemical potential of water in an artificial hydrate of structure II formed from a gas composition containing CH_4, C_2H_6 and C_3H_8. Solid curves are chemical potential for water in hydrate formed from various CO_2/N_2 ratios. H_2S amount has been added directly as molar ratio and the composition has been normalized. Top curve is for a mole % of CO_2 of 1%. The following curves are for hydrate formed from a mole % of respectively 2, 5, 10, 20, 40, 60, 80% CO_2 from top to bottom

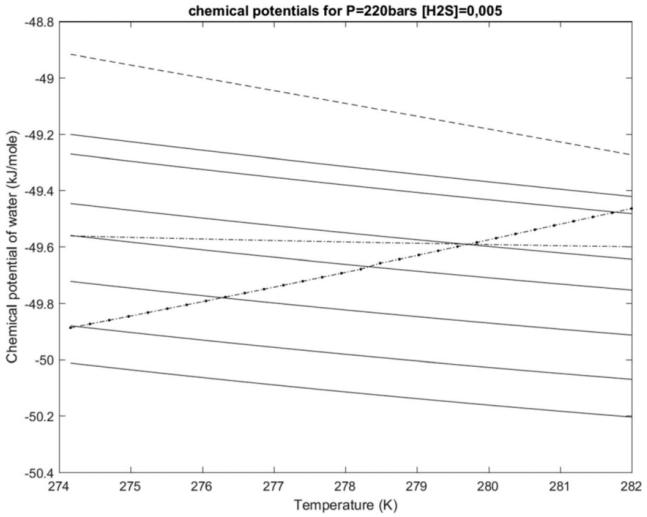

Fig. 24 Chemical potential as function of temperature of present components in the injection gas containing 0.5% H_2S at P = 220 bar. The upper dashed curve is chemical potential of liquid water. The lower dashed curve is for chemical potential of water in methane hydrate. The dash-dot curve is the chemical potential of water in an artificial hydrate of structure II formed from a gas composition containing CH_4, C_2H_6 and C_3H_8. Solid curves are chemical potential for water in hydrate formed from various CO_2/N_2 ratios. H_2S amount has been added directly as molar ratio and the composition has been normalized. Top curve is for a mole % of CO_2 of 1%. The following curves are for hydrate formed from a mole % of respectively 2, 5, 10, 20, 40, 60, 80% CO_2 from top to bottom

yielded the 200 bar - 250 bar pressure range and 274 K to 282 K temperature range, facilitating the estimation of chemical potential for the different relevant components. These results are plotted in Figs. 8, 9, 10, 11, 12, 13, 14, 15, 16, 17, 18, 19, 20, 21, 22, 23, 24, 25, 26 and 27 below, where the solid lines represent different concentration of CO_2 $[CO_2] = 0.01$; 0.02; 0.05; 0.1; 0.2; 0.4; 0.6; 0.8. The dashed line corresponds to water, the dot dashed line to methane hydrate structure I (the only one relevant in our case), and the double dash dotted line to methane hydrate structure II. Analysis of the present figures show several points that should be highlighted.

As reservoir pressure increases, chemical potential of CO_2 becomes progressively lower, indicating easier CH_4 substitution by CO_2, but we must exercise caution when it comes to the stability of CO_2 hydrates. Indeed, if CO_2 hydrate formation is too fast, it may seal off the reservoir close to the injection zone. CO_2 would then form hydrates directly from free

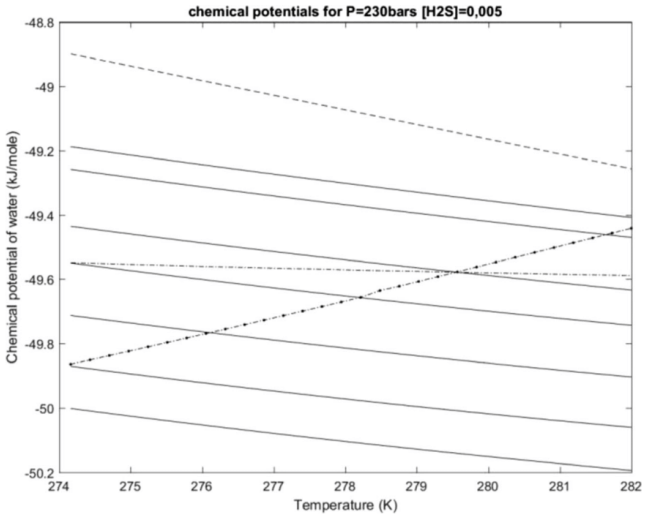

Fig. 25 Chemical potential as function of temperature of present components in the injection gas containing 0.5% H_2S at P = 230 bar. The upper dashed curve is chemical potential of liquid water. The lower dashed curve is for chemical potential of water in methane hydrate. The dash-dot curve is the chemical potential of water in an artificial hydrate of structure II formed from a gas composition containing CH_4, C_2H_6 and C_3H_8. Solid curves are chemical potential for water in hydrate formed from various CO_2/N_2 ratios. H_2S amount has been added directly as molar ratio and the composition has been normalized. Top curve is for a mole % of CO_2 of 1%. The following curves are for hydrate formed from a mole % of respectively 2, 5, 10, 20, 40, 60, 80% CO_2 from top to bottom

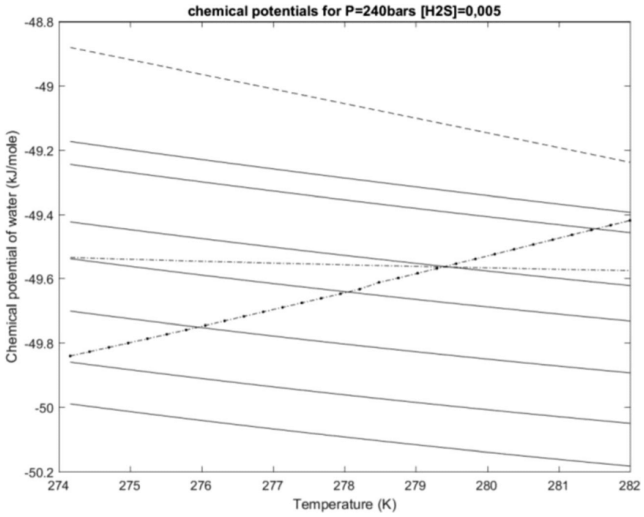

Fig. 26 Chemical potential as function of temperature of present components in the injection gas containing 0.5% H_2S at P = 240 bar. The upper dashed curve is chemical potential of liquid water. The lower dashed curve is for chemical potential of water in methane hydrate. The dash-dot curve is the chemical potential of water in an artificial hydrate of structure II formed from a gas composition containing CH_4, C_2H_6 and C_3H_8. Solid curves are chemical potential for water in hydrate formed from various CO_2/N_2 ratios. H_2S amount has been added directly as molar ratio and the composition has been normalized. Top curve is for a mole % of CO_2 of 1%. The following curves are for hydrate formed from a mole % of respectively 2, 5, 10, 20, 40, 60, 80% CO_2 from top to bottom

water present in the reservoir, and may never encounter methane hydrates it is supposed to react with. CH_4 substitution by CO_2 in hydrates is limited by the rate of solid diffusion, a slow kinetic phenomenon, which would take place after new hydrates formation, so the CO_2 concentration in injected gas must be calculated to allow CO_2 the time to travel close to the CH_4 hydrates. Therefore, the injected gas composition will be of crucial importance; the amount of N_2 present in the gas should be judged wisely to optimise hydrate formation without plugging the system.

One of the great advantages of the Natuna gas field lies in its virtual lack of hydrogen sulphide, which acts as inhibitor for chemical transformation of natural gas in addition to being an intensively corrosive agent. This fact allowed us to calculate chemical potential profiles for all the components while ignoring a possible presence of H_2S.

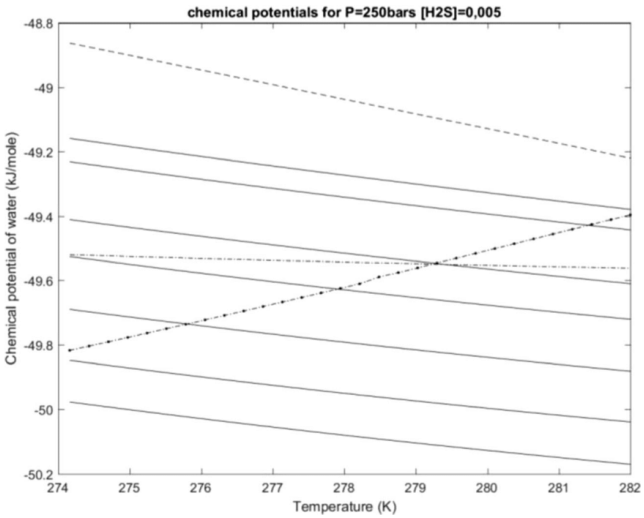

Fig. 27 Chemical potential as function of temperature of present components in the injection gas containing 0.5% H_2S at P = 250 bar. The upper dashed curve is chemical potential of liquid water. The lower dashed curve is for chemical potential of water in methane hydrate. The dash-dot curve is the chemical potential of water in an artificial hydrate of structure II formed from a gas composition containing CH_4, C_2H_6 and C_3H_8. Solid curves are chemical potential for water in hydrate formed from various CO_2/N_2 ratios. H_2S amount has been added directly as molar ratio and the composition has been normalized. Top curve is for a mole % of CO_2 of 1%. The following curves are for hydrate formed from a mole % of respectively 2, 5, 10, 20, 40, 60, 80% CO_2 from top to bottom

Nevertheless, data compiled in the above figures should prive quite relevant for any potential industrial trial considerations.

These figures above clearly show that there exists a range of temperatures and compositions where CO_2 can replace CH_4 in the structure I hydrate. Table 7 below groups these ranges for the pressures concerned.

To summarise, the CO_2 storage coupled with CH_4 recovery from hydrates fields appears to offer a sustainable alternative to combine with gas extraction from high CO_2 concentrated fields. Figures used to illustrate this study are based on seismic data that could be refined further for the purposes of a practical industrial implementation. Nevertheless, the ranges selected are wide enough to include temperatures and variations the most probable in such hydrates fields.

tin formation of CO_2-dominated hydrate and thus enable a rapids mechanism for formation of CO_2 hydrate and release of methane due to heat generated dissociation of *in situ* methane hydrate. A fraction of injected CO_2 will dissolve in the groundwater and adsorb on mineral surfaces. The "enrichment" of CO_2 when it either adsorbs on mineral surfaces or becomes trapped by adsorbed water layers can enhance the overall nucleation rate of the new CO_2 hydrate formation in sediments. But a rigorous estimate of the lowest limit of CO_2 needed in the injection gas will require a detailed modelling for each reservoir in question to make sure that the fast conversion mechanism is retained throughout the reservoir. The extremely slow mechanism of direct solid-state exchange is of not practical importance, but as indicated by Figs. 8 to 25, the concentration of CO_2 in the N_2-dominated mixture needed by the solid-state exchange is higher. In the absence of H_2S in the gas mixture, roughly 5 to 12% CO_2 will be required. These limits will decrease to between 4 to 5% for 0.5% H_2S in the gas mixture and to between 2 to 3% for the case of 1% H_2S. Since the Natuna gas has a very limited presence of higher hydrocarbons, the artificial structure-II gas mixture is not particularly relevant. It is included to provide a qualitative indication of the situation in a reservoir with similar conditions but more thermogenic gas.

7 Conclusion

In this work, we have investigated the Natuna gas as well as two realistic separated streams, a CO_2-rich stream and a methane-rich stream, to determine the maximum water fraction that can be permitted without invoking the risk of hydrate formation. Our estimates suggest that pipeline transport conditions expected for all three streams will fall inside the hydrate formation region if liquid water becomes available either by condensing below the dew-point or adsorbing on rusty pipeline surfaces. The low chemical potential of water adsorbed on hematite (dominating form of rust) will result in substantially lower tolerance limits for the water content of transported gas. When the water dew-point is used as the criteria, the permitted water mole fraction in gas is roughly eighteen times higher than in the case of using the limit of adsorption on rust.

We have also studied the feasibility of the separated CO_2 for simultaneous safe long terms storage of CO_2 and release of methane from *in situ* hydrates in the North Makassar Basin hydrate field at offshore Indonesia. It was found that the minimum concentration of CO_2 required to create a new hydrate while retaining a fast exchange rate will be reasonably low in case of this deep reservoir. Even CO_2 fractions as low as 2 mol% in CO_2/N_2 gas will allow the new hydrate to form. This is of course a theoretical limit, in practice the injection gas mixture will have to be adjusted depending on hydrate consumption throughout the reservoir. While N_2 will mostly fill the small hydrate cavities, a tiny fraction of it may even enter the large cavities while competing with the far more thermodynamically favoured CO_2. Data available on the Natuna gas indicates that the combined fraction of N_2 and H_2S amounts to 1%. If H_2S accounts for only a half of the admixture, gas able to form a new hydrate is only required to contain as little as 1% of CO_2. Direct solid-state exchange between in situ CH_4 hydrate and CO_2 hydrate will be extremely restricted kinetically and of no practical importance. Nevertheless, the minimum level of CO_2 in N_2 required by this mechanism is higher. Roughly 5 to 12% CO_2 will be needed in the absence of H_2S, and 2 to 3% when the mixture contains 1% H_2S.

Compliance with ethical standards

Conflict of interests On behalf of all authors, the corresponding author states that there is no conflict of interests.

Publisher's Note Springer Nature remains neutral with regard to jurisdictional claims in published maps and institutional affiliations.

References

1. Kvamme B et al (2016) Hydrate formation during transport of natural gas containing water and impurities. J Chem Eng Data 61(2): 936–949
2. Kvamme B (2016) Thermodynamic Limitations of the CO2/N2 Mixture Injected into CH4 Hydrate in the Ignik Sikumi Field Trial. J Chem Eng Data 61(3):1280–1295
3. Fenter DJ, Hadiatno D (1996) Reservoir simulation modeling of natuna gas field for reservoir evaluation and development planning. In: In SPE Asia Pacific Oil and Gas Conference. Society of Petroleum Engineers
4. Soave G (1972) Equilibrium constants from a modified Redlich-Kwong equation of state. Chem Eng Sci 27:1197–1203
5. Kvamme B, Tanaka H (1995) Thermodynamic Stability of Hydrates for Ethane, Ethylene, and Carbon Dioxide. J Phys Chem 99(18):7114–7119

6. Kvamme B et al (2014) Consequences of CO2 solubility for hydrate formation from carbon dioxide containing water and other impurities. Phys Chem Chem Phys 16(18):8623–8638
7. Kvamme B et al (2013) Can hydrate form in carbon dioxide from dissolved water? Phys Chem Chem Phys 15(6):2063–2074
8. Kvamme B et al (2014) Hydrate phase transition kinetics from Phase Field Theory with implicit hydrodynamics and heat transport. International Journal of Greenhouse Gas Control 29:263–278
9. Van der Waals JH, Platteuw JC (1959) *Clathrate solutions*. Advances in Chemical Physics, vol 2. Interscience Publishers Inc, New York
10. Sloan ED (2003) Fundamental principles and applications of natural gas hydrates. Nature 426(6964):353–363
11. Fan S-S, Guo T-M (1999) Hydrate formation of CO2-rich binary and quaternary gas mixtures in aqueous sodium chloride solutions. J Chem Eng Data 44(4):829–832
12. Maekawa T (2001) Equilibrium conditions for gas hydrates of methane and ethane mixtures in pure water and sodium chloride solution. Geochem J 35(1):59–66
13. Jackson BA (2004) Seismic evidence forgas hydrates in the North Makassar Basin, Indonesia. Pet Geosci 10(3):227–238